AWARD NUMBER: W81XWH-21-1-0043

TITLE: Understanding Molecular Mechanisms of Secondary Resistance in Patients with Metastatic Castrate-Resistant Prostate Cancer

PRINCIPAL INVESTIGATOR: Samir Zaidi, MD, PhD

CONTRACTING ORGANIZATION: Sloan Kettering Institute for Cancer Research

REPORT DATE: JANUARY 2022

TYPE OF REPORT: Annual Technical

PREPARED FOR: U.S. Army Medical Research and Development Command
Fort Detrick, Maryland 21702-5012

REPORT DOCUMENTATION PAGE

Form Approved
OMB No. 0704-0188

1. REPORT DATE	2. REPORT TYPE	3. DATES COVERED
JANUARY 2022	Annual	01/01/2021 – 12/31/2021

4. TITLE AND SUBTITLE

Understanding Molecular Mechanisms of Secondary Resistance in Patients with Metastatic Castrate Resistant Prostate Cancer.

5a. CONTRACT NUMBER

5b. GRANT NUMBER
W81XWH-21-1-0043

5c. PROGRAM ELEMENT NUMBER

6. AUTHOR(S)

Samir Zaidi

E-Mail: zaidis@mskcc.org

5d. PROJECT NUMBER

5e. TASK NUMBER

5f. WORK UNIT NUMBER

7. PERFORMING ORGANIZATION NAME(S) AND ADDRESS(ES)

8. PERFORMING ORGANIZATION REPORT NUMBER

9. SPONSORING / MONITORING AGENCY NAME(S) AND ADDRESS(ES)

U.S. Army Medical Research and Development Command
Fort Detrick, Maryland 21702-5012

10. SPONSOR/MONITOR'S ACRONYM(S)

11. SPONSOR/MONITOR'S REPORT NUMBER(S)

12. DISTRIBUTION / AVAILABILITY STATEMENT

Approved for Public Release; Distribution Unlimited

13. SUPPLEMENTARY NOTES

14. ABSTRACT

One of the fundamental ways to slow down the progression of prostate cancer in men is to reduce the action of androgens, such as testosterone, on prostate cancer tissue. Certain drugs directly reduce androgen levels, while others, such as bicalutamide (Casodex), prevent androgen action on its receptor. However, even with these 'androgen–deprivation' therapies, a proportion of cancers escape and progress—this phenomenon is termed 'primary resistance'. To counteract this resistance, a second generation of anti–androgen therapies, namely enzalutamide (Xtandi), apalutamide (Erleada), darolutamide (Nubeqa) and abiraterone (Zytiga) has emerged over the last decade. While each drug effectively overcomes primary resistance, all tumors finally escape and progress. Such 'secondary resistance' currently poses a major clinical challenge, as patients rapidly follow a downhill course. The paucity of our understanding of mechanisms that underpin resistance has prevented us from developing new therapies. Mouse and cellular models have highlighted molecular pathways—however, not all are applicable to the prostate cancer patient. The focus of this study is therefore to understand the genetic and molecular events that lead to secondary resistance **at the level of each individual patient**. We will obtain biopsy tissue from 20 patients with lethal prostate cancer using state–of–the–art radiology called molecular imaging. As we know that the cellular composition of biopsy tissue is not homogenous, we will use technologies, such as single cell gene sequencing, to measure the expression of cancer–associated genes at the level of each single cell. We will then employ computational tools to understand which genes are potential drivers of the cancer and, importantly, of secondary resistance. Furthermore, by reconstructing the cellular architecture in three dimensional cultures termed 'organoids', we will manipulate target genes and study effects on cancer progression. In all, we expect to identify and characterize novel targets that could be interrogated by new drugs to overcome secondary resistance.

15. SUBJECT TERMS
Prostate cancer, single cell RNA sequencing, human tumors, patient derived organoids, CRISPR editing, secondary resistance

16. SECURITY CLASSIFICATION OF:			17. LIMITATION OF ABSTRACT	18. NUMBER OF PAGES	19a. NAME OF RESPONSIBLE PERSON
a. REPORT	b. ABSTRACT	c. THIS PAGE			USAMRDC
Unclassified	Unclassified	Unclassified	Unclassified	76	19b. TELEPHONE NUMBER *(include area code)*

Standard Form 298 (Rev. 8-98)
Prescribed by ANSI Std. Z39.18

TABLE OF CONTENTS

1. INTRODUCTION

Prostate cancer is the second leading cause of cancer–related mortality in men, accounting for ~31,000 deaths in the U.S. alone during 2019. Despite the remarkable success of second–generation anti–androgen therapies, notably enzalutamide and abiraterone, secondary resistance poses an ongoing **clinical challenge**. Androgen receptor (AR) reactivation through gene amplification or mutation contributes to secondary resistance in almost 70% of patients with advanced castrate–resistant prostate cancer (CRPC). Mutations have been described in certain *AR* regulators, such as *FOXA1*, a pioneer transcription factor, *NCOR1/2*, a negative regulator, and *ZBTB16*, an AR–inducible gene that negatively regulates AR. Alterations in the PI3 kinase pathway that are enriched in advanced CRPC have also been shown to modulate AR signaling. Nonetheless, there is increasing concern regarding the emergence of AR–independent pathways in CRPC patients that have the poorest prognosis. One such pathway arises from 'lineage plasticity', a transdifferentiation phenomenon that, in the context of prostate adenocarcinoma, refers to the loss of typical luminal features, accounting for ~20% of secondary resistance. Notably, these tumors are enriched for *TP53* and *RB1* co–deletions that evolve clonally during transdifferentiation. An extreme form of lineage plasticity is the transformation of prostate adenocarcinoma into a neuroendocrine cancer, importantly, with AR loss. Similar biologic processes are noted in *EGFR* mutated non–small cell lung cancers and *BRAF*–mutated melanomas.

There have been attempts to recapitulate the genomic and signaling alterations in both AR–driven and AR–independent CRPCs in cell lines and mouse models. For example, a random mutagenesis screen revealed a *de novo* AR(F877L) mutation in human prostate cancer cells, LNCaP, which were under selective pressure from enzalutamide. This promiscuous mutation caused enzalutamide to convert to an AR agonist. Furthermore, an AR bypass pathway dependent on glucocorticoid receptor signaling emerged in LREX cells, a clonal line derived from parent LNCaP–AR cells following long–term enzalutamide exposure. Interestingly, CHIP–seq on LREX cells revealed overlapping AR and GR cistromes. In the context of *TP53* and *RB1* co–deletions as a cause of secondary AR–independent resistance, shRNA–mediated knock down of both genes in LNCaP and CWR22Pc-EP cells triggered the transition from a luminal to a basal epithelial phenotype with AR loss. This was, in part, mediated through a 10– to 50–fold upregulation of the epigenetic reprogramming gene *SOX2*, with androgen sensitivity being restored partially upon *SOX2* inhibition. Lineage plasticity has similarly been observed in mutant mice lacking *Tp53*, *Rb1* and *Pten* [19]. Notably, a population of cells from these compound mutants display neuroendocrine features and increased *Sox2* and *Ezh2* expression. Our data also show that organoids derived from $Tp53^{fl/fl}/Rb1^{fl/fl}$ mice lose their luminal features after ~4 weeks of lentiviral–*Cre* transduction, and that this transdifferentiation is accelerated with enzalutamide. Despite these functional studies, and substantial efforts at delineating genomic and transcriptomic landscapes for patients with advanced CRPC, we still lack robust drug–able targets to counter the resistance to second–generation AR–directed therapies.

Here, we present a unique platform whereby we will leverage whole body molecular imaging to prospectively guide the acquisition of AR–positive and AR–negative CRPC biopsies, which will be subjected to single cell transcriptomic analyses and organoid–based functional assays. Indeed, it is now possible to determine radiographically AR expression in metastases using highly specific radiotracer probes for imaging. As expected, patients who are strongly avid for the uptake of ^{18}F–dihydrotestosterone (F-DHT) and ^{68}Ga–prostate–specific membrane antigen (PSMA) are mostly AR–driven, while F-DHT– and PSMA–negative tumors are likely to be AR–independent. Our **hypothesis** is that there are unique transcriptomic signatures, genes and pathways in residual metastatic cancer cell populations in CRPC patients, and that functional studies with patient–derived organoids will identify those that are actionable. Our overall **goal** is therefore to utilize our **imaging–sequencing–organoid** platform towards two Specific Aims.

Specific Aim 1: To identify potentially actionable target genes in CRPC metastases utilizing molecular imaging to guide biopsies for single cell transcriptomic analyses.

Specific Aim 2: To determine the function of the identified target genes through CRISPR knockdown and/or doxycycline–induced overexpression in patient–derived organoid lines.

2. KEYWORDS

Prostate cancer, single cell RNA sequencing, human tumors, patient derived organoids, CRISPR editing, secondary resistance

3. ACCOMPLISHMENTS

a. Research Specific Goals

	Months	MSKCC
SPECIFIC AIM 1: **To identify potentially actionable target genes in CRPC metastases utilizing molecular imaging to guide biopsies for single cell transcriptomic analyses.**		
Major Task 1: Collect metastatic prostate cancer biopsies for generation of single cell RNA–sequencing and patient–derived organoids.		
Subtask 1: Use advanced molecular imaging, namely ^{68}Ga-PSMA and ^{18}F-DHT PET imaging to guide biopsies. Number of human biopsies: 20 Protocols: Biopsies and advanced imaging performed under approved IRB 12–245 and 06-107, and 16-306 and 00-095, respectively.	1–24	80%
Subtask 2: Digest tumors into a single cell suspension in preparation for single cell RNA–sequencing and organoid generation. Number of human biopsies: 20 [example HMP04 in Project Narrative] Method(s): Collagenase, trypsin, and FACS–sorted live cells are prepared. Single cell sequencing using 10X Chromium Kit. Organoids seeded in matrigel with adaptive media conditions.	1–24	80%
Milestone(s) Achieved: Generation on an ongoing basis of high–quality single cell RNA–sequencing data and matched patient-derived organoids.	1–24	80%
Major Task 2: Analyze single cell RNA–sequencing data using complex bioinformatic pipelines.		
Subtask 1: Process single cell RNA–sequencing data for identification of candidate genes Number of scRNA-seq files: 20 Methods: Pre-processing using SEQC, visualization of data, graph–based subpopulation clustering, trajectory inference, and identification of differentially expressed genes [refer to 'Project Narrative'].	1–24	80%
Milestone(s) Achieved: *Identification of candidate genes.*	1–24	80%
SPECIFIC AIM 2: **To determine the function of the identified target genes through CRISPR knockdown and/or doxycycline–induced overexpression in patient–derived organoid lines.**		
Major Task 3: Perform CRISPR knockdown or doxycycline inducible overexpression of candidate genes in organoid models.		
Subtask 1: CRISPR knockdown of *HES6* and *MLLT11* in HMP–04, and *SERPINE2* and *SFRP1* in MSK-PCA3 organoids Lines: HMP-04 and MSK-PCA3 organoid lines.	1–3	0%

Method: Transduction of lentivirus–containing sgRNA and Cas9 at an MOI of 10^5. Confirmation of knockdown by Western blot.		
Subtask 2: CRISPR knockdown or doxycycline–inducible overexpression of newly–identified candidate genes by scRNA-sequencing. Lines: Matched patient–derived or patient–xenograft–derived organoid line. Method: CRISPR knockdown or doxycycline–inducible overexpression	4–24	100%
***Milestone(s) Achieved**: Successful knockdown or overexpression of candidate genes.*	1–24	50%
Major Task 4: Use functional assays to study the function of candidate genes in matched patient–derived or patient–xenograft derived organoids.		
Subtask 1: Immunohistochemistry of HES6 and MLLT11 for HMP04, and SERPINE2 and SFRP1 in MSK-PCA3. Lines: Non–targeted and mutant HMP04 and MSK-PCA3 organoids. Methods: Immunohistochemistry with HES6 (Abcam #218037), MLLT11 (Abcam #109016), SERPINE2 (Abcam #154591), and SFRP1 (Abcam #4193) antibodies	1–3	0%
Subtask 2: Hematoxylin and eosin staining, immunohistochemistry for luminal, basal, and neuroendocrine markers, and immunohistochemistry of other candidate genes in patient derived organoids. Lines: Matched non–targeted and mutant organoid line. Method: Hematoxylin and eosin staining, immunohistochemistry for CK5 (basal), CK8 (luminal), and SYP and CGA (neuroendocrine), and immunohistochemistry with antibody directed to candidate gene.	4–24	100%
Subtask 3: Enzalutamide–sensitivity after knockdown or overexpression of HES6 and MLLT11 in HMP04 and SERPINE2 and SFRP1 in MSK–PCA3. Line: Non–targeted and mutant HMP04 and MSK–PCA3 organoids (~5000). Method: Viability measured in triplicate by Cell Titer-Glo.	1–24	0%
Subtask 4: Enzalutamide–sensitivity after knockdown or overexpression of newly–identified candidate genes. Line: Matched non–targeted and mutant organoids (~5000). Method: Viability measured in triplicate by Cell Titer-Glo.	1–24	100%
Subtask 5: Orthotopically engraft non–targeted or mutant HMP04 and MSK–PCA3 organoids in SCID mice and measure tumor response to enzalutamide. Lines: 24 SCID mice [6 mice for 3 triplicates of non–targeted and mutant organoids x 4 genes]. IACUC 06-07-012. Method: Organoids will be marked with GFP and orthotopically engrafted into SCID mice. Treatment with enzalutamide or vehicle will be followed by tumor volume measurements.	1–11	0%
Subtask 6: Orthotopically engraft non–targeted or mutant organoids for newly identified select candidate genes in SCID mice and measure tumor response to enzalutamide.	12–24	50%

Lines: SCID mice [6 mice for 3 triplicates of non–targeted and mutant organoids x *N* genes]. *N* – will be determined based on scRNA–seq and *in vitro* data. Method: Organoids will be marked with GFP and orthotopically engrafted into SCID mice. Treatment with enzalutamide or vehicle will be followed by tumor volume measurements.		
Milestone(s) Achieved: Publication or submission of work to peer–reviewed journal	22–24	100%

b. What was accomplished under these goals?

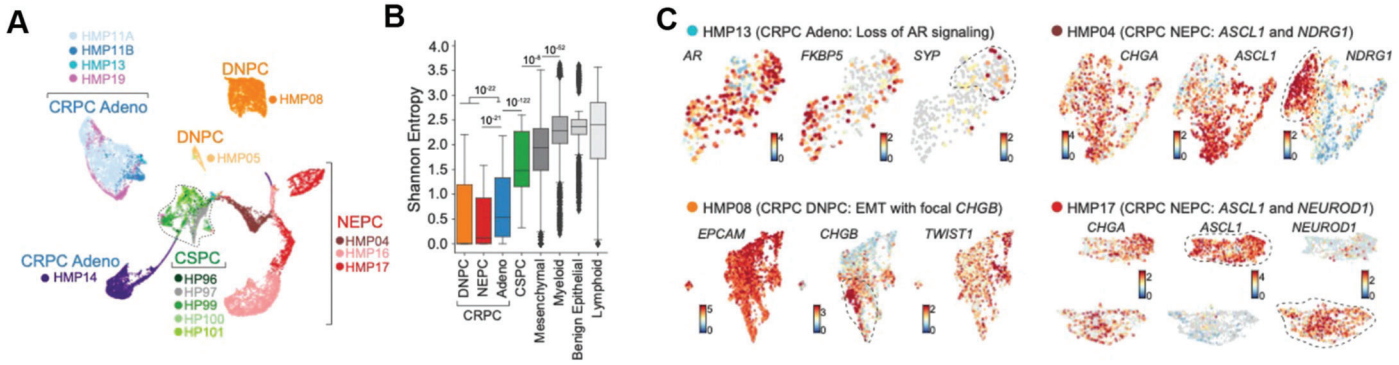

Figure 1: Candidate Gene and Program Identification By Human scRNA–Seq Of Prostate Tumors. We interrogated the complexity of prostate cancer by performing scRNA–seq analysis of sixteen human samples. Six patients had early–stage castration–sensitive prostate cancer (CSPC) and ten patients had late–stage metastatic castration–resistant prostate cancer (CRPC) representing three clinically recognized phenotypes: CRPC adenocarcinoma (AR+, SYP–); double negative prostate cancer (DNPC) (AR–, SYP–); and neuroendocrine prostate cancer (NEPC) (AR–, SYP+). All three CRPC phenotypes were enriched for alterations in *TP53*, *PTEN* and *RB1*. **(A)** Shown is UMAPs of tumor cells (N=29,373 cells), colored by tumor ID and grouped by tumor type. **(B)** Inter–patient heterogeneity measured by Shannon entropy based on tumor frequencies. To control for cell sampling, 100 cells were subsampled from each Phenograph cluster (*k*=30) within epithelial, immune, and mesenchymal compartments 100 times with replacement (Bonferroni–adjusted Student's t–test). **(C)** UMAPs of individual CRPC biopsies: HMP13 (N=354 cells, CRPC adeno), HMP08 (N=4,279 cells, DNPC), HMP04 (N=1791 cells, NEPC), and HMP17 (N=2,845 cells, NEPC). For each biopsy, cells are colored based on normalized expression (log_2X+1) for select genes demonstrating heterogenous and divergent intra–tumoral molecular resistance programs.

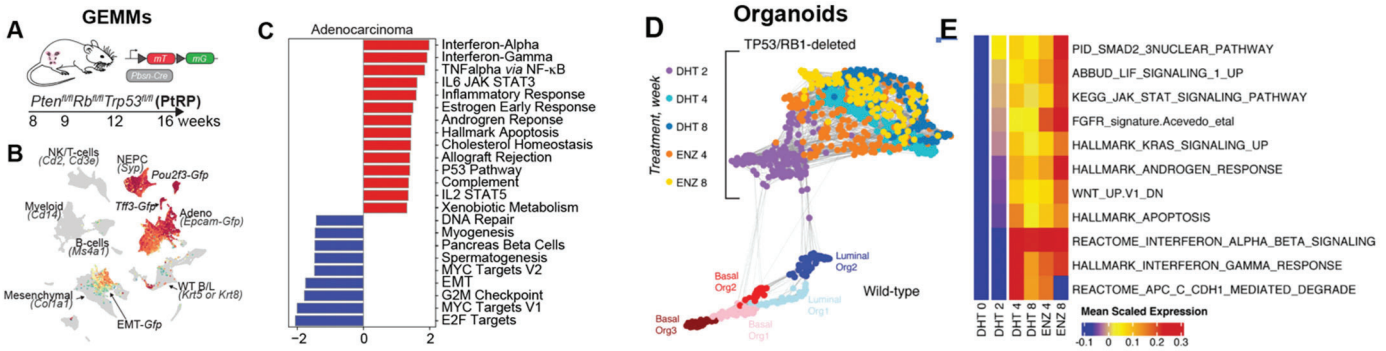

Figure 2: Upregulation of JAK/STAT and FGFR Signaling as a Function of Plasticity. To delineate the molecular programs involved in the progression of lineage plasticity after *Tp53* and *Rb1* deletion, we performed single cell RNA–sequencing (scRNA–seq) in both GEMM (*Tp53*$^{fl/fl}$;*Rb1* $^{fl/fl}$;*Pten*$^{fl/fl}$ mice) and *Tp53*/*Rb1*–deleted organoids. In GEMM plastic and stem–like adenocarcinoma cells, JAK/STAT and interferon–α/γ expression programs were significantly up–regulated. **(A)** Shown is data from 9 wild type mice and 13 GEMM mice at labelled time points. **(B)** UMAP of GEMMs (*N*=67,622 cells) shown for all cell types based on imputed *Gfp* expression as a marker for mutant cells. **(C)** Enriched signaling pathways using GSEA in plastic adenocarcinoma cells highlighting inflammation and JAK/STAT pathways (scale -2.5 to 2, normalized enrichment score, *P*<0.05). To determine whether a similar plasticity phenotype can be propagated *ex vivo,* we transduced *Cre*–expressing lentivirus in *Tp53*$^{fl/fl}$/*Rb1*$^{fl/fl}$ murine prostate organoids. In this reductionist system, we observed a gradual loss of cystic morphology and luminal markers by 4 weeks (hyperplastic) with the gain of migratory neural protrusions by ~8–10 weeks (referred to as 'slithering'). Organoids at 4 and 8

weeks showed a gain of mesenchymal markers, such as *Snai1, Zeb2,* and *Vim.* Strikingly, by performing scRNA–seq, we quantified tumoral plasticity (entropy based) and noted that JAK/STAT was the top correlated genetic program. **(D)** Shown above is a force directed layout (FDL) of *Tp53/Rb1*–deleted single cells from organoids colored by treatment (dihydrotestosterone, DHT; enzalutamide, ENZ) and timepoint (wildtype or 2–, 4–, and 8–weeks post–deletion). Wild-type cells are grouped into Basal Org 1–3 and Luminal Org 1–2 based on Phenograph clusters and canonical basal and luminal markers. **(E)** Heatmap of pathways most highly correlated with a measure of plasticity (entropy based) across timepoints. Each pathway is measured as the average Z–score of gene expression. Moreover, as our organoid media lacked serum, we reasoned that JAK/STAT maybe activated by other highly correlated ligand–receptor pairs. This analysis identified FGF1/FGFR, where the addition of the FGF1 ligand enhanced slithering in our organoid system.

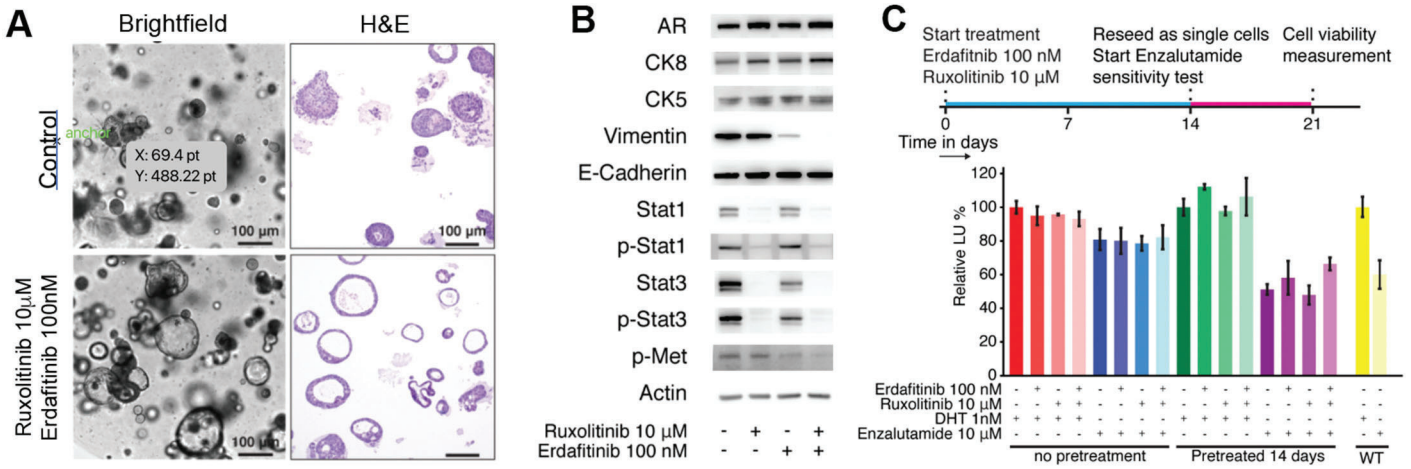

Figure 3: Reversal of Plasticity and Restoration of ARSI Sensitivity by Co–Inhibition of JAK and FGFR. As JAK/FGFR were upregulated after *Tp53*/*Rb1* deletion, we perturbed these pathways using a combination of genetic and pharmacologic approaches. CRISPR knockout or pharmacologic inhibition by ruxolitinib of JAK1/JAK2 reversed organoid phenotype from hyperplastic to cystic (from ~5% to 20%). Combinatorial treatment with ruxolitinib and the pan–FGFR inhibitor erdafitinib led to strikingly enhanced cystic reversion up to 60% and a dose–dependent increase in AR expression. **(A)** Shown are representative bright field micrographs and H&E staining for *Tp53/Rb1*–deleted organoids with CRISPR knockout of *Jak1/Jak2* or after 14 days exposure to DMSO or ruxolitinib (10μM) and/or erdafitinib (100 nM) (scale bar: 100 μm). **(B)** Western blots showing the effect of dual inhibition with ruxolitinib and erdafitinib for 14 days. Notable is the loss of VIM, a mesenchymal marker, and increased CK8 and AR expression. We next asked whether dual inhibition resulted in a re–sensitization to ARSIs. Of note is that ruxolitinib and/or erdafitinib did not display anti–proliferative effect; instead, there was a prominent effect in restoring cystic morphology. **(C)** Importantly, however, in the reprogramed organoids, enzalutamide (10 μM) reduced proliferation by 50%—this effect magnitude was strikingly comparable to the anti–proliferative effect of enzalutamide on untreated wild–type ARSI–sensitive organoids (10,000 cells *per* well in triplicate; viability by CellTiterGlo after 7 days treatment).

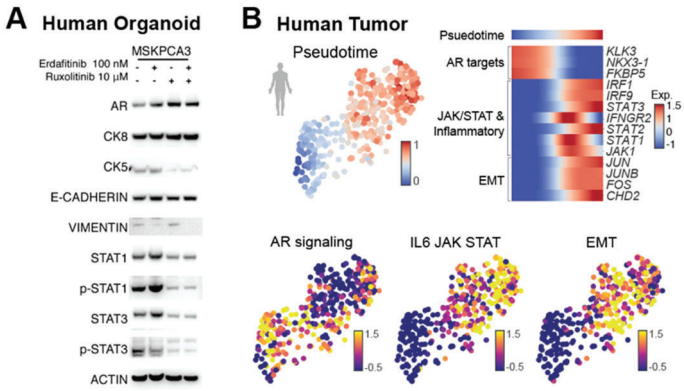

Figure 4: Validation of JAK/STAT and FGFR in Human Tumors. To extend our findings to human prostate tumors, we selected a set of three *TP53* and *RB1* null tumor–derived organoids. **(A)** One organoid line, MSK–PCA3, which retained a low level of AR, when exposed to ruxolitinib (10 μM) and erdafitinib (100 nM) for 14 days underwent reprogramming towards a luminal lineage (high AR and CK8, Western blot) and away from a mesenchymal lineage (reduced VIM), with a modest (20%) re–sensitization to enzalutamide. The other two lines, MSK–PCA1 and MSK–PCA6, were devoid of AR, fully transformed to small cell prostate cancer lines, and did not respond ruxolitinib and erdafitinib (not shown). These results, in combination with our GEMM data (Figure 2, above), establish a requirement for low levels of AR expression for JAK/STAT and FGFR mediated reprogramming. Furthermore, based on ATAC profiles, MSK–PCA3 has been allocated to the stem–like and inflammatory group of resistant prostate cancer, which may be uniquely susceptible to JAK/STAT and FGFR

reprogramming. **(B)** Our scRNA–seq data in a human tumor sample shows that low AR expression and high EMT markers correlate with JAK/STAT signaling. Shown above is a UMAP of a heavily–treated, resistant human tumor (*N*=353 cells) colored by pseudotime from cells with high to low AR signaling (top left). Heatmaps show gene trends for select DEGs (right; scale -1 to 1.5) (top right). Also shown is AR signature score or *Z*–score of leading edge of enriched GSEA terms IL6–JAK–STAT or EMT (scale, -0.5 to 1.5) (bottom).

c. What opportunities for training and professional development has the project provided?

Training:
Art of Flow Sorting, MSKCC
Mouse Training and Xenografts, MSKCC

Professional Development:
Invited Talk, Human Oncology Pathogenesis Program, MSKCC, 2020
Invited Talk, Drug Resistance and Sensitivity (DRSN Moonshot) Meeting, Cancer Moonshot Initiative
American Association for Cancer Research, 2022 (Abstract Submitted)
Presentation at lab meetings every other month

d. How were the results disseminated to communities of interest?

Manuscripts describing our analysis of human scRNA–seq and the identified candidate genes and programs involved in enzalutamide resistance were released as pre–prints on ***bioRxiv*** (below and in appendices). The manuscripts are *in review* at ***Science***.

1. **Zaidi S**[φ], Zhao JL[φ], Chan JM[φ], Roudier MP, Wadosky M, Gopalan A, Karthaus WR, Choi J, Lawrence K, Chaudhary O, Xu T, Masilionis I, Mazutis L, Chaligne R, Nawy T, Linkov I, Barlas A, Jungbluth A, Rekhtman N, Silber J, Manova-Todorova K, Watson PA, True LD, Nelson PS, Scher HI, Rathkopf DE, Morris MJ, Haffner MC, Goodrich DW, Pe'er D, Sawyers CL. (2021) Multilineage plasticity in prostate cancer through expansion of stem-like luminal epithelial cells with elevated inflammatory signaling. ***bioRxiv.*** 2021.11.01.466599. Accessed November 13, 2021. https://doi.org/10.1101/2021.11.01.466599. (Under review in ***Science***). ([φ]**Joint first authors**)

2. Karthaus WR.[φ], Chan J[φ], Setty M[φφ], Love JR[φφ], **Zaidi S**, Choo Z, Persad S, LaClair J, Lawrence KE, Chaudhary O, Xu T, Masilionis I, Mazutis L, Chaligne R, Pe'er D, Sawyers CL. (2021). Reversal of lineage plasticity in RB1/TP53–deleted prostate cancer through FGFR and Janus kinase inhibition. ***bioRxiv***. 2021.11.01.466615. Accessed November 13, 2021. https://doi.org/10.1101/2021.11.01.466615. (Under review in ***Science***). ([φ]Joint first authors or [φφ]equal contribution)

e. What do you plan to do during the next reporting period to accomplish the goals?

Towards **Specific Aim 1**, we have obtained additional human metastatic samples to complete the proposed sequencing of 20 biopsies. The aggregate data will lead to the identification of additional candidate genes and programs that may be mediating enzalutamide resistance. In addition, we will probe the tumor microenvironment to see whether there are novel candidates that mediate of resistance from either the stromal or immune compartments. We have also optimized the protocol to process bone metastases.

Towards **Specific Aim 2**, we will focus on performing *in vitro* and *in vivo* studies to characterize the role of *HES6, MLLT11, SERPINE2* and *SFRP1* in enzalutamide resistance as outlined in our original proposal. We will also characterize the *in vivo* effects of our discovery of JAK/STAT and FGFR inhibition (refer to data in 'Accomplishments', Figures 2 to 4) on *in vivo* orthotopic models of enzalutamide resistance. Based on in–depth and robust systems and models we have generated, we believe the remainder of these studies are achievable within the final year of this grant.

4. IMPACT

a. What was the impact on the development of the principal discipline(s) of the project?
Our studies are highly impactful as, for the first time, as we have identified novel JAK/STAT and FGFR pathways that interact to underpin lineage plasticity and AR–insensitivity in both murine and human tumors. Further *in vivo* studies, which are ongoing in the next reporting period, should help validate JAK/STAT and FGFR as targets for triple combinatorial therapy using currently FDA–approved agents, namely ruxolitinib, erdafitinib, and ARSI. The significance of these findings to treating resistant disease, without the need to develop a new therapeutic, could be of great benefit to our patients. Furthermore, we are continuing to grow our bank of human prostate tumors that have undergone scRNA–sequencing with an aim to elucidate meaningful targets and further inform non–tumor intrinsic mechanisms of resistance. Lastly, while we have focused on the JAK/STAT and FGFR pathway in Specific Aim 2 given its immediate therapeutic implications, in the next reporting period, we will also characterize the functional significance of *HES6* and *MLLT11* for HMP04, and *SERPINE2* and *SFRP1* in MSK-PCA3 in ARSI resistance.

b. What was the impact on other disciplines?
While these findings have clear mechanistic and therapeutic implications on prostate cancer progression and ARSI resistance, there is likely conservation of the plasticity program and its components in *EGFR*– and *KRAS*– mutant lung cancers, which also develop with *TP53* and *RB1* alterations, and, when exposed to next generation inhibitors transform in small cell lung cancer.

c. What was the impact of technology transfer?
Nothing to report

d. What was the impact on society beyond science and technology?
Our work is ultimately focused on improving patient care. We are hopeful these findings, particularly the potential for triple therapy using JAK/STAT, FGFR and AR directed agents, will translate into the clinic and benefit both patient survival and quality of life.

5. CHANGES/PROBLEMS

a. Changes in approach and reasons for change
As noted above, we discovered in our expanded cohort of human scRNA–seq data, that JAK/STAT signaling was upregulated in patient samples that underwent lineage plasticity. We also have strikingly noted a similar up–regulation of JAK/STAT (and FGFR) signaling pathway(s) in complementary models—namely, *Tp53, Rb1,* and/or *Pten* deleted GEMMs and organoid models. Given the consistency and therapeutic import of these observations, we expanded our focus to study this pathway and established additive effects in restoring ARSI sensitivity of co–inhibiting *Jak1/2* and *Fgfr,* both genetically and pharmacologically. During the next reporting period, we will focus on the relative contributions of *HES6*, *MLLT11, SERPINE2,* and *SFRP1* as additional modulators of enzalutamide resistance.

b. Actual or anticipated problems or delays and actions or plans to resolve them
Nothing to report

c. Changes that had a significant impact on expenditures
Nothing to report

d. Significant changes in use of human subjects, vertebrate animals, biohazards, and/or select agents?
Nothing to report

e. Significant changes in use or care of human subjects
Nothing to report

f. Significant changes in use or care of vertebrate animals.
Nothing to report

6. PRODUCTS

Publications, conference papers, and presentations:

Journal publications:

Two manuscripts (shown below) pertaining to this work have been released in bioRxiv and are under review at *Science*.

Zaidi S[φ], Zhao JL[φ], Chan JM[φ], Roudier MP, Wadosky M, Gopalan A, Karthaus WR, Choi J, Lawrence K, Chaudhary O, Xu T, Masilionis I, Mazutis L, Chaligne R, Nawy T, Linkov I, Barlas A, Jungbluth A, Rekhtman N, Silber J, Manova-Todorova K, Watson PA, True LD, Nelson PS, Scher HI, Rathkopf DE, Morris MJ, Haffner MC, Goodrich DW, Pe'er D, Sawyers CL. (2021) Multilineage plasticity in prostate cancer through expansion of stem-like luminal epithelial cells with elevated inflammatory signaling. ***bioRxiv.*** 2021.11.01.466599. Accessed November 13, 2021. https://doi.org/10.1101/2021.11.01.466599. (Under review in ***Science***). ([φ]**Joint first authors**)

Karthaus WR.[φ], Chan J[φ], Setty M[φφ], Love JR[φφ], **Zaidi S**, Choo Z, Persad S, LaClair J, Lawrence KE, Chaudhary O, Xu T, Masilionis I, Mazutis L, Chaligne R, Pe'er D, Sawyers CL. (2021). Reversal of lineage plasticity in RB1/TP53–deleted prostate cancer through FGFR and Janus kinase inhibition. ***bioRxiv***. 2021.11.01.466615. Accessed November 13, 2021. https://doi.org/10.1101/2021.11.01.466615. (Under review in ***Science***). ([φ]Joint first authors or [φφ] equal contribution)

Other publications include:

Bellone S, Roque DM, Siegel ER, Buza N, Hui P, Bonazzoli E, Guglielmi A, Zammataro L, Nagarkatti N, **Zaidi S**, Lee J, Silasi DA, Huang GS, Andikyan V, Damast S, Clark M, Azodi M, Schwartz PE, Tymon-Rosario JR, Harold JA, Mauricio D, Zeybek B, Menderes G, Altwerger G, Ratner E, Alexandrov LB, Iwasaki A, Kong Y, Song E, Dong W, Elvin JA, Choi J, Santin AD. A phase 2 evaluation of pembrolizumab for recurrent Lynch-like versus sporadic endometrial cancers with microsatellite instability. ***Cancer***. (2021) Dec 7. doi: 10.1002/cncr.34025. Epub ahead of print. PMID: 34875107.

Miyahira AK, Zarif J, Coombs C, Flavell RR, Ruso JW, **Zaidi S**, Zhao D, Zhao SG, Pienta KJ, Soule HR. (2021) Prostate cancer research in the 21st century: report from the 2021 Coffey-Holden Prostate Cancer Academy Meeting. ***Prostate.*** (2021). Nov 3. doi: 10.1002/pros.24262. PMID: 34734426.

Choi J, Manzano A, Dong W, Bellone S, Bonazzoli E, Zammataro L, Yao X, Deshpande A, **Zaidi S,** Guglielmi A, Gnutti B, Nagarkatti N, Tymon-Rosario JR, Harold J, Mauricio D, Zeybek B, Menderes G, Altwerger G, Jeong K, Zhao S, Buza N, Hui P, Ravaggi A, Bignotti E, Romani C, Todeschini P, Zanotti L, Odicino F, Pecorelli S, Ardighieri L, Bilguvar K, Quick CM, Silasi DA, Huang GS, Andikyan V, Clark M, Ratner E, Azodi M, Imielinski M, Schwartz PE, Alexandrov LB, Lifton RP, Schlessinger J, Santin AD. (2021) Integrated mutational landscape analysis of uterine leiomyosarcomas. ***Proceedings of the National Academy of Sciences*** 118(15):e2025182118. doi: 10.1073/pnas.2025182118. PMID: 33876771; PMCID: PMC8053980.

Books or other non-periodical, one–time publications.
Nothing to report

Other publications, conference papers, and presentations.
Invited Talk, Drug Resistance and Sensitivity (DRSN Moonshot) Meeting, Cancer Moonshot Initiative (11/18/2021).

Website or other internet sites
Nothing to report

Technologies or techniques
Nothing to report

Inventions, patent applications and/or licenses
Nothing to report

Other Products
Data: N/A
Research material: N/A

7. PARTICIPANTS AND OTHER COLLABORATING ORGANIZATION

What individuals have worked on the project?

Samir Zaidi (Principal Investigator, 10.8 months)
Joe Chan (Post–doctoral fellow in Dr. Pe'er laboratory, 0.96 months)
Wouter Karthaus (Post–doctoral fellow in Dr. Sawyers laboratory, 0.96 months)
Jimmy Zhao (Post–doctoral fellow in Dr. Sawyers laboratory, 0.96 months)

Has there been a change in the active other support of the PD/PI(s) or senior/key personnel since the last reporting period?
Yes. Samir Zaidi (PI) and Charles Sawyers (Mentor). Please see their other supports attached.

What other organizations were involved as partners?
Not applicable

8. SPECIAL REPORT REQUIREMENT

COLLABORATIVE AWARDS:
Not applicable

QUAD CHARTS:
Not applicable

9. APPENDICES

We have attached two bioRxiv pre–prints describing our human single cells efforts and identification of plasticity dependence of interferon-α/γ and JAK/STAT pathways (Zaidi *et al.* and Karthaus *et al.*, BioRxiv, 2021)

PREVIOUS/CURRENT/PENDING SUPPORT

Zaidi, Samir

CURRENT SUPPORT

2020YI2880 (PI: Zaidi) 09/01/2020–08/31/2023 0.00* calendar months
Prostate Cancer Foundation (PCF)
Title: Studying the Mechanisms of Lineage Plasticity in Prostate Cancer
Major Goal: Our overall goal is to delineate, both through the use of novel human systems and previously identified functional candidates, mechanisms of lineage plasticity that are downstream of, or parallel to, TP53 and RB1.
Aim 1: Identify changes in transcriptional factor and gene programs in a wild–type human organoid model deleted for *TP53* and *RB1* over a time course
Aim 2: Characterize *Runx2* and *Barx2*, identified through single cell RNA–sequencing, in a genetically modified mouse model (GEMM) conditionally deleted for *Tp53*, *Rb1* and *Pten*.
Role: Principal Investigator [Mentor: Charles Sawyers, MD]
Overlap: None
*Effort not required by the sponsor.

PC200086 (PI: Zaidi) 1/1/2021–12/31/2022 10.80 calendar months
Department of Defense (DOD), Prostate Cancer Research Program:
Title: Understanding Molecular Mechanisms of Secondary Resistance in Patients with Metastatic Castrate Resistant Prostate Cancer
Major Goal: This proposal will characterize novel molecular signatures in metastases from CRPC patients with an overarching goal to identify potentially actionable targets.
Aim 1: To identify potentially actionable target genes in CRPC metastases utilizing molecular imaging to guide biopsies for single cell transcriptomic analyses.
Aim 2: To determine the function of the identified target genes through CRISPR knockdown and/or doxycycline–induced overexpression in patient–derived tumor organoid lines.
Role: Principal Investigator [Mentor: Charles Sawyers, MD]
Overlap: N/A.

GC260796 (PI: Zaidi) 7/1/2021–6/30/2022 0.00* calendar months
Conquer Cancer Foundation of the American:
American Society of Clinical Oncology
Title: Systemic Investigation of Mouse Derived Organoids Undergoing Lineage Plasticity with Human PDX Validation
Major Goal: This study is on mechanistic detail using organoids derived from a mouse model of prostate cancer to validate these findings, particularly the interferon signaling pathway and copy number instability, in human xenografts.
Aim 1: Investigate evolving transcription factor changes using *mouse* prostate organoids deleted for *Tp53/Rb1* using single cell ATAC- and RNA-sequencing.
Aim 2: Explore the role of interferon signaling and copy number instability in organoids from patient-derived xenografts displaying loss of *TP53/RB1*.
Role: Principal Investigator [Mentor: Charles Sawyers, MD]
Overlap: N/A
*Effort not required by the sponsor.

PREVIOUS SUPPORT

5F30HL123238-02 (Trainee: Zaidi) 12/01/2014–05/31/2016 12.00 calendar months
NHLBI
Title: Genomic and Functional Architecture of Congenital Heart Disease (CHD)
Major Goals: This F30 is to support pre–doctoral research into the genetic architecture of CHD by whole exome sequencing.
Role: Trainee [Mentor: Richard Lifton, MD, PhD]
Overlap: N/A

2 T32 CA009207-41 (Bajorin/Wolchok) 08/01/1977–08/31/2024 12.00 calendar months
NCI
Title: T32 Investigational Cancer Therapeutics Training Program (ICTTP), Memorial Sloan Kettering Cancer Center (MSKCC)
Major Goals: This is a T32 grant awarded to highly select physician trainees in hematology and medical oncology at MSKCC with the research training necessary for successful careers in the translation of cancer biology discoveries into novel molecular, immune, or cell-based therapeutics, and those experimental treatments.
Role: Trainee (appointment: 9/1/2019-12/31/2020)
Overlap: Support from the T32 will end prior to the start date of the DoD grant.

PENDING SUPPORT

None

Previous/Current/Pending Support

Sawyers, Charles L.

PREVIOUS SUPPORT

5 R01 CA155169-05 (PI: Sawyers) 5/1/12-3/31/17 2.40 calendar
NCI/NIH
Understanding Resistance to Next Generation Antiandrogens
Specific Aims: To explore the molecular basis by which GR selectively activates certain AR target genes (Aim 1), the functional role of GR, AR and the GR/AR target gene SGK1 in maintaining drug resistance (Aim 2), and the clinical relevance of these findings in circulating tumor cells obtained from patients at treatment start and at relapse (Aim 3).
Agency Contact: Grants Management Specialist: Renee Carruthers, carruthersr@mail.nih.gov, Phone: 301-496-9310, Fax: 301-451-5391
Overlap: None

W81XWH-15-1-0274 (PI: Mu) 8/1/2015 - 7/31/2017 0.12 calendar
Congressionally Directed Medical Research Prgms
Identifying biomarkers of antiandrogen resistance: An shRNA-based in vivo screening approach
We aim to elucidate mechanism of RB1 and TP53 associated antiandrogen resistance in both in vitro and in vivo contexts.
Specific Aims: (1) To investigate the underlying mechanisms of enzalutamide resistance caused by disruption ofRB1 and TP53 pathways and determine potential therapeutic targets and clinical relevance. **(2)** To perform an shRNA-based *in vivo* screen of the prostate cancer deletome to identify the biomarker genes that confer resistance to enzalutamide.
Agency Contact: Janet Kuhns, Tel: 301-619-2827, email: janet.p.kuhns.civ@mail.mil
Overlap: None

W81XWH-15-1-0276 (PI: Wise) 8/1/2015 - 7/31/2017 0.12 calendar
Congressionally Directed Medical Research Prgms
Identifying androgen receptor-independent mechanisms of prostate cancer resistance to second generation anti-androgen therapy
Major Goals: This project will focus on identifying androgen receptor-independent mechanisms of prostate cancer resistance to second generation anti-androgen therapy.
Agency Contact: Janet Kuhns, Tel: 301-619-282, email: janet.p.kuhns.civ@mail.mil
Overlap: None

3 P30 CA008748-52 S1 (PI: Thompson/Sawyers) 1/1/2017 - 12/31/2018 0.12 calendar
NCI
Cancer Center Support Grant
DNA sequencing of tumors provides remarkable clarity and precision to the diagnosis of many cancers, resulting in better treatment outcomes. For more patients to benefit from this technology, it is important for sequencing data to be shared across cancer centers to accelerate progress. This supplement will support the sharing of these data through a consortium of cancer centers called AACR Project GENIE.
Agency Contact: Funmi Elesinmogun, Email: elesinmf@mail.nih.gov, Phone: (240) 276-6313
Overlap: None

I10-0062 (PI: Sawyers) 1/1/2017 - 12/31/2018 0.60 calendar
Starr Cancer Consortium
Transcriptional Reprogramming Drives Cancer Cell Heterogeneity and Drug Resistance

To elucidate the transcriptional regulators of lineage plasticity across a broader range of molecular contexts of tumor suppressor loss of function (PTEN, RB1)
Major Goals: To elucidate the transcriptional regulators of lineage plasticity across a broader range of molecular contexts of tumor suppressor loss of function (PTEN, RB1)
Specific Aims: Aim 1. Define the transcriptional changes associated with lineage plasticity driven by SOX2 and SATB2 in prostate cancer and melanoma, in mammalian and zebrafish models **Aim 2.** Define the chromatin alterations (new enhancers) responsible for the common transcriptional changes associated with lineage plasticity driven by SOX2 and SATB2 **Aim 3.** To elucidate the transcriptional regulators of lineage plasticity across a broader range of molecular contexts of tumor suppressor loss of function (PTEN, RB1)
Agency Contact: Sylvie Le Blancq, Email: leblancs@mskcc.org
Overlap: None

1 U54 CA224079-02 S1 (PI: Sawyers) 9/30/2017 – 8/31/2019 0.00 calendar
National Cancer Institute
The MSKCC-UW/Fred Hutch Prostate Cancer Drug Resistance and Sensitivity
The research in this grant aims to use a collection of patient-derived prostate cancer models to test resistance and sensitivity to novel drugs and therapeutic combinations quickly and efficiently. This supplement will support a collaboration to use related approaches in mouse models of prostate cancer to corroborate our findings and gain insight into mechanisms of drug response.

3 P30 CA008748 52 S2 (PI: Thompson) 1/1/2014 - 12/31/2019 0.00 calendar
NCI
Cancer Center Support Grant
We propose to establish a two-year Science Enrichment Program (SEP) at Memorial Sloan Kettering Cancer Center (MSK) for high school students who don't have easy access to resources that would help to develop their scientific curiosity.
Agency Contact: Funmi Elesinmogun, Email: elesinmf@mail.nih.gov, Phone: (240) 276-6313
Role: Program Director

I12 0007 (PI: Sawyers) 1/1/2019 - 12/31/2020 0.36 calendar
Starr Cancer Consortium
Defining prostate cancer cells of origin through single cell profiling
This proposal fits the RFA category of "Disease Applications" because it applies the relatively new molecular technology of single cell RNA sequencing (scRNA seq) to the study of prostate cancer.
Agency Contact: Sylvie Le Blancq, Email: leblancs@mskcc.org
Overlap: None

5 R01 CA193837-05 (PI: Sawyers) 4/1/2015-1/31/2020 1.90 calendar
NCI
Defining the Role of ERG in Modulating the AR Cistrome and Antiandrogen Sensitivity
Major Goals: This project will shed light on the molecular mechanism by which ERG causes prostate cancer and the impact of ERG on response to therapies directed against the androgen receptor, the common form of treatment for metastatic prostate cancer.
Specific Aims: Aim 1. Decipher the mechanism of ERG-mediated reprogramming of the AR cistrome
Aim 2. Understand the role of PTEN loss in modulating the ERG transcriptome.
Aim 3. Determine the role of ERG expression in sensitivity to AR and PI3K inhibition.
Agency Contact: Funmi Elesinmogun, Email: elesinmf@mail.nih.gov, Phone: (240) 276-6313
Overlap: None

1 P01 CA228696 02 (PI: Kantoff/ Sawyers) 9/1/2019 - 8/31/2024* 0.60 calendar
NCI

The Impact of DNA Damage Repair Abnormalities in Prostate Cancer (RP3: Functional Evaluation and Interpretation of DNA Damage Response Variants in Prostate Cancer)
Alterations in genes that help repair damaged DNA are seen in 25% of men with metastatic castration resistant prostate cancer, the lethal form of prostate cancer.
Role: Project Leader
Agency Contact: Kelly Filipski, Kelly.Filipski@nih.giv
Overlap: None
*Dr. Sawyers was replaced as Project Leader on this award as of 8/31/2021. Dr. Sawyers therefore committed no effort past 8/31/2021.

CURRENT SUPPORT

Howard Hughes Medical Institute (PI: Sawyers) 3/1/2008- 8/31/2025
Major Goals of this project: Patient oriented research into molecularly targeted therapy of cancer
Agency Contact: Edit Biro, MAS, Howard Hughes Medical Institute, 1230 York Ave, Box 269, New York, NY 10065
Overlap: None

2 R01 CA155169-10 (PI: Sawyers) 5/1/2012-12/31/2022 1.81 calendar
NCI/NIH
Understanding Resistance to Next Generation Antiandrogens
Major Goals: This project focuses on a novel mechanism of acquired resistance to hormone therapy in castration resistant prostate cancer (CRPC) called lineage plasticity. During the initial 5 year funding cycle, we focused primarily on two other mechanisms of resistance: mutation or amplification of the androgen receptor (AR) and bypass of AR signaling through upregulation of the closely related glucocorticoid receptor.
Agency Contact: Grants Management Specialist: Rogers Gross, (240) 276-7589, rogers.gross@nih.gov
Overlap: None

5 R01 CA193837-06 (PI: Sawyers) 2/9/2021-1/31/2026 1.80 calendar

NCI
Role of ETS factors in specifying prostate luminal cell identity and androgen receptor dependence
Major Goals: In this proposal, we investigate how mutations in ETS factors, clinically important oncogenic drivers of prostate cancer, promote luminal cell identity and regulate chromatin architecture of cancerous prostate tissues, including by co option of AR function.
Agency Contact: Funmi Elesinmogun, Email: elesinmf@mail.nih.gov, Phone: (240) 276-6313
Overlap: None

1 U54 CA224079-04 (PI: Sawyers) 9/1/2017-8/31/2022
NCI/NIH
The MSKCC-UW/Fred Hutch Prostate Cancer Drug Resistance and Sensitivity Center
- Admin Core (PI: Sawyers) 0.91 calendar
- Project 1 (PI: Sawyers) 0.91 calendar
- Project 2 (PI: Chen; Co-I: Sawyers) 0.46 calendar

Major Goals: 26,000 men die each year in the US from metastatic prostate cancer because the disease develops resistance to the primary treatment, called hormone therapy. DNA sequencing studies of tumors from these patients has revealed new strategies to treat prostate cancer with novel drugs in combination with hormone therapy. This application assembles a team of experts on this topic to work together to test these new therapies in laboratory models of prostate cancer developed directly from patients and identify those that should be accelerated into clinical development.
Agency Contact: Funmi Elesinmogun, Email: elesinmf@mail.nih.gov, Phone: (240) 276-6313
Overlap: None

3 U54 CA224079 04 S1 (PI: Sawyers/Nelson) 9/30/2020 - 8/31/2022 0.00 calendar*
NCI
Major Goals: The MSKCC UW/Fred Hutch Prostate Cancer Drug Resistance and Sensitivity Center (Supplement)
The overarching goal of this DRSC proposal is to evaluate translational therapies across a unique set of preclinical organoid and patient derived xenograft (PDX) models, and to catalyze the initiation of clinical studies in patients most likely to benefit based on appropriate biomarker profiles.
Agency Contact: Funmi Elesinmogun, Email: elesinmf@mail.nih.gov, Phone: (240) 276-6313
Overlap: None
*No effort required. The work for this supplement will take place at the partnering Site, Fred Hutch, under the direction of Dr. Peter Nelson.

2 P50 CA092629-19 (PI: Scher) 9/1/2016 – 8/31/2022
National Institutes of Health
MSKCC Spore in Prostate Cancer
- RP-3 (PI: Sawyers) 0.60 calendar
  Heterogeneity in metastatic CRPC and the role of TP53 mutation as a molecular determinant
- Core F (PI: Sawyers) 0.60 calendar
  Administrative Core

Major Goals of this Project: As a public health concern, prostate cancer is the second deadliest cancer in men. The translational research projects in this program aim to use knowledge of animal and human prostate cancer biology to develop and test interventions related to the prevention, early detection, diagnosis, prognosis, and treatment of prostate cancer in men.
This allocation is split between the following: Development Research Program; Core F, Administrative Core; Project 3, Heterogeneity in metastatic CRPC and the role of TP53 mutation as a molecular determinant; and Project 4, Investigating and targeting the glucocorticoid receptor (GR) in enzalutamide- and abiraterone.
Role: Core Co-Director of Core F, Co-Director of Development Research Program, Principal Investigator of Project 3 and Project 4.
Specific Aims of the Overall Grant:
1. To interrogate the genomics and molecular pathways relevant to prostate cancer progression
2. To improve prognostic models for early detection of potentially lethal cancers
3. To identify and validate clinically relevant biomarkers
4. To develop novel agents and therapeutic strategies
Agency Contact: Renee Carruthers, Email: carruthersr@mail.nih.gov Phone: 301-631-3018 Fax: 301-451-5391
Overlap: None

5 P30 CA008748-54 (PI: Thompson) 1/1/2014-12/31/2023 1.20 calendar
NCI
Cancer Center Support Grant (Cancer Biology and Experimental Pathology Program)
The CCSG funds support MSK's research infrastructure. These shared resources facilitate the research activities of the clinical, translational and laboratory programs at the Cancer Center.
Agency Contact: Funmi Elesinmogun, Email: elesinmf@mail.nih.gov, Phone: (240) 276-6313
Overlap: None

2 T32 CA160001-10 (PI: Sawyers) 8/1/2016 - 7/31/2022 (NCE) 0.00 calendar
NCI
Translational Research in Oncology Training Program
Major Goals: The training program for translational cancer research will provide opportunities to postdoctoral PhD trainees to learn about human oncology and pathogenesis, and work collaboratively with clinicians to advance the treatment of cancer patients. The goals are: to help basic scientists to develop a strong clinical

background so that they may effectively bring discoveries from bench to bedside; and to foster interdisciplinary research and collaboration.
Specific Aims: 1) To provide broad and intensive translational research training for PhDs by offering enhanced opportunities to orient their research to biomedically relevant problems. 2) To prepare Trainees to successfully collaborate during their career with researchers with different backgrounds. 3) To prepare and assist Trainees to successfully transition to research independence.
Agency Contact: Renee Carruthers, Email: carruthersr@mail.nih.gov, Phone: 301-631-3018, Fax: 301-451-5391
Overlap: None

W81XWH-20-1-028, PC190310 (PI: Sawyers) 9/30/2020 - 9/30/2023 0.60 calendar
Congressionally Directed Medical Research
Programs
Defining Transcription Factor Networks Governing Androgen Receptor Null Prostate Cancer
Major Goals: Aim 1. Determine gene expression and chromatin landscape changes associated with potent AR inhibition Aim 2. Identify vulnerabilities responsible for maintenance of the AR low/null state Aim 3. Characterize the AR low/null state in CRPC patients using single cell and organoid technologies
Role: Principal Investigator
Agency Contact: Joshua Mckean, Joshua.D.Mckean3.Civ@Mail.Mil
Overlap: None

GC260677 (PI: Leslie) 9/1/2020 - 8/30/2022 0.12 calendar
Geoffrey Beene Cancer Research Center
Epigenetic and transcriptional regulation in FOXA1 mutant prostate and breast cancer
Major Goals: The goal of this project is to elucidate the molecular details of how this co-option of pioneering TF activity occurs.
Aim 1. Characterize the epigenetic and transcriptional effects of mutant FOXA1 at a single cell level.
Aim 2. Decipher the motif grammar of mutant FOXA1 alleles through analysis of TF cistromes.
Role: Co-PI
Agency Contact: Vicky Baudin, baudinv@mskcc.org
Overlap: None

SK2020-1592 (PI: Sawyers) 12/1/2020 – 11/30/2023 0.00 calendar*

Calico Life Sciences
MSK - Calico Single Cell Collaboration
Major Goals: The MSK-Calico collaboration is centered around two initial research projects. Project 1 focuses on lineage plasticity in adenocarcinomas of the lung and prostate as a mechanism of acquired drug resistance. Project 2 focuses on the dynamics of tumor microenvironment change, including response to therapy and PTPN2 treatment, in prostate, lung, liver, pancreatic, and rectal cancers. The Sawyers lab will share relevant prostate cancer models and data to support the collaboration.
Role: Principal Investigator
Agency Contact: Bob Cohen, Calico Principal Investigator; rlc@calicolabs.com
Overlap: None
*No effort required by sponsor.

5 R25 CA057732-27 (PI: Sawyers) 07/11/2016 - 05/31/2021 0.50 calendar NIH/ NCI
Molecular Biology in Clinical Oncology Workshop
Major Goals: The workshop is primarily designed for oncologists in training at the fellow level. Space is also made available to a limited number of senior oncologists. The development and application of a range of cellular and molecular biological approaches to the study of gene structure and expression, cellular growth

control, and malignant transformation have resulted in remarkable advances in the diagnosis, treatment, and prevention of cancer.
Agency Contact: Jeannette F Korczak, korczakj@mail.nih.gov
Overlap: None

(This Award)
PC200086 (PI: Zaidi) 9/30/2021–9/29/2023 0.00 calendar months
Department of Defense (DOD), Prostate Cancer Research Program:
Title: Understanding Molecular Mechanisms of Secondary Resistance in Patients with Metastatic Castrate Resistant Prostate Cancer
Major Goal: This proposal will characterize novel molecular signatures in metastases from CRPC patients with an overarching goal to identify potentially actionable targets.
Aim 1: To identify potentially actionable target genes in CRPC metastases utilizing molecular imaging to guide biopsies for single cell transcriptomic analyses.
Aim 2: To determine the function of the identified target genes through CRISPR knockdown and/or doxycycline–induced overexpression in patient–derived organoid lines.
Role: Mentor
Overlap: N/A

PENDING SUPPORT

P01 (PI: Shen, Columbia University) 9/1/2021 - 8/31/2026 1.80 calendar
Columbia University
Investigating cell intrinsic and extrinsic interactions in prostate cancer at the single cell level.
P01 Consortium application with Dr. Michael Shen and Columbia University
Role: Project Leader and Subcontract Lead at MSK

T32 CA160001-11 (PI: Sawyers) 7/1/2022 - 6/30/2027 0.90 calendar
NCI
Translational Research in Oncology Training Program
The goal of the Translational Research in Oncology Training (TROT) program is to offer PhD scientists from a basic science background experience in clinically applied research. Trainees learn how to collaborate effectively to advance translational research for the treatment of cancer. Fellows are supported for two years, undertake formal coursework in human oncology and pathogenesis, and learn precision oncology approaches under the mentorship of a laboratory preceptor and clinical advisor.
Role: Principal Investigator
Agency Contact: N/A
Overlap: None

2 P50 CA092629-21 (PI: Scher) 9/1/2022 - 8/31/2027
National Institutes of Health
MSKCC Spore in Prostate Cancer

- RP-3 1.80 calendar

  Therapeutic Targeting of Lineage Plasticity in Castration-Resistant Prostate Cancer trials to predict and monitor patient response to these types of therapies.
  Recent genomics studies have shown that men with castration-resistant metastatic prostate cancer harbor an unexpectedly high frequency of alterations in the tumor suppressor genes TP53 and RB. In laboratory studies, we have found that these alterations lead tumor cells to change their identity and thereby become resistant to anticancer therapies that target the androgen receptor. In this project, we will characterize these altered tumor cells through single-cell analysis, evaluate four inhibitory therapies that may delay, prevent, or

even reverse the changes that cause resistance, and develop blood-based biomarkers that can be incorporated into clinical.
Role: Project Leader

- Administrative Core (PI: Scher) 0.30 calendar
The purpose of the Administrative Core is to support the translational research objectives of our SPORE in Prostate Cancer by serving as the organizational hub, optimizing collaboration among SPORE investigators within and outside the MSKCC.
Role: Executive Committee Member

P01 (PI: Sawyers) 7/1/2022 - 6/30/2027 1.20 calendar
NCI
Title: Leveraging Observational (Real World) Data to Advance Precision Oncology
Major Goal: Our proposal is highly synergistic as it brings together a multi-institutional team of distinguished investigators in population science, population genetics, cancer genomics and experimental therapeutics, with a substantial track record of collaborative interactions, who will work together to address these important topics in precision oncology.
Aim 1: Use the existing AACR Project GENIE (GENIE) infrastructure to serve as central hub for data collection, harmonization, storage, distribution, visualization, and analysis among Project and Core Teams.
Aim 2: Develop, deploy, and monitor project communications plan to ensure effective communication between project teams and cores, the EAB and IAB, the NCI and the broader scientific community and general public.
Aim 3: Provide centralized administrative and financial management support to monitor scientific progress, data integrity, and budget allocation and expenditures.
Role: Principal Investigator and Administrative Core Lead
Agency Contact: N/A
Overlap: None

Title: Multilineage plasticity in prostate cancer through expansion of stem–like luminal epithelial cells with elevated inflammatory signaling.

Authors: Samir Zaidi[1,2]†, Jimmy L. Zhao[1,2]†, Joseph M. Chan[3]†, Martine P. Roudier[4,10], Kristine M. Wadosky[5], Anuradha Gopalan[6], Wouter R. Karthaus[1,2], Jungmin Choi[7], Kayla Lawrence[1,2], Ojasvi Chaudhary[3], Tianhao Xu[3], Ignas Masilionis[3], Linas Mazutis[3], Ronan Chaligné[3], Irina Linkov[6], Afsar Barlas[8], Achim Jungbluth[6], Natasha Rekhtman[6], Joachim Silber[6], Katia Manova–Todorova[8], Philip A. Watson[1,2], Lawrence D. True[10], Peter S. Nelson[4], Howard I. Scher[9], Dana E. Rathkopf[9], Michael J. Morris[9], Michael C. Haffner[4,10], David W. Goodrich[5], Dana Pe'er[3]*, Charles L. Sawyers[1,2]*

Affiliations:

[1]Human Oncology and Pathogenesis Program, Memorial Sloan Kettering Cancer Center, New York, NY 10065, USA.

[2]Howard Hughes Medical Institute, Memorial Sloan Kettering Cancer Center, New York, NY 10065, USA.

[3]Program for Computational and Systems Biology, Sloan Kettering Institute, Memorial Sloan Kettering Cancer Center, New York, NY 10065, USA

[4]Divisions of Human Biology and Clinical Research, Fred Hutchinson Cancer Research Center, Seattle, WA 98195, USA.

[5]Department of Pharmacology and Therapeutics, Roswell Park Cancer Institute, Buffalo, NY 14263, USA.

[6]Department of Pathology, Memorial Sloan Kettering Cancer Center, New York, NY 10065, USA.

[7]Department of Biomedical Sciences, Korea University College of Medicine, Seoul, Korea.

[8]Molecular Cytology Core Facility, Memorial Sloan Kettering Cancer Center, New York, NY 10065, USA.

[9]Department of Genitourinary Oncology, Memorial Sloan Kettering Cancer Center, New York, NY 10065, USA.

[10]Department of Pathology, University of Washington, Seattle, WA 98195, USA

† These authors contributed equally to this work

* Corresponding authors. Email: peerd@mskcc.org (D.P), sawyersc@mskcc.org (C.L.S)

Abstract:

Lineage plasticity is a well–established mechanism of resistance to targeted therapies in lung and prostate cancer, where tumors transition from adenocarcinoma to small–cell or neuroendocrine carcinoma. Through single–cell analysis of a cohort of heavily–treated castration–resistant human prostate cancers (CRPC), we report a greater degree of plasticity than previously appreciated, with multiple distinct neuroendocrine (NEPC), mesenchymal (EMT–like), and other subpopulations detected within single biopsies. To explore the steps leading to this plasticity, we turned to two genetically engineered mouse models of prostate cancer that recapitulate progression from adenocarcinoma to neuroendocrine disease. Time course studies reveal expansion of stem–like luminal epithelial cells (*Sca1*+, *Psca*+, called L2) that, based on trajectories, gave rise to at least 4 distinct subpopulations, NEPC (*Ascl1*+), POU2F3 (*Pou2f3*+), TFF3 (*Tff3*+) and EMT–like (*Vim*+, *Ncam1*+)—these populations are also seen in human prostate and small cell lung cancers. Transformed L2–like cells express stem–like and gastrointestinal endoderm–like transcriptional programs, indicative of reemerging developmental plasticity programs, as well as elevated Jak/Stat and interferon pathway signaling. In sum, while the magnitude of multilineage heterogeneity, both within and across patients, raises considerable treatment challenges, the identification of highly plastic luminal cells as the likely source of this heterogeneity provides a target for more focused therapeutic intervention.

One Sentence Summary: Multilineage plasticity results from expansion of stem–like luminal cells with JAK/STAT activation, serving as a therapeutic target.

Main Text:

Acquired resistance to precision oncology therapies is often due to mutations in the drug target present in rare subclones, which eventually emerge during treatment (*1, 2*). This understanding has spurred the development of several next–generation targeted therapies that can overcome such "on target" resistance and extend survival (*3-5*). However, the expanded clinical use of these more effective inhibitors has led to the recognition that acquired resistance is often associated with a change in tumor histology, typified by the adenocarcinoma to neuroendocrine carcinoma transition seen in lung and prostate cancer (*6*). This histologic transition, often termed lineage plasticity, refers broadly to cell–state changes that allow cells to adapt to environmental stresses, such as those associated with invasion and metastasis, as well as to the selective pressure of drug therapy (*7*). Work across a range of model systems has shown that transcriptional programs associated with plasticity typically resemble those seen in stem and progenitor cells of various tissues and in various developmental pathways (*8-10*). Unlike the more conventional mechanism of drug resistance due to "on target" mutation, lineage plasticity does not appear to be associated with the acquisition of new mutations; however, mutational contexts such as loss of tumor suppressor genes can predispose to acquiring a state of plasticity (*11-14*).

To better understand the process by which plasticity begins and subsequently evolves in a common human tumor, we used single cell genomics to characterize a cohort of early and late stage human prostate cancers and two genetically engineered mouse prostate cancer models (GEMM) that undergo an adenocarcinoma to neuroendocrine lineage transition (*9*) (**Fig. 1A**). Integrative computational analysis of these mouse and human datasets, together with human small cell lung cancer data, reveals conservation of plasticity–derived cell types and transcriptional programs, pointing toward a specific luminal subpopulation as the source of plasticity.

Recent single–cell analyses of normal human and mouse prostate tissue have defined a complex array of previously unappreciated cell types, particularly within the luminal epithelial compartment (*15-20*). We interrogated this complexity in the context of prostate cancer by first performing single–cell RNA sequencing (scRNA–seq) analysis of sixteen human samples (**Table S1**). Six patients had early–stage castration–sensitive prostate cancer (CSPC) (*2*) and ten patients had late–stage metastatic castration–resistant prostate cancer (CRPC) representing three clinically recognized phenotypes: CRPC adenocarcinoma (AR+, SYP–); double negative prostate cancer (DNPC) (AR–, SYP–); and neuroendocrine prostate cancer (NEPC) (AR–, SYP+). All three CRPC phenotypes were enriched for alterations in *TP53*, *PTEN* and *RB1 (8, 11)* (**Table S2 and Fig. S1**).

Unsupervised clustering (*21*) on batch–corrected data was used for iterative labeling of coarse cell types into lineages using canonical markers (**Fig. 1B, Fig. S2**). Primary benign and CSPC tumor cells were labelled *per* Karthaus *et al (2)*, whereas all epithelial cells derived from metastatic tumors were found to be malignant, except for a small benign hepatocyte population (**Fig. S2, Table S5** for DEGs**, refer to Methods**). To assess for inter–tumor heterogeneity, we determined the Shannon diversity of patient tumors (**refer to Methods**). As anticipated, CRPC samples were significantly more heterogeneous (lower entropy) than CSPC tumors ($P=1.5x10^{-205}$, **Fig. 1C**). Furthermore, while CRPC samples showed minimal overlap across samples and did not adhere to *a priori* defined pathologic groupings (**Fig. 1B)**, the CRPC adenocarcinoma subgroup showed less heterogeneity (higher entropy) than the DNPC or NEPC samples ($P=1.6x10^{-22}$, **Fig. 1C**).

We next explored the factors that contribute to intra–tumoral heterogeneity as tumors displaying plasticity may harbor distinct tumor phenotypes at the *per*–biopsy level. Recurring transcriptomic trends emerged within multiple tumor biopsies including focal loss of AR signaling, gain of EMT signals, emergence of rare and early NEPC cells, and differing NEPC lineages (**Fig. 1D, Figs. S3–S4**). For example, HMP13 (CRPC adenocarcinoma) showed consistent AR expression throughout but had clusters with loss of expression of AR target genes, such as *FKBP5* and *NKX3.1*, and rare gain of *SYP* or *INSM1*+ cells, likely indicative of early transition to NEPC (**Fig. 1D)**. HMP08, histologically classified as DNPC, showed evidence of EMT (*EPCAM+, TWIST1*+) and focal expression of the NEPC marker *CHGB* (**Fig. 1D**, **Fig. S4**). Two further samples, both classified histologically as NEPC, displayed either distinct clusters of *ASCL1*+ and *NDRG1*+ (an EMT

marker) (HMP04, **Fig. 1D**, **Fig. S4**) or *ASCL1*+ and *NEUROD1*+ cells (HMP17, **Fig. 1D**) that, in human small cell lung cancer, are considered distinct disease subtypes. Collectively, these cases (each of which serves as its own case study) illustrate the complexity of aberrant lineages that can emerge from a relatively uniform population of adenocarcinoma cells in response to the selective pressure of androgen receptor signaling inhibitors (ARSIs).

To gain more insight into the early stages of lineage plasticity, we turned to two prostate GEMMs that model the adenocarcinoma to NEPC transition following prostate–specific deletion of the human–relevant tumor suppressor genes *PTEN*, *RB1* and *TP53*. scRNA–seq was performed on whole prostates harvested from 29 mice [9 wildtype (WT); 7 *Pten*$^{-/-}$*Rb*$^{-/-}$ (PtR); 13 *Pten*$^{-/-}$*Rb*$^{-/-}$*Trp53*$^{-/-}$ (PtRP)] at relevant timepoints reflecting adenocarcinoma to NEPC transformation (**Fig. 2A, Fig. S5**). Transcriptomes from 67,622 cells were analyzed using *Gfp* to mark those that underwent Cre recombination and visualized by UMAP, with cell types identified by coarse labelling (**Fig. 2B, Fig. S5, refer to Methods**). In addition to the expected adenocarcinoma (*Epcam–Gfp*) and NEPC (*Syp*+) populations, we were surprised to see three additional *Gfp*+ clusters defined by expression of *Pou2f3* and *Dclk1* (*Pou2f3–Gfp*), *Vim, Twist2* and *Ncam1* (EMT–*Gfp*), and *Tff3* (*Tff3–Gfp*), respectively. POU2F3 is a transcription factor (TF) expressed by rare chemosensory cells in normal gut and lung tissue (often called tuft cells), whereas *Tff3* encodes a secreted protein expressed by intestinal columnar epithelial cells involved in maintaining mucosal integrity. Of note, POU2F3 also defines a non–neuroendocrine variant subtype of lung cancer with morphologic features of small cell carcinoma distinct from ASCL1 and NEUROD1 subtypes (*12, 22*).

We examined potential routes of plasticity by generating force–directed layouts (FDLs) for each genotype across different timepoints. We noted the early appearance of *Gfp*+ adenocarcinoma (*Epcam–Gfp*) as well as *Tff3–Gfp* cells, followed by the expansion of EMT–*Gfp* and NEPC and *Pou2f3–Gfp* populations, with some differences based on genotype (**Figs. 2C and 2D**). The presence of each of these subpopulations was confirmed by multiplex immunofluorescence (IF) and immunohistochemistry (IHC), which documented SYP+ (NEPC) and VIM+ (EMT) positive cells in a background of ECAD+ (or PANCK+) epithelial cells (top row), larger clusters of NEPC and EMT (middle and bottom rows) and foci of TFF3+ or POU2F3+ cells (right panel) (**Fig. 2E**, see **Fig. S6** for additional examples and PANCK staining).

To investigate the cellular origin of these early adenocarcinoma cells, we performed deconvolution of mixed wild–type epithelial phenotypes in mutant *Gfp*+ cells using Markov absorption classification (**refer to Methods**) and found the majority of cells associate with stem–like luminal 2 (*Sca1, Psca, Tacstd2*, and *Krt4,* adeno–L2) or basal (*Krt5* and *Krt14*, adeno–B) phenotypes. This conclusion was supported by bulk RNA–seq data from normal mouse L1, L2 and basal cells (**Fig. 3A, Fig. S7, refer to Methods**). While adenocarcinoma cells were readily annotated based on maximum likelihood (adeno–L1, –L2, and –B), these cells displayed significant basal and L2 phenotypic mixing (higher entropy) compared with wild–type cells ($P<10^{-16}$, **Fig. 3A,** right bar plot). We further found that NEPC cells had the highest similarity to wild–type L2 cells among the wild–cell types (**Fig. 3A, refer to Methods**). In all, our scRNA-seq and spatial imaging data together implicate stem–like luminal (L2) cells and potentially basal–like state as the source of plasticity following deletion of *Pten/Rb1* or *Pten/Rb1/Trp53* that can give rise to at least 4 distinct lineages, namely NEPC, *Pou2f3–Gfp*, EMT–*Gfp*, and *Tff3–Gfp*. While we cannot exclude that these lineages arise from early activation and/or leakiness of *Pbsn–Cre*, notably with respect to EMT–*Gfp,* there is compelling evidence through lineage tracing using luminal *Nkx3.1–Cre* and *Krt8–Cre* mice, and our spatial IF showing PANCK and SYP staining that transformed luminal cells readily transdifferentiate into NEPC (*23*). Specifically, and consistent with our data, L2 (SCA–1+) cells have an increased propensity to transdifferentiate to neuroendocrine cells upon androgen ablation compared with L1 (SCA–1–)(*24*).

Having documented a much greater than expected degree of lineage plasticity in human and mouse prostate cancers (i.e., beyond SYP+ NEPC alone), we studied transcriptional programs and transcription factors associated with these lineage transitions, starting with differentially expressed genes (DEG) and pathways using gene set enrichment analysis (GSEA) (**Tables S6, S7**). In addition to L2–like regenerative programs that we previously reported in the context of the normal castration response (*14*), lineage–specification programs of early gut development (*25, 26*) in *Gfp*+ luminal and basal adenocarcinoma cells emerged (**Fig. 3B and 3C**). Among these programs, and specifically highest in adenocarcinoma luminal–like cells, we noted an upregulation of *Hnf4a* (focal positivity confirmed by IHC in **Fig. S6**), *Hhex* and *Onecut2,* which are known lineage–

defining TFs in the developing foregut (*27, 28*). *Onecut2* is of particular interest due to its recently reported role in suppression of AR signaling in CRPC (*29*).

Given that the data suggest that reactivation of stem– and developmental–like programs in *Gfp*+ adenocarcinoma cells is the likely source of lineage plasticity, we looked more specifically at TFs that might be responsible, starting with a predefined set of known TFs (1637 genes, Transcription Factor Database, TFDB). Consistent with our FDLs (**Fig. 2B**), pseudotime analysis using Palantir (*30*) (**refer to Methods**) starting with an early adenocarcinoma state (cluster with low *Cdk2na* expression) revealed four terminal differentiated states: *Tff3–Gfp*, EMT–*Gfp*, *Pou2f3–Gfp* and NEPC (**Fig. S8**). To explore the set of perturbed TFs further and given its clinical relevance, we focused on the adenocarcinoma to NEPC transition, restricting to the PtRP model, and noted three major trends in TF expression, namely: (i) those active in adenocarcinoma alone, (ii) those expressed during the transition to NEPC and (iii) NEPC–specific regulators (**Figs. 3D and 3E, Fig. S8,** discussed later).

A closer look at the NEPC and non-neuroendocrine variant populations provided evidence for even more heterogeneity, consisting of three subsets defined by distinct DEG profiles designated as: (i) *Pou2f3–Gfp* (*Pou2f3, Dclk1*), (ii) NEPC–A (*Ascl1*), (iii) NEPC–Ar (**refer to Methods, Fig. 4A, Fig. S9**). Because the NEPC–Ar subset is largely based on scRNA-seq data from a single PtRP mouse, we confirmed the presence of NEPC–Ar populations by multiplex–IF in additional PtR and PtRP mice (**Fig. S9**). We further found a cluster of *Syp*+ cells that express both *Ar* and *Ascl1*. We asked if the diversity of NEPC lineages detected in the prostate GEMMs are also found in human CRPC (beyond that observed in our scRNA–seq cohort, **Figs. 1 and 4A**). To this end, we assessed expression of selected lineage markers across a cohort of tissue samples from a large rapid autopsy cohort (*31, 32*) containing tissue samples from multiple anatomically distinct metastatic sites *per* patient [16 patients, 139 tumors from distant metastases and the prostate gland; 2–21 metastatic sites per patient] (**Fig. 4B, 4C, Fig. S10, Table S8**). The analysis confirmed 2 of the 3 mouse NEPC subsets (NEPC–A and NEPC–Ar) in human CRPC. Human NEPC–A is notable for concordant INSM1 and DLL3 expression, consistent with the mouse profile, and reminiscent of ASCL1+ human SCLC. Human NEPC–AR samples were largely INSM1– and ASCL1–negative (**Fig 4B**). NEUROD1 and POU2F3 were absent in this subset at the TMA level.

Our TMA also revealed a subset of YAP1+ human high–grade carcinomas (HGC), while NEPC tumors largely showed absence or focal *YAP1* expression (*33*). Although the former finding may implicate altered Hippo pathway signaling in CRPC adenocarcinoma, important to note is that *YAP1* is also expressed in primary adenocarcinoma cells (*28*). Finally, when examining lineage marker expression across metastases, we found several examples of widespread SYP+ soft tissue metastases in patients whose bone lesions retained the expression of luminal epithelial markers (*AR*, *NKX3.1*, *CK8*), suggesting microenvironmental signals may influence lineage commitment (**Fig. 4B**, **Table S8,** patients 6,7, and 10, boxed in gray).

To determine whether there is a human counterpart to mouse *Pou2f3–Gfp*, we examined existing human CRPC (SU2C) and patient–derived xenograft datasets (PDXs, LuCAP) for expression of *POU2F3* and its signature (*12*) (**refer to Methods**). We also studied NEPC–N (*NEUROD1*) in both datasets; this subpopulation was found in patient HMP17 by scRNA–seq (**Fig 1D**), but not in mouse NEPC or by human TMA. Most NEPC samples in the SU2C dataset expressed *ASCL1,* as expected, but we did identify several *NEUROD1*–expressing samples (NEPC–N+) that also retained expression of ASCL1, in line with HMP17 and recent literature (*34*) (*Z*–score > 2, discussed above) (**Fig. 4D**). *Pou2f3–Gfp* was less convincing in that the extreme *POU2F3* outlier (by signature) is from a subcutaneous tumor, which may alternatively represent contamination from skin cells expressing high levels of POU2F3 (**Fig. 4D**). Similar to our GEMM data, analysis of the PDX dataset also revealed divergent NEPC–A and *Pou2f3–Gfp* phenotypes in two sublines derived from the same patient, LuCAP173. Notably, subline LuCAP173_2 (DNPC with rare foci of NEPC) showed high *POU2F3* expression, whereas subline LuCAP173.1 (fully NEPC) expressed low *POU2F3*, but high *INSM1, CHGA,* and *SYP* (**Fig. S11**). This is consistent with a recent cohort of human CRPC patients displaying some degree of POU2F3–positivity (*12*). While these findings are suggestive of the presence of these NEPC subsets, large scale tissue–based PDX and tumor IHC/IF are likely needed to delineate their prevalence. Lastly, we also found evidence of EMT–like programs in the SU2C dataset, although not exclusively linked to NEPC histology (**Fig. S11**). This observation was consistent with EMT programs being active in late stage CRPC, such as in our human single–cell analysis and enriched in HMP08 (DNPC, **Fig. 1E**). Furthermore, while *TFF3* was expressed in SU2C samples (highest *Z*–score of ~8), the *Tff3–Gfp* signature for

all samples fell below a *Z*–score of 1.5, perhaps because *TFF3* defines an early population not enriched in CRPC patients (as seen in the GEMM data, **Fig 2D, Fig. S11**).

Given the concordance of NEPC populations in the GEMM and human datasets (scRNA–seq, UW rapid autopsy, SU2C, and PDX), we asked whether the TFs that define these subsets are conserved across human SCLC subtypes. We found significant overlap of differentially expressed TFs in scRNA–seq data from human SCLC as well as in mouse and human NEPC subtypes (*35*) (**Fig. 4E, Fig. S7E**). Examples of shared NEPC and SCLC TFs include: *FOXA2, INSM1*, *SOX2*, *SOX4, TOX3* (ASCL1 subtype, $P=6x10^{-15}$, Fisher's exact test); *ASCL2*, *REST*, *IRF7, SOX9*, *MYC, MYB* (POU2F3 subtype, $P=4x10^{-5}$, Fisher's exact test) and *DACH1*, *NFIA*, *HLX*, *TCF4* (NEUROD1 subtype, $P=3x10^{-6}$, Fisher's exact test) **(Fig. S9**, additional overlap analyses). Collectively, these mouse/human and prostate/lung cancer pairs reveal a high level of conservation of the endoderm–derived lineage specification pathways, in essence, revealing how these can be hijacked to promote disease progression and drug resistance.

Because transition to NEPC portends a highly aggressive and lethal stage of prostate cancer, there is an acute need for novel therapies. Current drug development efforts are focused on actionable targets known to be expressed in NEPC, such as *EZH2*, *AURKA* and *DLL3*, with clinical trials currently underway. In light of the high degree of heterogeneity in NEPC seen through our single–cell analyses, we looked at expression of these and other common targets, such as *AR* and *PSMA* across our datasets. Not surprisingly, this analysis revealed a high degree of both intra–tumoral and inter–tumoral heterogeneity across both human and GEMM scRNA-seq (examples shown in **Fig. 5A**), raising obvious concerns about the clinical efficacy of these treatment strategies due to escape of target–negative tumor cells.

Our prostate GEMM time course analysis implicated stem–like luminal (L2) adenocarcinoma cells as the source of plasticity for NEPC, raising the possibility that pharmacologic targeting of this population may be a strategy to prevent NEPC transition. We thus explored the temporal activation of pathways across the adenocarcinoma to NEPC transition in our GEMMs, with an eye toward druggability. In the adeno–L2, pathway analysis revealed the majority of significantly enriched gene sets related to activation of Jak/Stat, IFN and other inflammatory response pathways (**Fig**

5B). The set of genes (GSEA leading edge) driving this enrichment overlapped with transition regulators, namely IRF1/7, JAK2, STAT1/2, showing the highest expression in the adeno–L2 high plastic state, but with reduced expression in the NEPC populations (**Fig. S8**). To assess human relevance, we explored whether these transcription drivers were activated in tumor biopsies displaying evidence of plasticity from AR–high to AR–low adenocarcinoma states. Strikingly, we found a similar enrichment of inflammatory (and EMT) pathways in humans across high to low AR signaling as seen in HMP13 and highest in cells displaying an L2–like state **(Fig 5C, Fig. S11)**. Mapping of TFs across diffusion pseudotime revealed a similar activation of transcriptional regulators, namely JAK1, STAT2/3, IRF1, and IRF7 (**Fig 5C, Fig. S11**).

Together, our data reveal a greater than expected degree of lineage plasticity in prostate cancers that develop resistance to androgen deprivation therapy and, through side–by–side analysis of human and mouse datasets, establish a set of transcriptional programs that define and likely mediate plasticity states in prostate cancer. The delineation of such novel signatures should inform clinical prognosis and could enhance precision in treatment selection. Most importantly, we define a stem–like luminal (L2) population as the likely source of plasticity and implicate the inflammatory JAK/STAT pathway as a potential target for therapeutic intervention (**Fig. 5D**), which we address functionally in the accompanying manuscript.

References and Notes:

1. P. A. Watson, V. K. Arora, C. L. Sawyers, Emerging mechanisms of resistance to androgen receptor inhibitors in prostate cancer. *Nat Rev Cancer* **15**, 701-711 (2015).
2. W. R. Karthaus *et al.*, Regenerative potential of prostate luminal cells revealed by single-cell analysis. *Science* **368**, 497-505 (2020).
3. T. M. Beer *et al.*, Enzalutamide in metastatic prostate cancer before chemotherapy. *The New England journal of medicine* **371**, 424-433 (2014).
4. J. S. de Bono *et al.*, Abiraterone and increased survival in metastatic prostate cancer. *The New England journal of medicine* **364**, 1995-2005 (2011).
5. H. I. Scher *et al.*, Increased survival with enzalutamide in prostate cancer after chemotherapy. *The New England journal of medicine* **367**, 1187-1197 (2012).
6. A. Quintanal-Villalonga *et al.*, Lineage plasticity in cancer: a shared pathway of therapeutic resistance. *Nat Rev Clin Oncol* **17**, 360-371 (2020).
7. H. Beltran *et al.*, Divergent clonal evolution of castration-resistant neuroendocrine prostate cancer. *Nat Med* **22**, 298-305 (2016).
8. E. G. Bluemn *et al.*, Androgen Receptor Pathway-Independent Prostate Cancer Is Sustained through FGF Signaling. *Cancer Cell* **32**, 474-489 e476 (2017).
9. S. Y. Ku *et al.*, Rb1 and Trp53 cooperate to suppress prostate cancer lineage plasticity, metastasis, and antiandrogen resistance. *Science* **355**, 78-83 (2017).
10. P. Mu *et al.*, SOX2 promotes lineage plasticity and antiandrogen resistance in TP53- and RB1-deficient prostate cancer. *Science* **355**, 84-88 (2017).
11. W. Abida *et al.*, Genomic correlates of clinical outcome in advanced prostate cancer. *Proc Natl Acad Sci U S A* **116**, 11428-11436 (2019).
12. N. J. Brady *et al.*, Temporal evolution of cellular heterogeneity during the progression to advanced AR-negative prostate cancer. *Nat Commun* **12**, 3372 (2021).
13. J. W. Park *et al.*, Reprogramming normal human epithelial tissues to a common, lethal neuroendocrine cancer lineage. *Science* **362**, 91-95 (2018).
14. H. Beltran *et al.*, The Role of Lineage Plasticity in Prostate Cancer Therapy Resistance. *Clin Cancer Res* **25**, 6916-6924 (2019).
15. L. Crowley *et al.*, A single-cell atlas of the mouse and human prostate reveals heterogeneity and conservation of epithelial progenitors. *Elife* **9**, (2020).
16. D. Gao *et al.*, Organoid cultures derived from patients with advanced prostate cancer. *Cell* **159**, 176-187 (2014).
17. M. X. He *et al.*, Transcriptional mediators of treatment resistance in lethal prostate cancer. *Nat Med* **27**, 426-433 (2021).
18. G. H. Henry *et al.*, A Cellular Anatomy of the Normal Adult Human Prostate and Prostatic Urethra. *Cell Rep* **25**, 3530-3542 e3535 (2018).
19. W. R. Karthaus *et al.*, Identification of multipotent luminal progenitor cells in human prostate organoid cultures. *Cell* **159**, 163-175 (2014).
20. S. Chen *et al.*, Single-cell analysis reveals transcriptomic remodellings in distinct cell types that contribute to human prostate cancer progression. *Nat Cell Biol* **23**, 87-98 (2021).
21. J. H. Levine *et al.*, Data-Driven Phenotypic Dissection of AML Reveals Progenitor-like Cells that Correlate with Prognosis. *Cell* **162**, 184-197 (2015).
22. Y. H. Huang *et al.*, POU2F3 is a master regulator of a tuft cell-like variant of small cell lung cancer. *Genes Dev* **32**, 915-928 (2018).

23. M. Zou *et al.*, Transdifferentiation as a Mechanism of Treatment Resistance in a Mouse Model of Castration-Resistant Prostate Cancer. *Cancer Discov* **7**, 736-749 (2017).
24. O. J. Kwon, L. Zhang, D. Jia, L. Xin, Sox2 is necessary for androgen ablation-induced neuroendocrine differentiation from Pten null Sca-1(+) prostate luminal cells. *Oncogene* **40**, 203-214 (2021).
25. S. Nowotschin *et al.*, The emergent landscape of the mouse gut endoderm at single-cell resolution. *Nature* **569**, 361-367 (2019).
26. J. Cao *et al.*, The single-cell transcriptional landscape of mammalian organogenesis. *Nature* **566**, 496-502 (2019).
27. R. I. Sherwood, T. Y. Chen, D. A. Melton, Transcriptional dynamics of endodermal organ formation. *Dev Dyn* **238**, 29-42 (2009).
28. S. Shukla *et al.*, Aberrant Activation of a Gastrointestinal Transcriptional Circuit in Prostate Cancer Mediates Castration Resistance. *Cancer Cell* **32**, 792-806 e797 (2017).
29. M. Rotinen *et al.*, ONECUT2 is a targetable master regulator of lethal prostate cancer that suppresses the androgen axis. *Nat Med* **24**, 1887-1898 (2018).
30. M. Setty *et al.*, Characterization of cell fate probabilities in single-cell data with Palantir. *Nat Biotechnol* **37**, 451-460 (2019).
31. L. Brady *et al.*, Inter- and intra-tumor heterogeneity of metastatic prostate cancer determined by digital spatial gene expression profiling. *Nat Commun* **12**, 1426 (2021).
32. M. P. Labrecque *et al.*, Molecular profiling stratifies diverse phenotypes of treatment-refractory metastatic castration-resistant prostate cancer. *J Clin Invest* **129**, 4492-4505 (2019).
33. K. Asrani *et al.*, Reciprocal YAP1 loss and INSM1 expression in neuroendocrine prostate cancer. *J Pathol*, (2021).
34. P. Cejas *et al.*, Subtype Heterogeneity and Epigenetic Convergence in Neuroendocrine Prostate Cancer. *bioRxiv*, 2020.2009.2013.291328 (2020).
35. J. M. Chan *et al.*, Signatures of plasticity, metastasis, and immunosuppression in an atlas of human small cell lung cancer. *Cancer Cell*, (2021).
36. A. Zehir *et al.*, Mutational landscape of metastatic cancer revealed from prospective clinical sequencing of 10,000 patients. *Nat Med* **23**, 703-713 (2017).
37. H. Sun *et al.*, E2f binding-deficient Rb1 protein suppresses prostate tumor progression in vivo. *Proc Natl Acad Sci U S A* **108**, 704-709 (2011).
38. S. Wang *et al.*, Prostate-specific deletion of the murine Pten tumor suppressor gene leads to metastatic prostate cancer. *Cancer Cell* **4**, 209-221 (2003).
39. J. Drost *et al.*, Organoid culture systems for prostate epithelial and cancer tissue. *Nat Protoc* **11**, 347-358 (2016).
40. E. Azizi *et al.*, Single-Cell Map of Diverse Immune Phenotypes in the Breast Tumor Microenvironment. *Cell* **174**, 1293-1308 e1236 (2018).
41. A. T. L. Lun *et al.*, EmptyDrops: distinguishing cells from empty droplets in droplet-based single-cell RNA sequencing data. *Genome Biol* **20**, 63 (2019).
42. J. S. Adam Gayoso, JonathanShor/DoubletDetection: doubletdetection v3.0 (v3.0). *Zenodo*, (2020).
43. C. Hafemeister, R. Satija, Normalization and variance stabilization of single-cell RNA-seq data using regularized negative binomial regression. *Genome Biol* **20**, 296 (2019).

44. L. Haghverdi, A. T. L. Lun, M. D. Morgan, J. C. Marioni, Batch effects in single-cell RNA-sequencing data are corrected by matching mutual nearest neighbors. *Nat Biotechnol* **36**, 421-427 (2018).
45. J. M. Chan *et al.*, Single cell profiling reveals novel tumor and myeloid subpopulations in small cell lung cancer. *bioRxiv*, 2020.2012.2001.406363 (2020).
46. E. Becht *et al.*, Dimensionality reduction for visualizing single-cell data using UMAP. *Nat Biotechnol*, (2018).
47. M. Jacomy, T. Venturini, S. Heymann, M. Bastian, ForceAtlas2, a continuous graph layout algorithm for handy network visualization designed for the Gephi software. *PLoS One* **9**, e98679 (2014).
48. D. van Dijk *et al.*, Recovering Gene Interactions from Single-Cell Data Using Data Diffusion. *Cell* **174**, 716-729 e727 (2018).
49. I. Tirosh *et al.*, Dissecting the multicellular ecosystem of metastatic melanoma by single-cell RNA-seq. *Science* **352**, 189-196 (2016).
50. W. Guo *et al.*, Single-cell transcriptomics identifies a distinct luminal progenitor cell type in distal prostate invagination tips. *Nat Genet* **52**, 908-918 (2020).
51. A. M. Laughney *et al.*, Regenerative lineages and immune-mediated pruning in lung cancer metastasis. *Nat Med* **26**, 259-269 (2020).
52. F. A. Wolf, P. Angerer, F. J. Theis, SCANPY: large-scale single-cell gene expression data analysis. *Genome Biol* **19**, 15 (2018).
53. H. Hieronymus *et al.*, Gene expression signature-based chemical genomic prediction identifies a novel class of HSP90 pathway modulators. *Cancer Cell* **10**, 321-330 (2006).
54. P. S. Nelson *et al.*, The program of androgen-responsive genes in neoplastic prostate epithelium. *Proc Natl Acad Sci U S A* **99**, 11890-11895 (2002).
55. G. Finak *et al.*, MAST: a flexible statistical framework for assessing transcriptional changes and characterizing heterogeneity in single-cell RNA sequencing data. *Genome Biol* **16**, 278 (2015).
56. G. Korotkevich *et al.*, Fast gene set enrichment analysis. *bioRxiv*, 060012 (2021).
57. C. Tabula Muris *et al.*, Single-cell transcriptomics of 20 mouse organs creates a Tabula Muris. *Nature* **562**, 367-372 (2018).

Acknowledgments: Authors are thankful to the members of the Pe'er and Sawyers laboratories for their extensive and productive critiques and discussions. We are incredibly grateful to the prostate cancer patients who participated in this research. We further appreciate the efforts of the Memorial Sloan Kettering Cancer Center (MSK) Genitourinary faculty for recruitment of prostate cancer tumor specimens. We thank the MSK core facilities for their invaluable help, namely the Molecular Cytology Core and Pathology Core for their help with confocal microscopy and IHC, and the Flow Cytometry Core for their help with FACS experiments. We are appreciative of the generous help of Sonja Nowotschin, PhD to curate a list of canonical gut tube specification transcription factors. We are similarly thankful to Matan Hofree, PhD for providing us with certain sets of developmental DEGs from published single cell data.

Funding: S.Z. is supported by the Department of Defense (DoD) Prostate Cancer Research Program Early Investigator Research Award, Prostate Cancer Foundation Young Investigator Award, and Conquer Cancer Foundation of the American Society of Oncology Young Investigator Award. J.L.Z. is supported by Conquer Cancer Foundation of the American Society of Oncology Young Investigator Award, K12 Paul Calabresi Career Development Award for Clinical Oncology from NIH, and Prostate Cancer Foundation Young Investigator Award. J.M.C is supported by the Conquer Cancer Foundation of the American Society of Oncology Young Investigator Award, AACR-AstraZeneca Lung Cancer Research Fellowship, and the Alan and Sandra Gerry Metastasis and Tumor Ecosystems Center. J.C. is supported by the National Research Foundation of Korea (NRF–2019R1A4A1029000). P.S.N. is supported by NCI P50CA097186, U54CA224079, R01CA234715 and Challenge Awards from Prostate Cancer Foundation. M.C.H is supported by the Department of Defense (DoD) Prostate Cancer Research Program (W81XWH-21-1-0229, W81XWH-20-1-0111) and by Grant 2021184 from the Doris Duke Charitable Foundation**.** D.P. is supported by HHMI; NCI U54 CA209975**,** Alan and Sandra Gerry Metastasis and Tumor Ecosystems Center and Parker Institute for Cancer Immunotherapy. C.L.S. is supported by HHMI; National Institute of Health (CA193837, CA092629, CA224079, CA155169, and CA008748), and Starr Cancer Consortium (I12–0007).

Author contributions: S.Z., J.L.Z., J.M.C., D.P., and C.L.S. conceived the project. S.Z., J.L.Z., J.M.C., D.P., and C.L.S. wrote the manuscript. H.I.S, D.E.R, and M.J.M provided human tumor

specimens. A.G., M.R. and M.F. interpreted histology and staining for prostate cancer patients. S.Z., J.L.Z., K.L., W.R.K and P.W. performed human tumor tissue dissociation. S.Z, J.L.Z., A.B. performed mouse staining and/or confocal microscopy. J.L.Z., K.W., K.L. performed all mouse work. M.P.R., N.R., I.L, J.S, A.J, and A.G. performed tissue microarray studies. P.S.N., C.M. and M.P.R. enrolled patients into rapid autopsy protocols, provided rapid autopsy biospecimens and RNA–seq data from PDX tumors. M.P.R. and M.C.H. interpreted and scored human tissue microarray. O.C., I.M., and T.X. performed single-cell sequencing. L.M., R.C. and D.P. oversaw the single-cell–sequencing experiments. S.Z. J.M.C., and J.C. performed computational analyses. D.P. and C.L.S. oversaw the project.

Competing Interests: C.L.S is on the board of directors of Novartis, is a confounder of ORIC Pharmaceuticals, and is a coinventor of the prostate cancer drugs enzalutamide and apalutamide, covered by U.S. patents 7,709,517, 8,183,274, 9,126,941, 8,445,507, 8,802,689, and 9,388,159 filed by the University of California. C.L.S. is on the scientific advisory boards of the following biotechnology companies: Agios, Beigene, Blueprint, Column Group, Foghorn, Housey Pharma, Nextech, KSQ Therapeutics, Petra Pharma, and PMV Pharma, and is a cofounder of Seragon Pharmaceuticals, purchased by Genentech/Roche in 2014. D.P is on the scientific advisory board of Insitro.

Data and Material Availability: Human raw data for CSPC samples, as per *Karthaus et al*., are available at the Data Use and Oversight System controlled access repository https://duos.broadinstitute.org/ (accession no. DUOS-000115, samples: HP95NT/T, HP96NT/T, HP97NT/T, HP98NT, HP99NT/T, HP100NT/T, and HP101NT/T). Human raw data and 10X formatted files for CRPC samples are available at dbGAP (study submitted, accession no. in process). GEMM raw data and 10X formatted files for WT, PtR and PtRP are available at Gene Expression Omnibus respository (accession no. in process). Software and tools used for the enclosed data analysis will be provided open source at https://github.com/dpeerlab/.

Supplementary Materials:

**References 36-57 only used in materials and methods section.

Figure 1

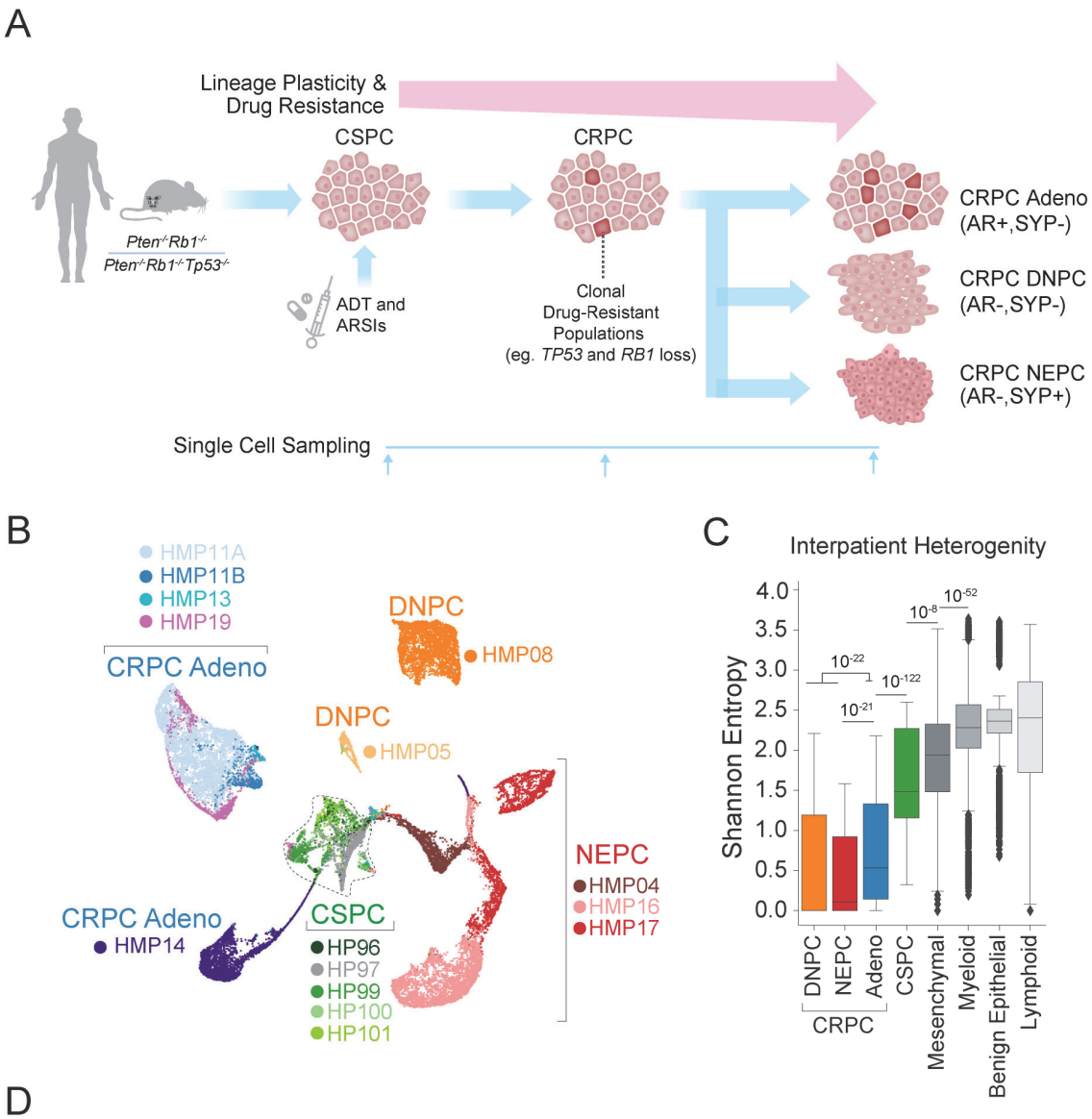

Figure 1. Drivers of Resistance in Metastatic Human Castration–Resistant Prostate Cancer. **(A)** Schematic of an investigative platform to explore drug resistance and lineage plasticity in early– and late–stage human prostate cancer and two autochthonous genetically engineered mouse prostate cancer models (GEMM). Human prostate cancer samples include castrate–sensitive prostate cancer (CSPC) and castrate–resistant prostate cancer (CRPC). The latter includes CRPC adenocarcinoma (AR+, SYP–), double–negative prostate cancer (DNPC) (AR–, SYP–), and transformed neuroendocrine prostate cancer (NEPC) (AR–, SYP+). GEMMs include organ–specific deletion (*Probasin*–Cre) of *Pten* and *Rb1* (PtR), or *Pten, Rb1,* and *Tp53* (PtRP) at relevant timepoints reflecting adenocarcinoma to NEPC transformation. **(B)** UMAPs of tumor cells (N=29,373 cells), colored by tumor ID and grouped by tumor type. **(C)** Inter–patient heterogeneity measured by Shannon entropy based on tumor frequencies. To control for cell sampling, 100 cells were subsampled from each Phenograph cluster (k=30) within epithelial, immune, and mesenchymal compartments 100 times with replacement (Bonferroni–adjusted Student's t–test, **refer to Methods**). **(D)** UMAPs of individual CRPC biopsies: HMP13 (N=354 cells, CRPC adeno), HMP08 (N=4,279 cells, DNPC), HMP04 (N=1791 cells, NEPC), and HMP17 (N=2,845 cells, NEPC). For each biopsy, cells are colored based on normalized expression ($\log_2$X+1) for select genes demonstrating heterogenous and divergent intra–tumoral molecular resistance programs.

Figure 2

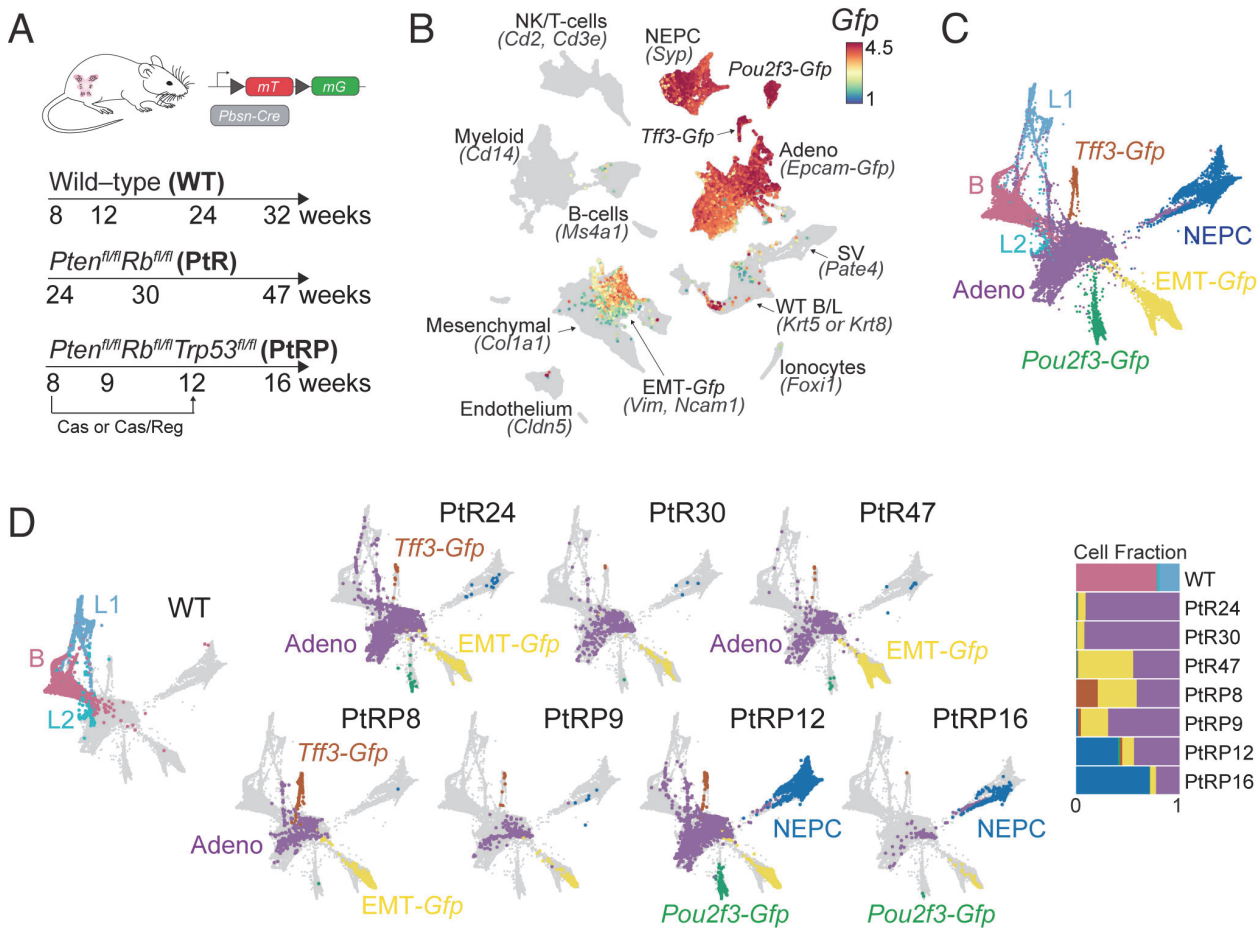

Figure 2. Modeling Multilineage Plasticity in GEMMs. (A) Experimental design includes WT (9 mice), PtR (7 mice, *PbCre*:*Rosa26*$^{mT/mG}$*Pten*$^{fl/fl}$*Rb1*$^{fl/fl}$), and PtRP (13 mice, *PbCre*: *Rosa26*$^{mT/mG}$*Pten*$^{fl/fl}$*Rb1*$^{fl/fl}$*Tp53*$^{fl/fl}$) at labelled time points. **(B)** UMAP of GEMMs (N=67,622 cells) shown for all cell types based on imputed *Gfp* expression (restricted to non–immune cells) as a marker for mutant cells (**refer to Methods**). **(C)** Mutant *Gfp*–positive and wild–type cells (N=28,934) were subsetted. Shown is a force–directed layout (FDL) colored by wild–type and mutant cell types. **(D)** FDLs separated by genotypes and timepoints and colored by cell types (left, WT with N=7,435 cells; top PtRP 24/30/47 weeks with N=2,565/662/1,441 cells; bottom PtRP 8/9/12/16 weeks with N=981/353/4,984/569 cells) with stacked bar plot of fraction of cell types *per* genotype and time point (right). **(E)** Validation of mutant subtypes, including adenocarcinoma to NEPC transition, NEPC, and EMT by hematoxylin/eosin and multiplex immunofluorescence (mIF) (40x). Shown are GFP (mG, green), DAPI (nuclei, blue), VIM (mesenchymal, red), SYP (synaptophysin, purple), and E–CAD (e–cadherin, white). Also shown is mIF of adenocarcinoma state (20x) with zoomed in (80x) hematoxylin/eosin and immunohistochemistry of TFF3– and POU2F3–positive cells in mutant tissue.

Figure 3

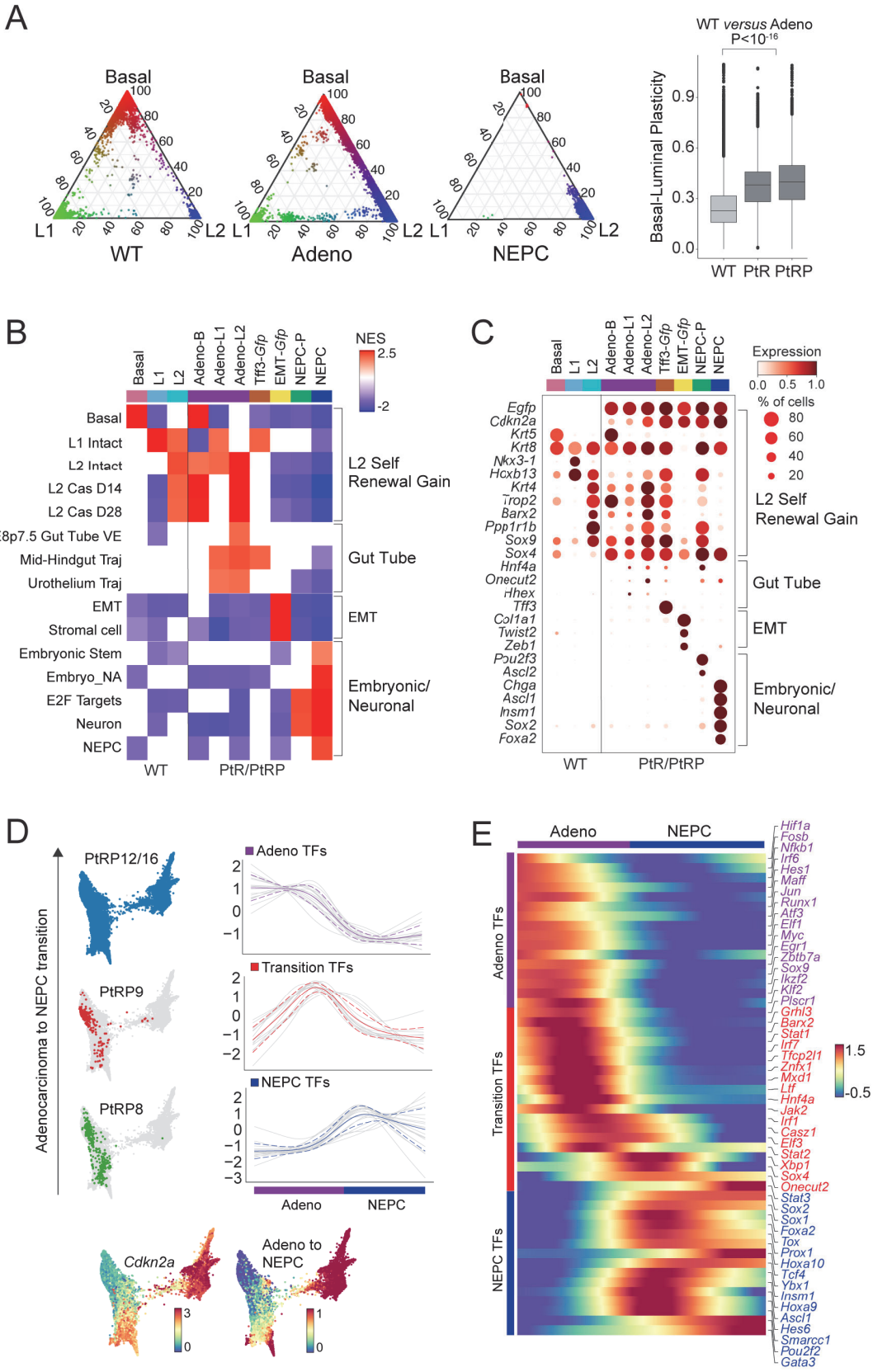

Figure 3. Stem– and Developmental–Like Programs Highest in L2–Like State with Mapping of Inferred Transition TFs. (A) Ternary plots of wild–type epithelial cells, adenocarcinoma or NEPC cells (left to right labelled 'WT', 'Adeno', and 'NEPC') based on three coordinates–basal (B), luminal 1 (L1), and luminal 2 (L2) Markov absorption probabilities. A preponderance of 'Adeno' cells (middle) along the B–L2 side of the triangle suggests an increased mixed phenotype compared with 'WT'. Ternary plot of 'NEPC' cells (right) demonstrating skew to luminal 2 (L2) absorption probabilities. Box plot of basal–luminal plasticity *per* single cell, as measured by Shannon entropy of re–normalized Markov absorption probabilities for B, L1 and L2 phenotypes comparing WT *versus* mutant Adeno in PtR and PtR (Mann–Whitney U test comparing entropies of WT *versus* mutant Adeno in PtR/PtRP, **refer to Methods**). **(B)** Heatmap of significantly enriched gene sets *per* cell type (scale from -2 to +2.5 of GSEA normalized enrichment score, $P<0.05$, **refer to Methods**). **(C)** Dot plot of select differentially expressed genes (DEGs), stratified by cell type (mean normalized $\log_2X+1$ expression scaled from 0 to 1; size of dot represents percent of cells expressing the respective gene) grouped by L2, gut tube specification, EMT, and embryonic/neuronal genes. (**D)** FDL of mutant adenocarcinoma (restricted to PtR model, including adeno–B and adeno–L2) and NEPCs cells (total N=16,593 cells) colored by genotype and time (left). Shown below are FDLs colored by normalized $\log_2X+1$ expression of *Cdkn2a* or pseudotime scaled from 0 to 1 (bottom). Gene trends for TF DEGs across the adenocarcinoma to NEPC branch probability were determined as described in Palantir using a generalized additive model with cubic splines used as the smoothing function across 500 equally sized bins. Gene trends were grouped using Phenograph cluster (k=30*)*. Solid and dashed lines represent the mean and standard deviation of the gene trends for each cluster (**Refer to Methods**). TFs groups include early adenocarcinoma (purple), transition (red), and NEPC (blue). (**E**) Heatmap of gene trends of select TF DEGs (Phenograph cluster versus rest, refer to **Methods: 'Identifying DEGs'**) from each category are ordered by the adenocarcinoma to NEPC transition and colored by aforementioned groups (right; scale gene trends of imputed expression, -0.5 to 1.5).

Figure 4

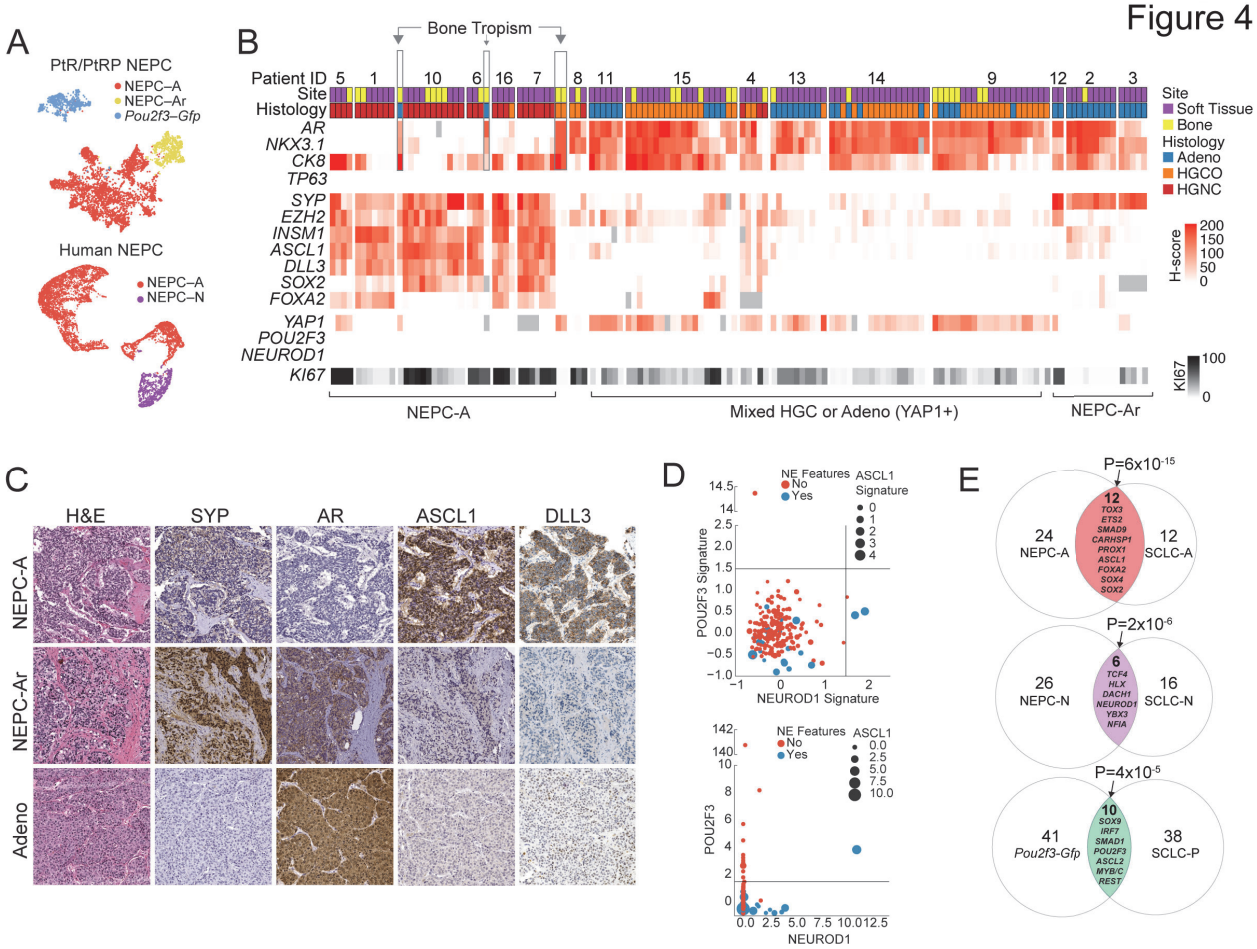

Figure 4. Conservation of Transcription Factors in NEPC Subtypes. (A) UMAP colored by NEPC subtypes based on *Ascl1* (A), *Ar* (Ar) and *Pou2f3* (P) in GEMMs (N=4,973 cells) (A) and *ASCL1* (A) and *NEUROD1* (N) in human samples (from HMP04, HMP16, and HMP17, N=9,572 cells). **(B)** Heatmap of human CRPC tissue microarray *H*-score (immunohistochemical score, scale 0 to 200, red gradient) and proliferative score (KI67, 0 to 100, black gradient) shown with corresponding patient ID, site (soft tissue, purple; bone, yellow), and histology (adenocarcinoma, blue; high-grade carcinoma, NOS, orange; high-grade neuroendocrine, red) confirming NEPC–A and NEPC–Ar subsets. Arrow denotes bone tropism of AR positivity in patients 6, 7 and 10. **(C)** Representative immunohistochemistry shown for NEPC–A, NEPC–Ar, and high-grade adenocarcinoma (additional examples and stain shown in **Fig. S10**). **(D)** Scatter plot shows *Z*–score of expression of genes in the SU2C database of *Pou2f3*–*Gfp* (y–axis) and NEPC-N (x–axis) signatures (top, **Refer to Methods**), and canonical transcriptional regulators *POU2F3* (y–axis) and *NEUROD1* (x–axis) (bottom). Red and blue dots denote non–NEPC or NEPC features as *per* SU2C database, respectively. Size of dot corresponds to the Z–score of NEPC–A signature (top) or ASCL1 expression (bottom). Dotted lines denote Z–score cutoff of 1.5. **(E)** Venn diagrams of differentially expressed TFs in corresponding *ASCL1*, *NEUROD1* and *POU2F3*–high subtypes in small cell lung cancer and neuroendocrine prostate cancer. The overlap between NEPC and SCLC subsets is assessed by Fisher's exact test. Key overlapping TFs are annotated suggesting conserved transcriptional regulation.

Figure 5

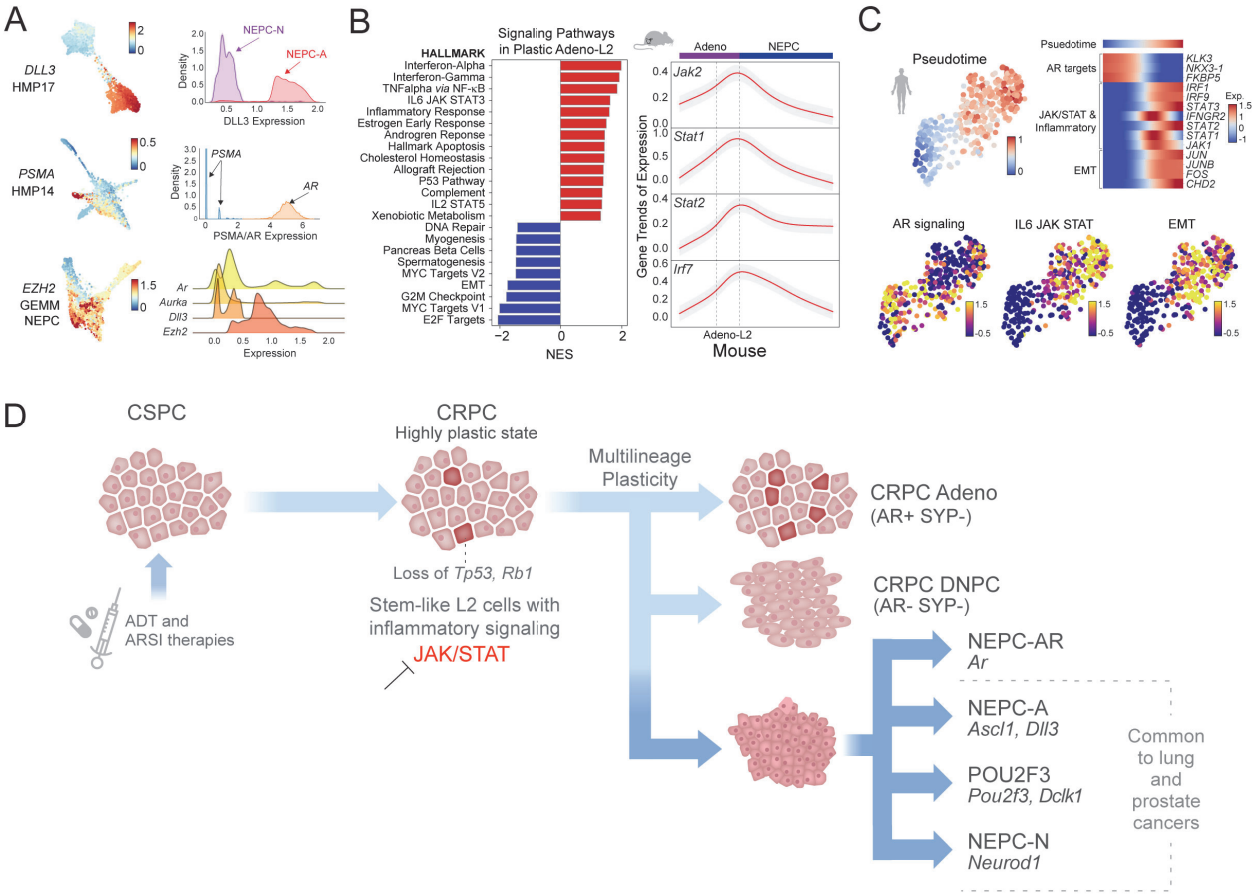

Figure 5. Identification of Targetable Transcriptional Mediators of Plasticity Across Human and GEMM Datasets. (A) FDL and kernel density estimate plots of imputed gene expression (MAGIC, *k*=30, t=3) are shown of current and select prostate cancer drug targets. FDL of *DLL3* expression is shown for HMP17 (NEPC, 2,845 cells, top) with density of expression stratified by NEPC–A (purple) and NEPC–N (red). FDL of *PSMA* expression is shown for HMP14 (CRPC adenocarcinoma, 3,351 cells, middle) highlighting both low *PSMA* (blue) and high *AR* (orange) expression. FDL of *Ezh2* expression is shown for GEMM NEPC tumors (N=4,973 cells, bottom) with ridgeline plots of imputed expression shown for *Ar, Aurka, Dll3, and Ezh2*. **(B)** Enriched signaling pathways using GSEA in adeno–L2 state highlighting inflammation and JAK/STAT pathways (scale -2.5 to 2, normalized enrichment score, P<0.05). Plotted gene trends of *Jak2*, *Stat1*, *Stat2, Irf7* were determined as described in Palantir across adenocarcinoma (purple bar) to NEPC (blue bar) using a generalized additive model with cubic splines used as the smoothing function across 500 divided equally sized bins. **(C)** UMAP of HMP13 (N=353 cells) colored by pseudotime from cells with high to low AR signaling (**refer to Methods**, top left). Corresponding robustness analysis of pseudotime detailed in **Fig. S11** (**refer to Methods**). Heatmaps showing gene trends for select DEGs and mouse transition TF markers ordered by the high to low AR signaling—early NEPC transition (right; scale -1 to 1.5, **refer to Fig. S11**). Gene trends were determined as described in Palantir and above in (B). AR signature score (**refer to Methods**) or Z–score of leading edge of enriched GSEA terms IL6–JAK–STAT or EMT are shown (scale, -0.5 to 1.5) (bottom). **(D)** Schematic of lineage plasticity progression and its mediators highlighting plastic L2–like cells enriched for *TP53, RB1, and/or PTEN* loss with emergence of developmental and stem–like program and upregulation of Jak/Stat and interferon signaling genes (ISGs). This cellular state is primed for multi–lineage plasticity with inhibition of Jak/Stat re–sensitizing to AR directed therapy (refer to accompanying manuscript). NEPC and neuroendocrine variant cells states, *ASCL1*, *NEUROD1*, and *POU2F3*, are common to both lung and prostate cancers with conservation of TFs. The identification of stem–like transformed L2 state provides a target for more focused therapeutic intervention.

Reversal of lineage plasticity in RB1/TP53-deleted prostate cancer through FGFR and Janus kinase inhibition

Wouter R. Karthaus[1†], Joseph Chan[2,3†], Manu Setty[3,4‡], Jillian R. Love[1‡] Samir Zaidi[1], Zi-ning Choo[3], Sitara Persad[3,5], Justin LaClair[1], Kayla E Lawrence[1], Ojasvi Chaudhary[3], Tianhao Xu[3], Ignas Masilionis[3], Linas Mazutis[3,6], Ronan Chaligne[3], Dana Pe'er[3§], Charles L Sawyers [1,7§]

[1]Human Oncology and Pathogenesis Program, Memorial Sloan Kettering Cancer Center, New York, NY 10065, USA

[2]Department of Medicine, Thoracic Oncology Service, Memorial Sloan Kettering Cancer Center, New York, NY 10065, USA.

[3]Program for Computational and Systems Biology, Sloan Kettering Institute, Memorial Sloan Kettering Cancer Center, New York, NY 10065, USA.

[4]Current address: Basic sciences division and translational data science IRC, Fred Hutchinson Cancer research center

[5] Department of Computer Science, Columbia University, New York, NY 10027, USA.

[6] Institute of Biotechnology, Life Sciences Centre, Vilnius University, Vilnius, Lithuania

[7] Howard Hughes Medical Institute

† These authors contributed equally

‡These authors contributed equally

§ Corresponding authors to whom correspondence should be addressed

Abstract (167 words)

The inherent plasticity of tumor cells provides a mechanism of resistance to many molecularly targeted therapies, exemplified by adeno-to-neuroendocrine lineage transitions seen in prostate and lung cancer. Here we investigate the root cause of this lineage plasticity in a primary murine prostate organoid model that mirrors the lineage transition seen in patients. These cells lose luminal identity within weeks following deletion of *Trp53* and *Rb1*, ultimately acquiring an Ar-negative, Syp+ phenotype after orthotopic *in vivo* transplantation. Single-cell transcriptomic analysis revealed progressive mixing of luminal-basal lineage features after tumor suppressor gene deletion, accompanied by activation of Jak/Stat and Fgfr pathway signaling and interferon-a and -g gene expression programs prior to any morphologic changes. Genetic or pharmacologic inhibition of Jak1/2 in combination with FGFR blockade restored luminal differentiation and sensitivity to antiandrogen therapy in models with residual AR expression. Collectively, we show lineage plasticity initiates quickly as a largely cell-autonomous process and, through newly developed computational approaches, identify a pharmacological strategy that restores lineage identity using clinical grade inhibitors.

Main (~3450 words)

Although resistance to molecularly targeted therapies is often due to mutations in the drug target, there is growing recognition of other modes of tumor escape, particularly with next-generation inhibitors designed to circumvent target-based resistance mechanisms. For example, in EGFR- and KRAS-mutant lung cancer and in metastatic prostate cancer, tumor cells can undergo a lineage transition from adenocarcinoma to squamous or neuroendocrine histology following treatment with the respective inhibitors (*1*–*6*). Similarly, BRAF-mutant melanomas can transition from a MITF+ differentiated melanocyte phenotype to a more mesenchymal AXL+ cell state or neural crest stem-like state in response to BRAF inhibition (*7*–*9*). Transcriptomic analyses of these changing cell states share features of normal developmental, regenerative and stem cell signatures, suggesting that tumor cells co-opt these gene expression programs to escape lineage-dependent therapies (*10*). Importantly, these plasticity mechanisms are not associated with new genomic alterations and are potentially reversible (*11*, *12*).

The increasing prevalence of this mode of tumor escape has sparked numerous investigations into the underlying mechanism. Analysis of patient specimens, particularly at the single-cell level, has been particularly instructive in defining the complexity of the problem, revealing remarkable heterogeneity within and across patients, as exemplified in our accompanying manuscript and by others (*13*, *14*) . Because these studies typically capture a single snapshot during tumor evolution, it is difficult to discern precisely how plasticity arises. Furthermore, the complexity of genomic alterations in advanced cancers makes it challenging to distinguish between drivers of oncogenicity versus drivers of plasticity-associated drug resistance. To complement these patient-focused studies, we and others have identified several genetic perturbations that can induce plasticity and drug resistance in prostate cancer models, such as loss of tumor suppressor genes (TP53, RB1, PTEN) and activation of transcription factors (MYC, NMYC, SOX2, BRN2) in various combinations (*11*, *15*–*17*). In some cases, these same perturbations can also elicit plasticity phenotypes in lung, providing further evidence for the developmental conservation of these programs across endoderm-derived epithelial tissues(*5*, *15*).

We previously reported conditions for *in vitro* propagation and genetic manipulation of primary prostate organoids under defined, serum-free growth conditions (*18*). Because co-deletion of *Trp53* and *Rb1* in the mouse prostate has been shown to give rise to carcinomas displaying both luminal epithelial and neuroendocrine differentiation(*19*), we asked if a similar phenotype might be seen *ex vivo* by infection of *Trp53*$^{loxP/loxP}$, *Rb1* $^{loxP/loxP}$ organoids with Cre-expressing lentivirus. The presence of a mTmG reporter cassette allowed easy identification and tracking of *Trp53*$^{-/-}$; *Rb*$^{-/-}$ cells due to the red-to-green color change initiated by Cre expression (**Movie S1**). In contrast to the cystic appearance of uninfected organoids, those with *Trp53/Rb1* co-deletion lost their basal/luminal polarity and cystic lumens by ~4 weeks (hereafter called hyperplastic), followed by the appearance of migratory cells and cellular protrusions outside the normally sharp exterior organoid borders at ~8-10 weeks (hereafter called "slithering," based on similarity to the migratory phenotype reported for lung neuroepithelial bodies) (*20*)(**Fig 1A-B, Fig S1A, Fig S2, Movie S2**). This phenotype required deletion of both tumor suppressors and was also seen after CRISPR/Cas9-mediated co-deletion of *Trp53* and *Rb1* in wild-type organoids (**Fig S1B**).

To further characterize the changes induced by *Trp53/Rb1* co-deletion, we performed bulk RNA-seq, western blot analysis and *in situ* immunofluorescence (IF) or immunohistochemistry (IHC) for various lineage markers. The most dramatic finding was reduced expression of luminal lineage genes such as *Nkx3.1, Folh1* (Psma), *Dpp4* (CD26), *Krt18* and *Krt8* and increased expression of mesenchymal genes such as *Snai1*, *Zeb2*, *Vim* (**Fig 1C-D, S1C-D, Table S1**). Other notable gene expression changes include *Wnt5a* and the axon guidance ligand *Slit3*, both of which can promote migratory behavior, and *Fgfr1* which has been implicated in epithelial-mesenchymal transition (EMT) associated drug resistance in prostate cancer as well as EGFR-mutant lung cancer (*21*, *22*). However, unlike the Syp+ neuroendocrine cancer seen in the *Trp53*$^{-/-}$*;Rb1*$^{-/-}$ mouse prostate cancer model, we observed only modest levels of *Syp* and *Chgb* and failed to detect expression of *Chga*, *Ascl1* or *Neurod1*, even in *Trp53*$^{-/-}$*;Rb1*$^{-/-}$ organoids passaged for >12 months.

We postulated the lack of Syp or other neuroendocrine lineage gene expression might be due to absence of critical prostate microenvironmental factors in organoid culture media, and therefore asked if the organoid phenotype evolved further after orthotopic (OT) implantation of *Trp53*$^{-/-}$/*Rb1*$^{-/-}$ organoids into *Trp53*$^{+/+}$; *Rb1*$^{+/+}$ hosts. After confirming highly efficient engraftment of hyperplastic/slithering stage organoids at 4 weeks in a pilot experiment (by detection of GFP+ cells in the dorsal lobe of hormonally intact *NSG* mice), we scored lineage phenotype and tumorigenicity, as well as the effect of androgen blockade, in a larger cohort by treating half the mice with castration and daily enzalutamide (Enz) 4 weeks after OT injection. In the hormonally intact mice, engrafted cells remained Ar+, Syp- (as in organoid culture); however, large foci of Ar-, Syp+ engrafted cells were seen in all mice in the castration + Enz group, indicating progression to a neuroendocrine-like lineage (**Fig S3A-B**). This progression to an Ar-, Syp+ state following androgen receptor signaling inhibition (ARSI) was confirmed across four independent *Trp53/Rb1* co-deletion experiments (**Fig S3C**). To determine if this effect of *in vivo* androgen blockade on lineage plasticity is also observed in culture, we returned to the organoid model and compared the effect of dihydrotestosterone (DHT) versus Enz on the slithering phenotype following *Trp53/Rb1* co-deletion. The percentage of organoids scored as slithering increased from ~10% to >30% (~3-fold) after 7 days of Enz treatment **(Fig S3D**). Thus, sustained Ar signaling plays a role in preserving luminal lineage identity, a conclusion further supported by recent data from a human patient-derived xenograft model (*23*).

The above experiments demonstrate that lineage plasticity can be initiated by co-deletion of *Trp53* and Rb1 in normal mouse prostate organoids grown in bulk culture, which includes basal and luminal cells. To determine if acquisition of plasticity is restricted to either of these populations, we isolated basal (CD49f+) and luminal (CD24+) cells by FACS prior to lentiviral Cre infection and found that both basal and luminal cells can give rise to plasticity in response to co-deletion of *Trp53* and *Rb1* (**Fig 1F-G, S1E-F**).

Having developed a predictable model in which lineage plasticity initiates and evolves, we wanted to characterize the emerging plasticity and elucidate the molecular mechanisms through which this plasticity is induced following co-deletion of *Trp53* and *Rb1*. To characterize the transcriptional cell states and gene

programs that emerge over time, we collected single-cell RNA-sequencing (scRNA-seq) data, beginning 2 weeks after *Trp53/Rb1* co-deletion, prior to any morphologic evidence of plasticity, then at 4 and 8 weeks (**Fig 2A; Table S2**). These experiments were done in bulk-derived organoids in the presence of either DHT or Enz based on the effects of androgen blockade on plasticity described above (**Fig S3**).

We observed great transcriptional heterogeneity both within and between each time point/ condition. To catalog systematically the observed cell states that occurred in our prostate system, we started with the wildtype phenotypic landscape then followed how it remodels following perturbation. To gain a concise description of the observed phenotypic diversity, we used our SEACell algorithm (see methods) to calculate metacells separately within each sample timepoint, then ensured that the resulting metacells were robust (**Fig S4**). The metacell approach(*24*) creates a set of distinct, highly granular cell states by aggregating similar cells to generate a robust, full transcriptomic quantification for each cell state, thus mitigating noise and data sparsity in scRNA-seq. An added benefit of metacells is enumeration of observed cell states that are more amenable for comparison (see **Fig S5** for workflow of metacell versus single-cell analyses).

We first focused on the cell states present in the wild-type organoid. Applying Phenograph clustering (*25*), we identified 5 distinct subpopulations, which we classified as luminal (L-Org1, L-Org2) and as basal (B-Org 1, B-Org 2, B-Org 3) based on published transcriptomes of luminal and basal cells (**see Methods**)(**Fig 2B-C, S6A-B, Table S3-8**). L-Org1 cells share expression of stem-like genes (e.g. *Ly6d*) with L-Org2 cells but also express some basal genes (e.g. *Krt14*), perhaps indicative of a bi-potential population enriched in organoid culture. L-Org2 cells resemble stem-like (Ly6d+, Psca+) luminal cells seen *in vivo* (called L2 in Karthaus et al, LumP in Crowley et al) and *Prom1*, which marks secretory luminal cells seen *in vivo* (*26*, *27*). B-Org1 cells express canonical basal markers (*Krt5*+, *Krt14+*, *Tp63*+), B-Org2 cells express secretory proteins such calcitonin and inhibin A, whereas B-Org3 are largely distinguished by expression of proliferation markers (*Mki67*, *Aurka*).

Analyzing the entire dataset, we found no overlap between the cell states present in the wild-type organoid and the mutant cell states. We visualized all metacells from the entire time-course following *Trp53/Rb1* co-deletion using a force-directed layout (FDL). The metacells organized along the FDL based on time point, with a clearly distinct gap between the wild-type and 2-week timepoint. Strikingly, while the wild-type metacells organized into clear subpopulations, the mutant metacells formed a seemingly disorganized cloud of cell states lacking clear distinction from one another (**Fig 2D**). In a manner similar to the wild-type metacells, we used gene signatures derived from sorted luminal and basal cells to assign luminal versus basal identity to the mutant cells. While we observe clear basal and luminal phenotypes among some mutant metacells, the distinction is far less clear for the majority of the mutant metacells **(Fig S6C**), which express genes associated with both luminal (e.g., *KRT8*) and basal (e.g., *KRT5*) identities (**Fig S6D**). To ensure that the mixed basal-luminal phenotype is not a product of the metacell approach, we repeated the analysis at the level of individual cells and observed similar lineage mixing (**Fig S6E, see Methods**).

To explore and quantify the mixing of basal/luminal identity further, we deconvolved cell phenotype using a Markov-absorption classification approach(*25*) (**see Methods**) which calculates the probability of associating with each of the wild-type sub-populations based on transcriptomic similarity. The key advantage to this graph-based approach is that it scores similarity based on the key axes of gene variation along the phenotypic manifold, giving more weight to the genes that participate in a multitude of intermediate states. As a result, each cell is assigned a vector of classification probabilities for each wild-type subpopulation. While some cells are clearly associated with one subpopulation, others have an uncertain classification indicating basal-luminal mixing. To quantify this mixing, we calculated the entropy of these cell type probabilities and treat this entropy as a proxy measure of plasticity.

To visualize the basal luminal mixing, we plot the classification probabilities for the 3 predominant basal/luminal phenotypes (B-Org2, B-Org3, L-Org2) (**Fig S6F**) as a ternary plot, stratified by sample timepoint (**Fig 2E, Methods**). As expected, the undeleted cells favor a single assignment to their respective populations, but as time progresses, cell type probabilities become less committed to a single basal or

luminal phenotype, eventually converging towards maximal uncertainty at the center of the ternary plot. Interestingly, cells from the Enz-treated samples display even fewer cells favoring the L-Org2 phenotype, consistent with our early data showing that Ar inhibition accelerates loss of luminal identity. Using our entropy-based plasticity score, we observed a time-dependent increase following *Trp53/Rb1* co-deletion (**Fig 2F**) that was robust across parameters (**Fig S6G**). To demonstrate robustness further, we repeated the analysis using an alternative approach dependent only on gene signatures. By calculating a normalized average Z-score of DEGs for the undeleted (wild-type) basal and luminal subpopulations for each single cell (**see Methods**), we again observe increased basal-luminal mixing over time, with a phenotypic shift away from luminal phenotype with Enz treatment and an increase in entropy as a measure of plasticity over time (**Fig S6H-I**).

Having observed an increasing fraction of mixed-lineage cells over time, we sought to better characterize the mixed lineage cell-states. At each timepoint, metacells represent distinct cell states, and we visualize their structure using an FDL on the nearest-neighbor graph (**Fig 2G**). The wild-type metacells clearly partition into a luminal and a basal component with limited paths between them. At two weeks, while the organoids are still morphologically intact, we observe a diversity of distinct intermediate states that mediate an increasing number of connections between the basal and luminal components, suggesting multiple potential paths of transdifferentiation. Over time and with Enz treatment, the diversity of intermediate states and the connectivity between basal and luminal components continue to increase, which we quantify using diffusion distance as an inverse proxy measure of plasticity (**Fig 2H, S6J**).

In summary, our single-cell analyses identify transcriptional changes associated with lineage plasticity early within 2 weeks, well in advance of the morphologic changes that evolve over 4-8 weeks. Furthermore, we quantify an increase in both the fraction of mixed lineage cells and diversity of mixed lineage cell-states over both time and treatment. While lineage tracing is required to assess plasticity conclusively, our quantitative measures of entropy and diffusion distance consistently detect increasing plasticity over time, accelerated by drugs that inhibit Ar pathway signaling.

We next sought to elucidate the candidate pathways that increase plasticity in the mutant organoid. We leveraged our measure of plasticity that increases over time yet still displays a wide range within each timepoint/condition. Thus, for each cell, we correlated our measure of plasticity with gene programs using GSEA (**Table S9-10;** see **Methods**). While correlation does not imply causation, we reasoned that gene programs responsible for plasticity would: (1) correlate to our plasticity measure and (2) activate early in the time course when plasticity begins to arise even before morphological changes take place (week 2 following *Trp53/Rb1* deletion). The top candidate pathways were SMAD2 (EMT), LIF signaling, JAK-STAT and FGFR signaling (**Fig 3A-B, S7A-C; Table S11**). In addition to the expected EMT signature (SMAD2) based on our earlier characterization of bulk organoid cultures (**Fig 1D**), we were surprised to find gene sets consistent with inflammation (LIF signaling, JAK-STAT). Indeed, our entropy-based score was tightly correlated with JAK/STAT activity in each cell (**Fig 3C**). Additionally, these cells also display an interferon response signature (**Fig 3B**). We confirmed JAK/STAT signaling at the protein level by western blot analysis showing elevated phospho-Stat1 (pStat1) and phospho-Stat3 following Trp53/Rb1 deletion (**Fig 3D**).

To interrogate the role of Jak/Stat pathway activation in the initiation of plasticity further, we derived *Trp53*$^{loxP/loxP}$, *Rb1* $^{loxP/loxP}$ organoids in which either *Jak1* or *Jak2* alone or in combination was disrupted using CRISPR/Cas9-directed sgRNAs. We then deleted *Trp53* and *Rb1* by lentiviral Cre infection and scored the percentage of organoids with cystic, hyperplastic or slithering phenotypes at 8 weeks, as in **Fig 1B**. Disruption of *Jak1* or *Jak2* alone blunted upregulation of pStat1 and pStat3, but only modestly impacted development of the plasticity phenotype (a ~6% to ~13% (p=0.01, Jak1 guides) and ~15% (p=0.09 Jak2 guides) increase in cystic organoids and no change in slithering phenotype (~4% versus ~6%)), with most organoids progressing to the hyperplastic morphology (**Fig 3F-G)**. In contrast, organoids with combined *Jak1/Jak2* disruption (which more effectively blocked Stat1/3 phosphorylation) had substantial preservation of cystic morphology (>3-fold increase). This genetic dependence on Jak1 and Jak2 for the development of plasticity raised the question whether pharmacologic intervention might have similar effects, including potential reversal of the organoid morphology that had already progressed to a fully plastic state phenotype.

Indeed, treatment with the dual Jak1/2 kinase inhibitor Ruxolitinib (Rux) restored cystic morphology (from ~5% to ~40%) in a dose-dependent fashion (**Fig 3F, S7D**). As further evidence of reversion to a more luminal lineage, these morphological changes were accompanied by a substantial increase in Ar expression, as well as a return of elevated pStat1 and pStat3 levels back to baseline (**Fig 3E**).

Because our prostate organoids are cultured using defined, serum-free conditions that, notably, do not contain IFN or other known ligands that might activate IFN response genes, we explored potential mechanisms as to how the pathway might be stimulated following *Trp53/Rb1* co-deletion. The enrichment of JAK-STAT3 and LIF signaling signatures suggested that IFN response genes may be activated by cytokine receptors, perhaps through an autocrine loop. We reasoned that if a ligand-receptor pair activates JAK-STAT, then high abundance of the ligand-receptor should correlate with increased JAK-STAT signaling in the mutant organoid cells. A key advantage in our organoid model (versus an *in vivo* setting of plasticity), is that we only needed to consider autocrine ligand-receptor (L-R) interactions and were able to exclude cell type as a variable in L-R analysis. We evaluated a set of 74 L-R pairs known to activate JAK-STAT signaling and scored each candidate based on their correlation with a summary statistic of 33 JAK-STAT associated genes enriched following mutation (**Table S12-13;** see **Methods**).

The top ligand-receptor pairs identified by this analysis were LIF and its heterodimeric receptor (LIFR/IL6ST), FGF1/FGFR, IL15/IL15RA, the chemokines CCL2 and CCL5 and their cognate receptors CCR2 and CCR5, and HGF/MET (**Fig 4A, S8A**). Additionally, we reasoned that the ligand-receptor pairs responsible for an increase in plasticity should display: (1) upregulation of receptor expression early in the time course (week 2), and (2) further upregulation with antiandrogen treatment. Based on these criteria, FGFR and LIF (co)receptors remained as top candidate drivers, based on early expression of FGFR1-3 and LIFR following *Trp53/Rb1* co-deletion as well as increased expression of FGFR1, LIFR and IL6ST following ENZ treatment (**Fig 4B, S8C-D**).

As a first test of these two pathways, we added recombinant FGF1 or LIF to organoids following *Trp53/Rb1* co-deletion, reasoning that plasticity might be further enhanced by an artificial increase in ligand concentration. As a control for our prioritization schema, we included recombinant HGF since HGF was among the top candidates in our L-R analysis, but MET was not substantially upregulated early at week 2 following *Trp53/Rb1* co-deletion or after Enz (**Fig 4A-B, S8B-C**). FGF1, but not LIF or HGF, dramatically enhanced the magnitude of slithering (from 6% to 50% of matrigel surface) within 3 days (**Fig S9A**), providing further support for Fgfr signaling as a driver of plasticity.

The availability of a clinical grade FGFR inhibitor (erdafitinib), together with the fact that FGFR activation has been implicated in prostate cancer progression, including AR-negative, SYP-negative disease (*4*, *22*), led us to examine the functional consequences of pharmacological FGFR inhibition on plasticity, alone and in combination with JAK inhibition. Although treatment with the FGFR inhibitor erdafitinib (Erda) modestly reduced the percentage of organoids with the slithering phenotype, we observed a striking ~12-fold increase (5% to 60%) in cystic morphology when fully plastic organoids were co-treated with Erda + Rux (**Fig 4C-D**). Consistent with this dramatic morphologic change, western blot analysis showed near complete loss of expression of the mesenchymal lineage marker Vim and increased levels of the luminal marker Ck8 and Ar (**Fig 4E**). In contrast, the MET inhibitor Crizotinib had minimal activity and did not enhance the anti-plasticity effect of Rux. The remarkable restoration of cystic luminal organoids following combined Fgfr + Jak kinase inhibition led us to ask if sensitivity to antiandrogen therapy is also restored. First, we noted that neither Erda nor Rux, alone or in combination, had significant antiproliferative effects in *Trp53/Rb1*-deleted organoids, despite their substantial effects in restoring cystic morphology. However, once this cystic morphology was restored (after 14 days), Enz sensitivity was restored to previously Enz-resistant organoids (~50% decrease in proliferation, comparable to wild type organoids) (**Fig 4F, S9B**).

To ask if the *Jak*- and *Fgfr*-dependent plasticity observed in our murine organoid model extends to human prostate cancer, we selected three Enz-resistant patient-derived organoids with combined *TP53/Rb1* deletion to replicate the genetic context of our organoid model (*28*). Combination Rux + Erda treatment of

MSKPCA3 organoids, but not MSKPCA1 and MSKPCA6 organoids, led to enhanced expression of AR and CK8 as well as reduced CK5, consistent with reprogramming toward a luminal lineage phenotype, as well as induction of modest sensitivity to Enz (~20% growth reduction) (**Fig 4G-H, S9C-E**). One potential explanation for the differential sensitivity of the human organoids to Rux + Erda despite shared mutant-*TP53/RB1* genotypes is chromatin accessibility, as suggested by a recent analysis of CRPC tumors (including 2 of the 3 human organoids tested here) that defined 4 distinct subclasses based on transcription factor/transcriptome profiles (*29*). Of note, MSKPCA3 falls into a subclass defined by inflammation, IFN response and EMT pathway signaling, reminiscent of our mouse organoid model, whereas MSKPCA1 maps to a distinct subgroup. In addition, MSKPCA3 and our *Trp53/Rb1*-deleted mouse organoids retain modest levels of AR expression, whereas MSKPCA1 and MSKPCA6 are AR-negative, raising the possibility that reversal of plasticity is only possible in cells with some residual luminal gene expression.

In summary, co-deletion of the Trp53 and Rb1 tumor suppressor genes in normal mouse prostate epithelial cells initiates a program of transcriptional changes that, over a period of weeks, results in mixing of luminal and basal identities and eventual progression to mesenchymal and neuroendocrine lineage phenotypes. We find that execution of this lineage plasticity program is dependent on JAK and FGFR kinase signaling and is reversible through combination therapy with the clinically approved pharmacologic inhibitors Rux and Erda (**Fig 4I**). In the reduced complexity setting of our organoid model (with only epithelial cells present), we identify the IL-6 family cytokine LIF and FGF as the sources of JAK/STAT activation but recognize that microenvironmental stimuli (immune cells) are likely to play a role *in vivo*. Of note, IL-6 has been previously implicated in Ar-negative, pStat3+ tumor progression using cell lines derived from the TRAMP prostate cancer model, where Trp53 and Rb1 function are presumably disabled by expression of SV40 large T antigen (*30*), and LIF expression by pancreatic stellate cells can act as a paracrine factor to promote pancreas cancer progression (*31*). The dependence of tumor cells on JAK/STAT and FGFR signaling to initiate a plasticity program, while compelling from a translational perspective, raises questions about how these pathways intersect with the master regulator transcription factors associated with execution of specific lineage transitions (see accompanying manuscript). Our model suggests that EMT transcription factors are

upregulated commensurate with Jak/Stat and Fgfr activation whereas upregulation of canonical neuroendocrine factors (Ascl1, Neurod1) may occur later and/or require an appropriate microenvironmental niche. Whatever the mechanism, our current work has near term clinical relevance because reversion to luminal lineage identity is accompanied by restored sensitivity to ARSIs. Drugs such as Rux and Erda, as well as EZH2 inhibitors (*12*, *23*), are all compelling candidates to prevent or overcome ARSI resistance in patients at risk for lineage plasticity assuming, as suggested by our human organoid data, we can develop biomarker tools to identify those tumors most amenable to lineage reversion.

Acknowledgements:

Acknowledgements: The authors thank the Pe'er lab and the Sawyers lab for valuable critiques and discussions. Molecular Cytology Core Facility from MSKCC for help with confocal microscopy and IHC. Flow Cytometry Core Facility from MSKCC for help with FACS experiments.

Data accession

All sequencing data is deposited at the Gene Expression Omnibus (GEO) database.

Author contributions

W.R.K, J.C, D.P and C.L.S. conceived the project. W.R.K and C.L.S. designed organoid experiments. W.R.K, J.R.L and S.Z. performed organoid experiments and downstream benchwork. J.C and D.P. designed computational approach. J.C., M.S and D.P. developed computational methods. Z.C., S.P. and D.P. contributed computational methods. J.C. and M.S. performed computational analysis. J.R.L., J.L., K.E.L. and W.R.K. performed mouse work. I.M., O.C. and X.T performed single cell experiments. L.M. and R.C oversaw single cell experiments. D.P., C.L.S, J.C, W.R.K wrote the manuscript. D.P. and C.L.S. oversaw the project.

Grants

C.L.S. is supported by HHMI; National Institute of Health (CA193837, CA092629, CA224079, CA155169, and CA008748), and Starr Cancer Consortium (I12–0007). D.P is supported by U54CA209975 and Starr Cancer Consortium (I14-0023), Alan and Sandra Gerry Metastasis and Tumor Ecosystems Center (D.P., J.M.C., O.C., I.M. and L.M.), AACR Lung Cancer Fellowship (J.M.C.), ASCO Young Investigator Award (J.M.C.) W.R.K. is supported by the Prostate Cancer Foundation PCF 17YOUN10

Competing Interests: C.L.S is on the board of directors of Novartis, is a confounder of ORIC Pharmaceuticals, and is a coinventor of the prostate cancer drugs enzalutamide and apalutamide, covered by U.S. patents 7,709,517, 8,183,274, 9,126,941, 8,445,507, 8,802,689, and 9,388,159 filed by the University of California. C.L.S. is on the scientific advisory boards of the following biotechnology companies: Agios, Beigene, Blueprint, Column Group, Foghorn, Housey Pharma, Nextech, KSQ Therapeutics, Petra Pharma, and PMV Pharma, and is a cofounder of Seragon Pharmaceuticals, purchased by Genentech/Roche in 2014. D.P is on the scientific advisory board of Insitro. W.R.K. is a coinventor of organoid technology.

FIGURE LEGENDS

Figure 1 Establishment of an organoid model of spontaneous lineage plasticity:
A) *Upper:* Representative brightfield pictures of the various organoid phenotypes prior to and 4,6,8 and 10 weeks post *Tp53* and *Rb1* loss. *Lower:* Schematic representation of lineage plasticity development in *Tp53*$^{\Delta/\Delta}$ *Rb1*$^{\Delta/\Delta}$ organoids. Scale bar represents 50 μm.
B) *Left:* Representative H&E staining of LentiCre *Tp53*$^{\Delta/\Delta}$ *Rb1*$^{\Delta/\Delta}$ organoids ~10 weeks post deletion with cystic (A, blue), Hyperplastic (B, red) and slithering (C, silver) phenotypes. *Right:* Bargraph with percentage of organoids in given phenotypes during the time course. Scale bar represents 100 μm.
C) Bargraph of differentially expressed genes between ~10 weeks post deletion (LentiCre *Tp53*$^{\Delta/\Delta}$ *Rb1*$^{\Delta/\Delta}$ organoids) and wild-type (*Tp53*$^{loxP/loxP}$ *Rb1*$^{loxP/loxP}$ organoids) in bulk RNA-seq. DESeq2, FDR ≤ 0.05, Log2 fold change (for full parameters see **Methods**). Genes are colored by association to lineage (Luminal (Red), AR target (Orange), Basal (Green), Epithelial (Blue), Mesenchymal (Yellow), and CRPC (Magenta). Neuroendocrine marker genes were lowly expressed without major difference (*Cghb, Syp*) or not detected (*Cgha, NeuroD1, Ascl1*) in RNA-seq data (see supplementary Table 1).
D) Westernblot verification of differentially expressed genes identified in RNA-seq data in wild-type (*Tp53*$^{loxP/loxP}$ *Rb1*$^{loxP/loxP}$ organoids, left) and ~10 weeks post deletion (LentiCre *Tp53*$^{\Delta/\Delta}$ *Rb1*$^{\Delta/\Delta}$ organoids, right). Proteins as marked. Actin was used as a loading control.
E) Representative IHC of basal markers (p63, Ck5), luminal marker (Ck8) and Ar in wild-type (*Tp53*$^{loxP/loxP}$ *Rb1*$^{loxP/loxP}$ organoids, left) and ~10 weeks post deletion (LentiCre *Tp53*$^{\Delta/\Delta}$ *Rb1*$^{\Delta/\Delta}$ organoids, right). Scale bars represent 100 μm.
F) Schematic representation of single cell cloning experiment of Basal (CD49f^{+}) and Luminal (CD24^{+}) cells. Organoids harboring a Cre recombinase inducible Cas9 (Rosa26 lsl-Cas9 (*32*)) were transduced with guide RNA's targeting *Tp53* and *Rb1* (LentiGuide Puro, guide sequences **Table S__**). Basal and luminal cells were sorted based on CD49f^{+} (Basal) and CD24^{+} (Luminal) expression and subsequently Cas9 was activated by transduction with adenovirus expressing Cre. Approximately 1000 single cells were seeded and grown out. Nutlin-3 and Palbociclib were added 3 days post Cas9 activation to select for *Tp53* and *Rb1* mutant cells. 24 basal and 24 luminal clones were randomly chosen and expanded for 4 weeks.
G) Quantification whole culture phenotypes (Cystic or Hyperplastic) of single cell derived (CD49f^{+} or CD24^{+} FACS sorted) organoids after 4 weeks of culture. Left bargraph absolute number of cultures, right bargraph percentage of cultures in cystic or hyperplastic state.

Figure 2: Single-cell sequencing reveals increased basal-luminal plasticity in the prostate organoid following *RB1/TP53* deletion

A) Experimental design of scRNA-seq time-course sequenced at weeks 0, 2, 4, and 8, with weeks 4 and 8 subjected to either enzalutamide (ENZ) treatment or dihydrotestosterone (DHT) control. Each sample then undergoes enzymatic digestion and subsequent scRNA-seq.
B) Force-directed layout (FDL) of wild-type basal and luminal SEACell metacells, labeled by wild-type subpopulations determined by Phenograph clusters. Edges between metacells indicate the k-nearest neighbors (k = 6) (see **Methods**).
C) Heatmap of mean log2(X+1) expression of DEGs per basal and luminal subpopulation in the wild-type organoid.
D) FDL (k=10) of metacells in the prostate organoid before and after *RB1/TP53* deletion, annotated by either wild-type subpopulations or by time and treatment following mutation.
E) Ternary plots of cell-type classification (based on Markov absorption probabilities) for single cells in the organoid before and after mutation. Each ternary plot represents a timepoint/condition. Each dot is a single cell, plotted using 3 coordinates representing the classification probabilities of the 3 most frequent basal and luminal phenotypes in the wild-type organoid: Basal Org2 (green), Basal Org3 (red), and Luminal Org2 (blue). Color intensity of each dot corresponds to the certainty of cell-type classification, calculated by entropy of their classification probabilities (see **Methods**). Higher entropy indicates greater uncertainty of cell type assignment, increased basal-luminal mixing, a proxy for increased plasticity. The red line at 60%

probability of Luminal Org2 classification at weeks 4 and 8 highlights the decreased probability for Luminal Org2 in Enz-treated samples compared to DHT control.
F) Boxplot of entropy of cell-type classification probabilities for single cells per timepoint in (**G**) as a measure of basal-luminal mixing and plasticity over time and treatment (Wilcoxon rank-sum test). p-values: ***<0.001
G) FDL of metacells within each timepoint/treatment. Nodes represent metacells, and edges represent k-nearest neighbors (k = 3% of the number of metacells per timepoint). Metacell nodes are colored based on correlation to bulk-sorted basal CD49f+ and luminal CD24+ cells. Each FDL is divided into two predominantly basal vs luminal partitions, annotated by pale red (basal) and pale blue (luminal) polygons, determined by attributed stochastic block model (aSBM) (**see Methods**).
H) Boxplot of log mean diffusion distances between basal and luminal partitions for each FDL in (**G**), as an inverse measure of plasticity over time and treatment (Wilcoxon rank-sum test, see **Methods**). p-values: ***<0.001

Figure 3: JAK/STAT signaling drives increased plasticity in the *Rb1/Tp53*-deleted prostate organoid.

A) Heatmap of select pathways from the top 10% correlated to plasticity across timepoints (see **Figure S5C, Table S11**). Each pathway score is measured as the average Z-score of gene expression in each pathway among SEACells. Rows (pathways) are ordered by increasing pathway score from bottom to top in the early timepoint at week 2, with JAK/STAT and LIF signaling scoring the highest (see **Methods**).
B), FDL of SEACells in the prostate organoid cells before and after *RB1/TP53* deletion (same layout as **Fig 2D**), scored by key pathways enriched in the mutant setting. Scores are calculated by average Z-score of the leading-edge gene subsets calculated by GSEA for the following pathways from MSigDB: HALLMARK_IL6_JAK_STAT3_SIGNALING, ABBUD_LIF_SIGNALING_1_UP, REACTOME_INTERFERON_ALPHA_BETA_SIGNALING, and a curated signature of FGFR signaling in prostate adenocarcinoma based on Acevedo, et al.(*22*) combined with FGFR1-3 and FGF ligands (see **Methods**).
C) Scatterplot of JAK/STAT signaling score vs plasticity as measured by average entropy of cell-type classification probabilities per metacell. JAK/STAT score is measured by average Z-score of the leading-edge gene subset of KEGG_JAK_STAT_SIGNALING_PATHWAY and HALLMARK_IL6_JAK_STAT3_SIGNALING. For visualization, the entropy of classification probabilities was first calculated for each single cell and then averaged per metacell. A linear fit is shown with Pearson's correlation of 0.74.
D) Westernblot of Stat1 and phosphorylated Stat1 (p-Stat1) in LentiCre $Tp53^{\Delta/\Delta}$ $Rb1^{\Delta/\Delta}$ organoids cultured with 50 ng/ml or 0 ng/ml EGF for 7 days. Actin was used a loading control.
E) Westernblot of AR in 21-day Ruxolitinib treated (0, 10 nM, 100 nM, 5 μM, 10 μM, 10 μM) organoids
F) Bargraph with percentage of cystic (Blue), Hyperplastic (Red) and slithering (Silver) phenotypes in LentiCre $Tp53^{\Delta/\Delta}$ $Rb1^{\Delta/\Delta}$ organoids with CRISPR/Cas9 mediated Jak1 knockout (two independent guide RNA's), Jak2 Knockout (two independent guide RNA's), Jak1/Jak2 double knockout (Combination of two independent guide RNA's), a control non targeting guide RNA and Ruxolitinib treated organoids.
G) Westernblot of JAK-STAT signaling components in LentiCre $Tp53^{\Delta/\Delta}$ $Rb1^{\Delta/\Delta}$ organoids with CRISPR/Cas9 mediated knockout of Jak1 and/or Jak2 (2 separate gRNAs per target). Proteins probed as labeled, Actin was used as a loading control. Proteins as marked.

Figure 4: Pharmacological inhibition of JAK-STAT signaling and FGFR signaling resensitizes prostate cancer organoids to ARSI.
A) Barplot showing the top scoring ligand-receptor (L-R) interactions known to activate JAK/STAT signaling, based on adjusted R^2 (R_{adj}^2) of the regression $JAK\_STAT \sim L + R + L{:}R$, where *JAK_STAT* is the JAK/STAT signaling score, and *L* and *R* represent scaled imputed ligand and receptor expression (see **Methods**). Only L-R pairs with non-zero R_{adj}^2 are shown. Red asterisks indicate L-R pairs where *R* is overexpressed early at timepoint week 2 (see **Figure S8B**).

B) Heatmap of mean gene expression (rows) over sample timepoints (columns) for candidate receptors activating downstream JAK/STAT signaling in SEACells. Receptor genes are ordered by increasing expression in the early timepoint at week 2 from bottom to top.
C) Quantification of phenotypes cystic (Blue), Hyperplastic (Red) and slithering (Silver) of *Tp53*$^{\Delta/\Delta}$ *Rb1*$^{\Delta/\Delta}$ organoids treated for 14 days with indicated drugs, see methods for exact medium composition.
D) Representative brightfield pictures, H&E staining and IHC of CK8, Ck5 and Vimentin of *Tp53*$^{\Delta/\Delta}$ *Rb1*$^{\Delta/\Delta}$ organoids treated for 14 days with indicated drugs. Scale bars represent 100 μm.
E) Western blot of lineage markers and JAK-STAT signaling components in *Tp53*$^{\Delta/\Delta}$ *Rb1*$^{\Delta/\Delta}$ organoids treated for 14 days with indicated drugs, see methods for exact medium composition. Proteins probed as indicated. Actin was used as a loading control.
F) Top: Schematic overview of resensitization drug experiments. Organoids are treated with Erdafitinib 100 nM and Ruxolitinib 10 μM for 14 days in low Egf organoid medium (ENR+A83+DHT), control organoids were cultured in low EGF organoid medium for 14 days. Subsequently organoids (10000 cells per well, triplicate) are reseeded in organoid culture medium without EGF (NR+A83), containing an AR agonist (DHT 1 nM) or antagonist (Enzalutamide 10 μM). Viability was measured by CellTiterGlo after 7 days of Enzalutamide treatment of *Tp53*$^{\Delta/\Delta}$ *Rb1*$^{\Delta/\Delta}$ organoids treated for 14 days with indicated drugs (Lower). See methods for exact medium composition.
G) Westernblot of lineage markers and JAK-STAT signaling components in MSKPCA3 organoid after 14 days treatment with Erdafitinib 100 nM, Ruxolitinib 10 μM or with Erdafitinib 100 nM & Ruxolitinib 10 μM combination. Proteins probed as indicated. Actin was used as a loading control.
H) Representative histology and IHC (CK8, CK5 and Vimentin) of MSKPCA3 organoids after 14 days treatment with Erdafitinib (100 nM) & Ruxolitinib (10 μM) combination in full organoid medium (ENRFFPN, A83-01, Nicotinamide, DHT). See methods for exact medium composition. Scale bars represent 100 μm.
I) Proposed model system of lineage plasticity. JAK-STAT signaling activation and FGFR signaling activation leads to a AR^{low}, ARSI insensitive state that can be reprogrammed back to an ARSI sensitive state. Potentially the JAK-STAT^{high}, AR^{low}, ARSI insensitive state is a cellular state preceding AR negative ARSI insensitive CRPC.

Figure 1

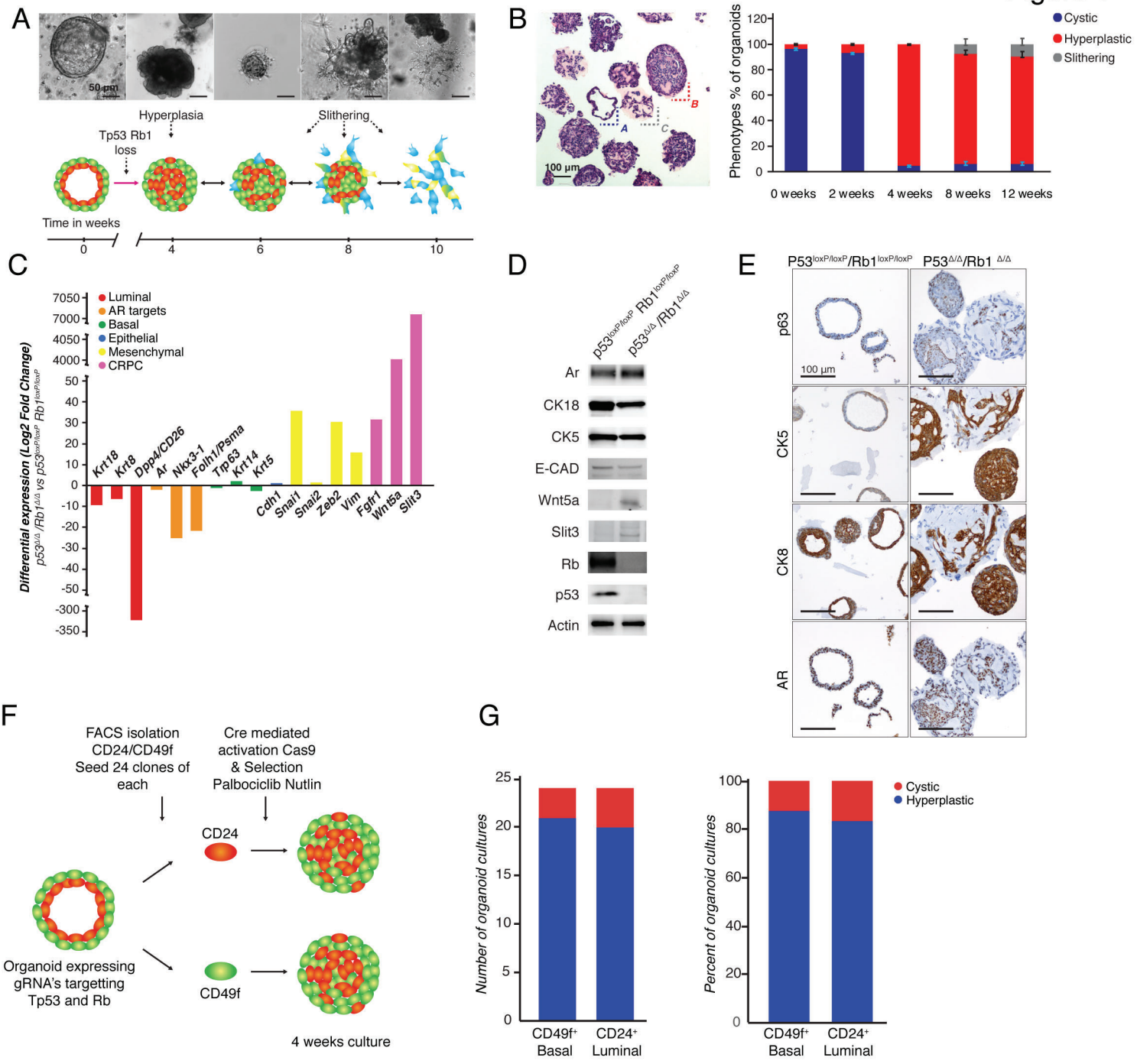

Figure 2

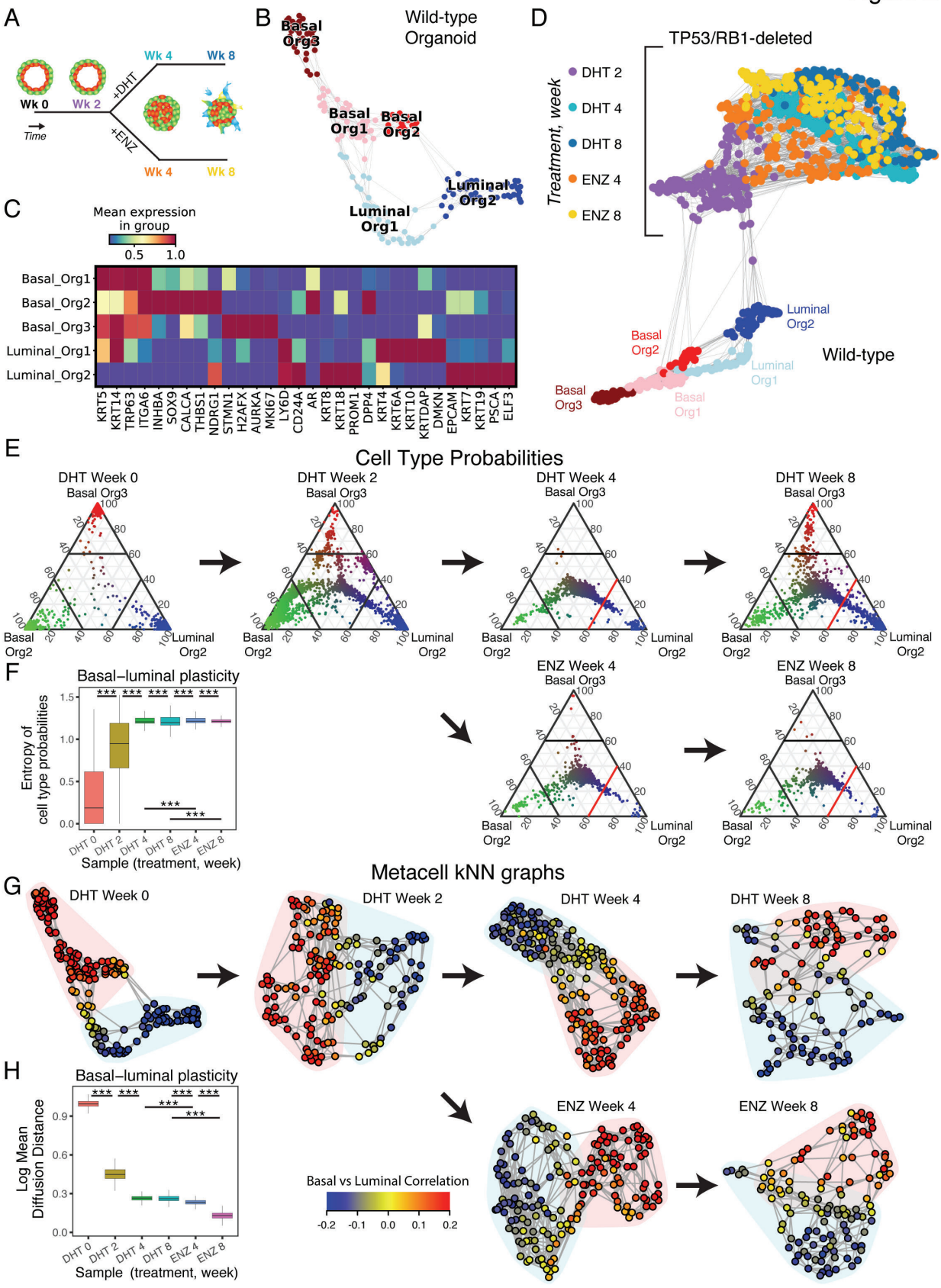

Figure 3

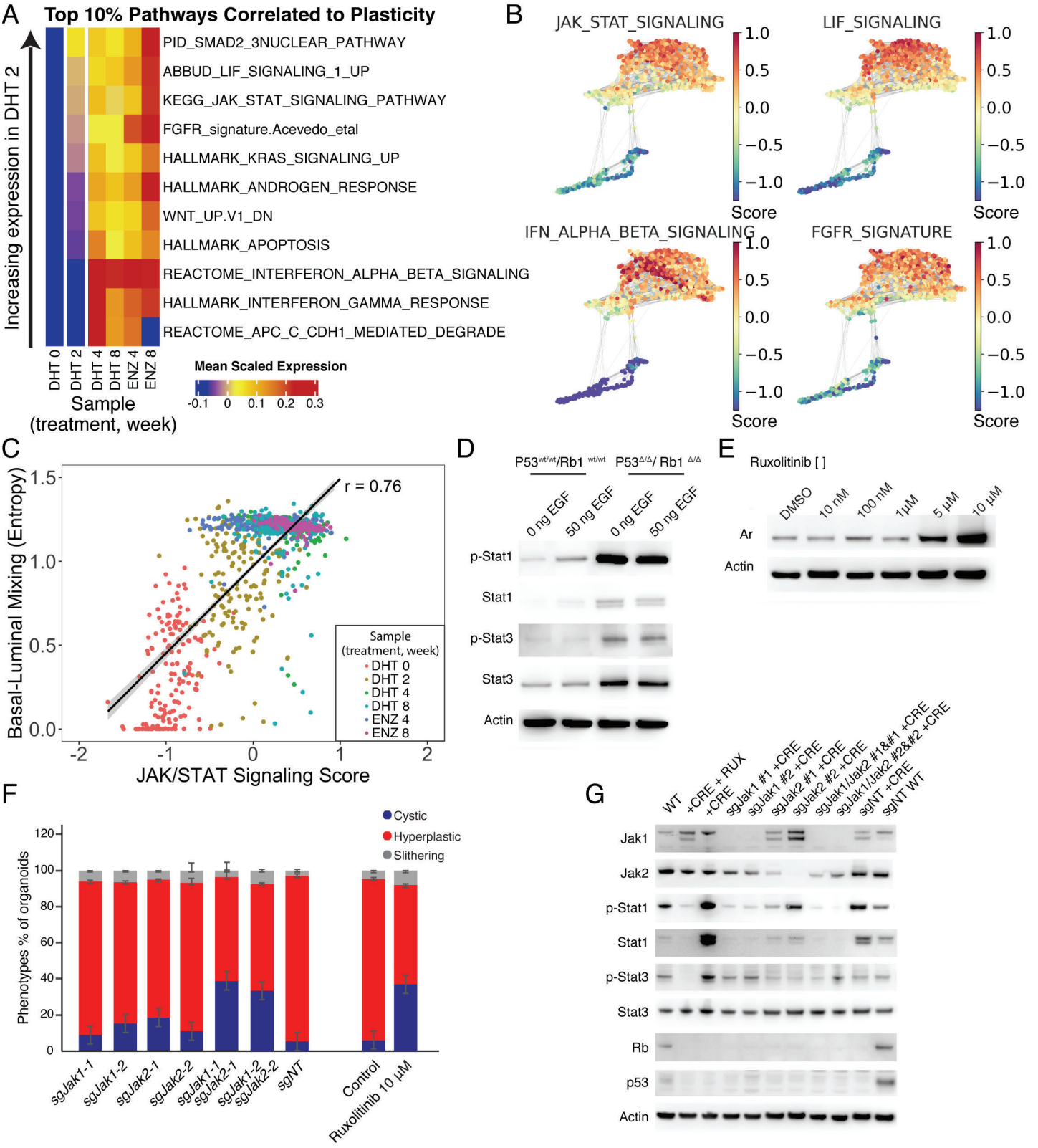

Figure 4

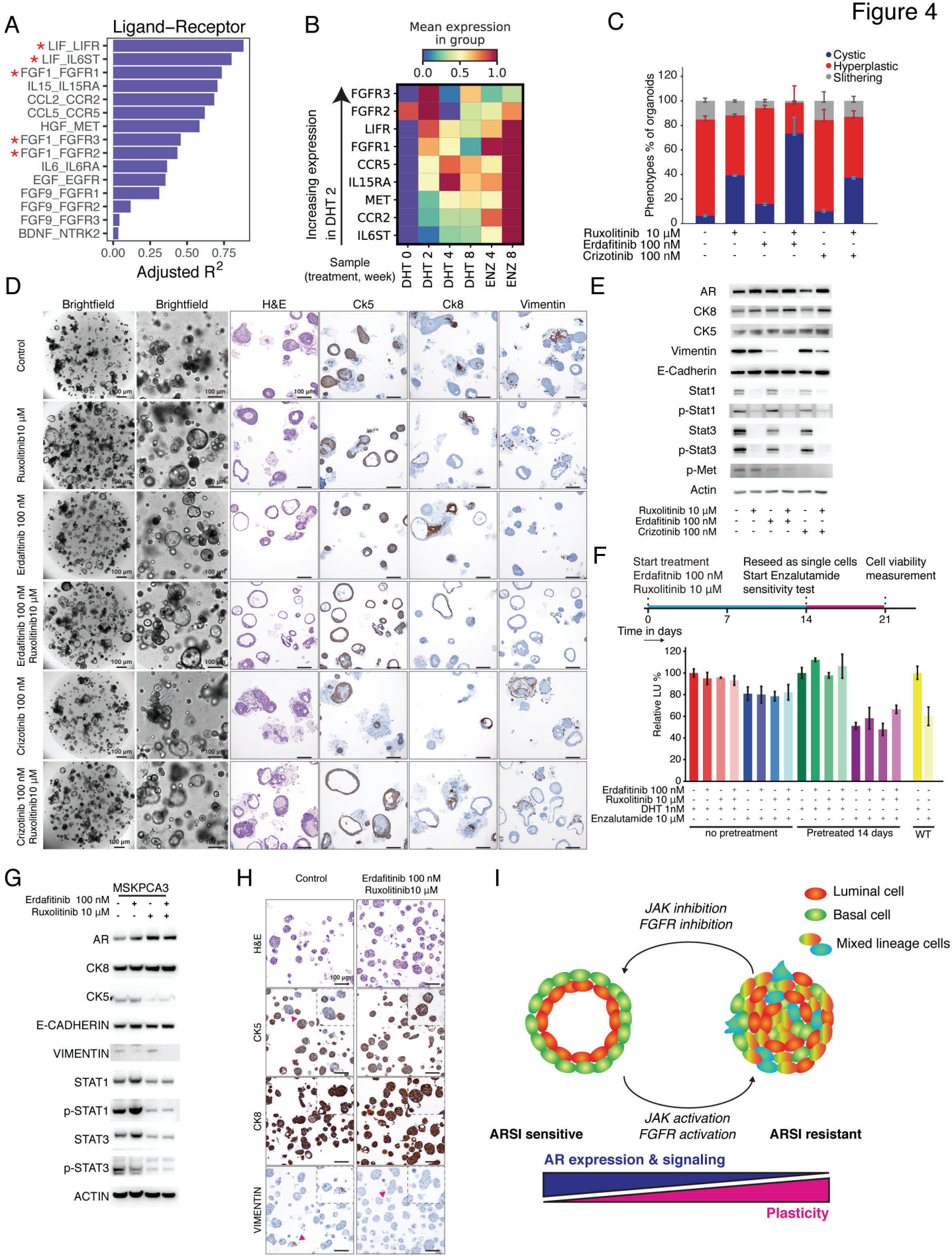

References

1. L. V Sequist, B. A. Waltman, D. Dias-Santagata, S. Digumarthy, A. B. Turke, P. Fidias, K. Bergethon, A. T. Shaw, S. Gettinger, A. K. Cosper, S. Akhavanfard, R. S. Heist, J. Temel, J. G. Christensen, J. C. Wain, T. J. Lynch, K. Vernovsky, E. J. Mark, M. Lanuti, A. J. Iafrate, M. Mino-Kenudson, J. A. Engelman, Genotypic and histological evolution of lung cancers acquiring resistance to EGFR inhibitors. *Sci. Transl. Med.* **3**, 75ra26 (2011).
2. M. M. Awad, S. Liu, I. I. Rybkin, K. C. Arbour, J. Dilly, V. W. Zhu, M. L. Johnson, R. S. Heist, T. Patil, G. J. Riely, J. O. Jacobson, X. Yang, N. S. Persky, D. E. Root, K. E. Lowder, H. Feng, S. S. Zhang, K. M. Haigis, Y. P. Hung, L. M. Sholl, B. M. Wolpin, J. Wiese, J. Christiansen, J. Lee, A. B. Schrock, L. P. Lim, K. Garg, M. Li, L. D. Engstrom, L. Waters, J. D. Lawson, P. Olson, P. Lito, S.-H. I. Ou, J. G. Christensen, P. A. Jänne, A. J. Aguirre, Acquired Resistance to KRAS G12C Inhibition in Cancer . *N. Engl. J. Med.* **384**, 2382–2393 (2021).
3. P. A. Watson, V. K. Arora, C. L. Sawyers, Emerging mechanisms of resistance to androgen receptor inhibitors in prostate cancer. *Nat. Rev. Cancer*. **15**, 701–711 (2015).
4. E. G. Bluemn, I. M. Coleman, J. M. Lucas, R. T. Coleman, S. Hernandez-Lopez, R. Tharakan, D. Bianchi-Frias, R. F. Dumpit, A. Kaipainen, A. N. Corella, Y. C. Yang, M. D. Nyquist, E. Mostaghel, A. C. Hsieh, X. Zhang, E. Corey, L. G. Brown, H. M. Nguyen, K. Pienta, M. Ittmann, M. Schweizer, L. D. True, D. Wise, P. S. Rennie, R. L. Vessella, C. Morrissey, P. S. Nelson, Androgen Receptor Pathway-Independent Prostate Cancer Is Sustained through FGF Signaling. *Cancer Cell*. **32**, 474-489.e6 (2017).
5. Á. Quintanal-Villalonga, J. M. Chan, H. A. Yu, D. Pe'er, C. L. Sawyers, T. Sen, C. M. Rudin, Lineage plasticity in cancer: a shared pathway of therapeutic resistance. *Nat. Rev. Clin. Oncol.* **17**, 360–371 (2020).
6. A. J. Schoenfeld, J. M. Chan, D. Kubota, H. Sato, H. Rizvi, Y. Daneshbod, J. C. Chang, P. K. Paik, M. Offin, M. E. Arcila, M. A. Davare, U. Shinde, D. Pe'er, N. Rekhtman, M. G. Kris, R. Somwar, G. J. Riely, M. Ladanyi, H. A. Yu, *Clin. Cancer Res.*, in press, doi:10.1158/1078-0432.CCR-19-3563.

7. I. Tirosh, B. Izar, S. M. Prakadan, M. H. Wadsworth, D. Treacy, J. J. Trombetta, A. Rotem, C. Rodman, C. Lian, G. Murphy, M. Fallahi-Sichani, K. Dutton-Regester, J.-R. Lin, O. Cohen, P. Shah, D. Lu, A. S. Genshaft, T. K. Hughes, C. G. K. Ziegler, S. W. Kazer, A. Gaillard, K. E. Kolb, A.-C. Villani, C. M. Johannessen, A. Y. Andreev, E. M. Van Allen, M. Bertagnolli, P. K. Sorger, R. J. Sullivan, K. T. Flaherty, D. T. Frederick, J. Jané-Valbuena, C. H. Yoon, O. Rozenblatt-Rosen, A. K. Shalek, A. Regev, L. A. Garraway, Dissecting the multicellular ecosystem of metastatic melanoma by single-cell RNA-seq. *Science (80-.).* **352**, 189–196 (2016).

8. D. J. Konieczkowski, C. M. Johannessen, O. Abudayyeh, J. W. Kim, Z. A. Cooper, A. Piris, D. T. Frederick, M. Barzily-Rokni, R. Straussman, R. Haq, D. E. Fisher, J. P. Mesirov, W. C. Hahn, K. T. Flaherty, J. A. Wargo, P. Tamayo, L. A. Garraway, A melanoma cell state distinction influences sensitivity to MAPK pathway inhibitors. *Cancer Discov.* **4**, 816–827 (2014).

9. F. Rambow, A. Rogiers, O. Marin-Bejar, S. Aibar, J. Femel, M. Dewaele, P. Karras, D. Brown, Y. H. Chang, M. Debiec-Rychter, C. Adriaens, E. Radaelli, P. Wolter, O. Bechter, R. Dummer, M. Levesque, A. Piris, D. T. Frederick, G. Boland, K. T. Flaherty, J. van den Oord, T. Voet, S. Aerts, A. W. Lund, J. C. Marine, Toward Minimal Residual Disease-Directed Therapy in Melanoma. *Cell.* **174**, 843-855.e19 (2018).

10. A. M. Laughney, J. Hu, N. R. Campbell, S. F. Bakhoum, M. Setty, V. P. Lavallée, Y. Xie, I. Masilionis, A. J. Carr, S. Kottapalli, V. Allaj, M. Mattar, N. Rekhtman, J. B. Xavier, L. Mazutis, J. T. Poirier, C. M. Rudin, D. Pe'er, J. Massagué, *Regenerative lineages and immune-mediated pruning in lung cancer metastasis* (Springer US, 2020), vol. 26.

11. P. Mu, Z. Zhang, M. Benelli, W. R. Karthaus, E. Hoover, C.-C. Chen, J. Wongvipat, S.-Y. Ku, D. Gao, Z. Cao, N. Shah, E. J. Adams, W. Abida, P. A. Watson, D. Prandi, C.-H. Huang, E. de Stanchina, S. W. Lowe, L. Ellis, H. Beltran, M. A. Rubin, D. W. Goodrich, F. Demichelis, C. L. Sawyers, SOX2 promotes lineage plasticity and antiandrogen resistance in TP53- and RB1-deficient prostate cancer. *Science*. **355**, 84–88 (2017).

12. S. Y. Ku, S. Rosario, Y. Wang, P. Mu, M. Seshadri, Z. W. Goodrich, M. M. Goodrich, D. P. Labbé, E. C. Gomez, J. Wang, H. W. Long, B. Xu, M. Brown, M. Loda, C. L. Sawyers, L. Ellis, D. W.

Goodrich, Rb1 and Trp53 cooperate to suppress prostate cancer lineage plasticity, metastasis, and antiandrogen resistance. *Science (80-.).* **355**, 78–83 (2017).

13. M. X. He, M. S. Cuoco, J. Crowdis, A. Bosma-Moody, Z. Zhang, K. Bi, A. Kanodia, M. J. Su, S. Y. Ku, M. M. Garcia, A. R. Sweet, C. Rodman, L. DelloStritto, R. Silver, J. Steinharter, P. Shah, B. Izar, N. C. Walk, K. P. Burke, Z. Bakouny, A. K. Tewari, D. Liu, S. Y. Camp, N. I. Vokes, K. Salari, J. Park, S. Vigneau, L. Fong, J. W. Russo, X. Yuan, S. P. Balk, H. Beltran, O. Rozenblatt-Rosen, A. Regev, A. Rotem, M. E. Taplin, E. M. Van Allen, Transcriptional mediators of treatment resistance in lethal prostate cancer. *Nat. Med.* **27**, 426–433 (2021).

14. B. Dong, J. Miao, Y. Wang, W. Luo, Z. Ji, H. Lai, M. Zhang, X. Cheng, J. Wang, Y. Fang, H. H. Zhu, C. W. Chua, L. Fan, Y. Zhu, J. Pan, J. Wang, W. Xue, W. Q. Gao, Single-cell analysis supports a luminal-neuroendocrine transdifferentiation in human prostate cancer. *Commun. Biol.* **3** (2020), doi:10.1038/s42003-020-01476-1.

15. J. W. Park, J. K. Lee, K. M. Sheu, L. Wang, N. G. Balanis, K. Nguyen, B. A. Smith, C. Cheng, B. L. Tsai, D. Cheng, J. Huang, S. K. Kurdistani, T. G. Graeber, O. N. Witte, Reprogramming normal human epithelial tissues to a common, lethal neuroendocrine cancer lineage. *Science (80-.).* **362**, 91–95 (2018).

16. A. Berger, N. J. Brady, R. Bareja, B. Robinson, V. Conteduca, M. A. Augello, L. Puca, A. Ahmed, E. Dardenne, X. Lu, I. Hwang, A. M. Bagadion, A. Sboner, O. Elemento, J. Paik, J. Yu, C. E. Barbieri, N. Dephoure, H. Beltran, D. S. Rickman, N-Myc-mediated epigenetic reprogramming drives lineage plasticity in advanced prostate cancer. *J. Clin. Invest.* **129**, 3924–3940 (2019).

17. J. L. Bishop, D. Thaper, S. Vahid, A. Davies, K. Ketola, H. Kuruma, R. Jama, K. M. Nip, A. Angeles, F. Johnson, A. W. Wyatt, L. Fazli, M. E. Gleave, D. Lin, M. A. Rubin, C. C. Collins, Y. Wang, H. Beltran, A. Zoubeidi, The Master Neural Transcription Factor BRN2 Is an Androgen Receptor–Suppressed Driver of Neuroendocrine Differentiation in Prostate Cancer. *Cancer Discov.* **7**, 54–71 (2017).

18. W. R. Karthaus, P. J. Iaquinta, J. Drost, A. Gracanin, R. van Boxtel, J. Wongvipat, C. M. Dowling, D. Gao, H. Begthel, N. Sachs, R. G. J. J. Vries, E. Cuppen, Y. Chen, C. L. Sawyers, H. C. Clevers,

Identification of Multipotent Luminal Progenitor Cells in Human Prostate Organoid Cultures. *Cell*. **159**, 163–175 (2014).

19. Z. Zhou, A. Flesken-Nikitin, D. C. Corney, W. Wang, D. W. Goodrich, P. Roy-Burman, A. Y. Nikitin, Synergy of p53 and Rb Deficiency in a Conditional Mouse Model for Metastatic Prostate Cancer. *Cancer Res.* **66**, 7889–7898 (2006).

20. C. S. Kuo, M. A. Krasnow, Formation of a Neurosensory Organ by Epithelial Cell Slithering. *Cell*. **163**, 394–405 (2015).

21. S. Raoof, I. J. Mulford, H. Frisco-Cabanos, V. Nangia, D. Timonina, E. Labrot, N. Hafeez, S. J. Bilton, Y. Drier, F. Ji, M. Greenberg, A. Williams, K. Kattermann, L. Damon, S. Sovath, D. P. Rakiec, J. M. Korn, D. A. Ruddy, C. H. Benes, P. S. Hammerman, Z. Piotrowska, L. V. Sequist, M. J. Niederst, J. Barretina, J. A. Engelman, A. N. Hata, Targeting FGFR overcomes EMT-mediated resistance in EGFR mutant non-small cell lung cancer. *Oncogene*. **38**, 6399–6413 (2019).

22. V. D. Acevedo, R. D. Gangula, K. W. Freeman, R. Li, Y. Zhang, F. Wang, G. E. Ayala, L. E. Peterson, M. Ittmann, D. M. Spencer, Inducible FGFR-1 activation leads to irreversible prostate adenocarcinoma and an epithelial-to-mesenchymal transition. *Cancer Cell*. **12**, 559–571 (2007).

23. A. Davies, S. Nouruzi, D. Ganguli, T. Namekawa, D. Thaper, S. Linder, F. Karaoğlanoğlu, M. E. Omur, S. Kim, M. Kobelev, S. Kumar, O. Sivak, C. Bostock, J. Bishop, M. Hoogstraat, A. Talal, S. Stelloo, H. van der Poel, A. M. Bergman, M. Ahmed, L. Fazli, H. Huang, W. Tilley, D. Goodrich, F. Y. Feng, M. Gleave, H. H. He, F. Hach, W. Zwart, H. Beltran, L. Selth, A. Zoubeidi, *An androgen receptor switch underlies lineage infidelity in treatment-resistant prostate cancer* (Springer US, 2021), vol. 23.

24. Y. Baran, A. Bercovich, A. Sebe-Pedros, Y. Lubling, A. Giladi, E. Chomsky, Z. Meir, M. Hoichman, A. Lifshitz, A. Tanay, MetaCell: analysis of single-cell RNA-seq data using K-nn graph partitions. *Genome Biol.* **20**, 206 (2019).

25. J. H. Levine, E. F. Simonds, S. C. Bendall, K. L. Davis, E. A. D. Amir, M. D. Tadmor, O. Litvin, H. G. Fienberg, A. Jager, E. R. Zunder, R. Finck, A. L. Gedman, I. Radtke, J. R. Downing, D. Pe'er, G. P. Nolan, Data-Driven Phenotypic Dissection of AML Reveals Progenitor-like Cells that

Correlate with Prognosis. *Cell*. **162**, 184–197 (2015).

26. W. R. Karthaus, M. Hofree, D. Choi, E. L. Linton, M. Turkekul, A. Bejnood, B. Carver, A. Gopalan, W. Abida, V. Laudone, M. Biton, O. Chaudhary, T. Xu, I. Masilionis, K. Manova, L. Mazutis, D. Pe'er, A. Regev, C. L. Sawyers, *Science (80-.).*, in press, doi:10.1126/science.aay0267.

27. L. Crowley, F. Cambuli, L. Aparicio, M. Shibata, B. D. Robinson, S. Xuan, W. Li, H. Hibshoosh, M. Loda, R. Rabadan, M. M. Shen, A single-cell atlas of the mouse and human prostate reveals heterogeneity and conservation of epithelial progenitors. *Elife*. **9**, 1–24 (2020).

28. D. Gao, I. Vela, A. Sboner, P. J. Iaquinta, W. R. Karthaus, A. Gopalan, C. Dowling, J. N. Wanjala, E. A. Undvall, V. K. Arora, J. Wongvipat, M. Kossai, S. Ramazanoglu, L. P. Barboza, W. Di, Z. Cao, Q. F. Zhang, I. Sirota, L. Ran, T. Y. MacDonald, H. Beltran, J.-M. M. Mosquera, K. A. Touijer, P. T. Scardino, V. P. Laudone, K. R. Curtis, D. E. Rathkopf, M. J. Morris, D. C. Danila, S. F. Slovin, S. B. Solomon, J. A. Eastham, P. Chi, B. Carver, M. A. Rubin, H. I. Scher, H. Clevers, C. L. Sawyers, Y. Chen, Organoid cultures derived from patients with advanced prostate cancer. *Cell*. **159**, 176–187 (2014).

29. T. Tang, F. F., W. Wang, S. S., W. Wong, C. K., L. Lee, C. J., C. Cohen, S. S., P. Park, J. J., H. Hill, C. E., E. Eng, K. K., B. Bareja, R. R., H. Han, T. T., L. Liu, E. M., P. Palladino, A. A., D. Di, W. W., G. Gao, D. D., A. Abida, W. W., B. Beg, S. S., P. Puca, L. L., B. Berger, M. F., G. Gopalan, A. A., D. Dow, L. E., M. Mosquera, J. M., B. Beltran, H. H., S. Sternberg, C. N., C. Chi, P. P., S. Scher, H. I., S. Sboner, A. A., C. Chen, Y. Y., K. Khurana, E. E., Chromatin accessibility profiles of castration-resistant prostate cancers reveal novel subtypes and therapeutic vulnerabilities. *bioRxiv Cancer Biol.* (2020).

30. A. Schroeder, A. Herrmann, G. Cherryholmes, C. Kowolik, R. Buettner, S. Pal, H. Yu, G. Muller-Newen, R. Jove, Loss of Androgen Receptor Expression Promotes a Stem-like Cell Phenotype in Prostate Cancer through STAT3 Signaling. *Cancer Res.* **74**, 1227–1237 (2014).

31. Y. Shi, W. Gao, N. K. Lytle, P. Huang, X. Yuan, A. M. Dann, M. Ridinger-Saison, K. E. DelGiorno, C. E. Antal, G. Liang, A. R. Atkins, G. Erikson, H. Sun, J. Meisenhelder, E. Terenziani, G. Woo, L. Fang, T. P. Santisakultarm, U. Manor, R. Xu, C. R. Becerra, E. Borazanci, D. D. Von Hoff, P. M.

Grandgenett, M. A. Hollingsworth, M. Leblanc, S. E. Umetsu, E. A. Collisson, M. Scadeng, A. M. Lowy, T. R. Donahue, T. Reya, M. Downes, R. M. Evans, G. M. Wahl, T. Pawson, R. Tian, T. Hunter, Targeting LIF-mediated paracrine interaction for pancreatic cancer therapy and monitoring. *Nature*. **569**, 131–135 (2019).

32. R. J. Platt, S. Chen, Y. Zhou, M. J. Yim, L. Swiech, H. R. Kempton, J. E. Dahlman, O. Parnas, T. M. Eisenhaure, M. Jovanovic, D. B. Graham, S. Jhunjhunwala, M. Heidenreich, R. J. Xavier, R. Langer, D. G. Anderson, N. Hacohen, A. Regev, G. Feng, P. A. Sharp, F. Zhang, CRISPR-Cas9 Knockin Mice for Genome Editing and Cancer Modeling. *Cell*, 1–16 (2014).

33. W. R. Karthaus, D. Gao, E. Driehuis, C. L. Sawyers, Y. Chen, J. Drost, H. Clevers, Organoid culture systems for prostate epithelial and cancer tissue. *Nat. Protoc.* **11**, 347–358 (2016).

34. B.-K. K. Koo, D. E. Stange, T. Sato, W. Karthaus, H. F. Farin, M. Huch, J. H. van Es, H. Clevers, Controlled gene expression in primary Lgr5 organoid cultures. *Nat. Methods*. **9**, 81–83 (2011).

35. N. E. Sanjana, O. Shalem, F. Zhang, Improved vectors and genome-wide libraries for CRISPR screening. *Nat. Methods*. **11**, 783–784 (2014).

36. K. J. Pappas, D. Choi, C. L. Sawyers, W. R. Karthaus, Prostate Organoid Cultures as Tools to Translate Genotypes and Mutational Profiles to Pharmacological Responses. *J. Vis. Exp.*, 1–7 (2019).

37. R. Bose, W. R. Karthaus, J. Armenia, W. Abida, P. J. Iaquinta, Z. Zhang, J. Wongvipat, E. V Wasmuth, N. Shah, P. S. Sullivan, M. G. Doran, P. Wang, A. Patruno, Y. Zhao, D. Zheng, N. Schultz, C. L. Sawyers, ERF mutations reveal a balance of ETS factors controlling prostate oncogenesis. *Nat. Publ. Gr.* **546**, 671–675 (2017).

38. E. Azizi, A. J. Carr, G. Plitas, A. E. Cornish, C. Konopacki, S. Prabhakaran, J. Nainys, K. Wu, V. Kiseliovas, M. Setty, K. Choi, R. M. Fromme, P. Dao, P. T. McKenney, R. C. Wasti, K. Kadaveru, L. Mazutis, A. Y. Rudensky, D. Pe'er, Single-Cell Map of Diverse Immune Phenotypes in the Breast Tumor Microenvironment. *Cell*. **174**, 1293-1308.e36 (2018).

39. A. T. L. Lun, S. Riesenfeld, T. Andrews, T. P. Dao, T. Gomes, J. C. Marioni, participants in the 1st H. C. A. Jamboree, EmptyDrops: distinguishing cells from empty droplets in droplet-based single-

cell RNA sequencing data. *Genome Biol.* **20**, 63 (2019).

40. C. Hafemeister, R. Satija, Normalization and variance stabilization of single-cell RNA-seq data using regularized negative binomial regression. *Genome Biol.* **20**, 296 (2019).

41. D. van Dijk, J. Nainys, R. Sharma, P. Kathail, A. J. Carr, K. R. Moon, L. Mazutis, G. Wolf, S. Krishnaswamy, D. Pe'er, MAGIC: A diffusion-based imputation method reveals gene-gene interactions in single-cell RNA-sequencing data. *bioRxiv*, 111591 (2017).

42. F. A. Wolf, P. Angerer, F. J. Theis, SCANPY: large-scale single-cell gene expression data analysis. *Genome Biol.* **19**, 15 (2018).

43. S. C. Wei, R. Sharma, N.-A. Anang, J. Levine, Y. Zhao, J. Wang, D. Pe'er, J. P. Allison, *J. Immunol.*, in press (available at http://www.jimmunol.org/content/200/1_Supplement/171.17.abstract).

44. C. Boutsidis, M. W. Mahoney, P. Drineas, An Improved Approximation Algorithm for the Column Subset Selection Problem (2010).

45. J. H. Levine, E. F. Simonds, S. C. Bendall, K. L. Davis, E. D. Amir, M. D. Tadmor, O. Litvin, H. G. Fienberg, A. Jager, E. R. Zunder, R. Finck, A. L. Gedman, I. Radtke, J. R. Downing, D. Pe'er, G. P. Nolan, Data-Driven Phenotypic Dissection of AML Reveals Progenitor-like Cells that Correlate with Prognosis. *Cell.* **162**, 184–197 (2015).

46. N. E. Hamilton, M. Ferry, Ggtern: Ternary diagrams using ggplot2. *J. Stat. Softw.* **87** (2018), doi:10.18637/jss.v087.c03.

47. L. Haghverdi, M. Büttner, F. A. Wolf, F. Buettner, F. J. Theis, Diffusion pseudotime robustly reconstructs lineage branching. *Nat. Methods*. **13**, 845–848 (2016).

48. M. Setty, V. Kiseliovas, J. Levine, A. Gayoso, L. Mazutis, D. Pe'er, Characterization of cell fate probabilities in single-cell data with Palantir. *Nat. Biotechnol.* **37**, 451–460 (2019).

49. M. Setty, M. D. Tadmor, S. Reich-Zeliger, O. Angel, T. M. Salame, P. Kathail, K. Choi, S. Bendall, N. Friedman, D. Pe'Er, Wishbone identifies bifurcating developmental trajectories from single-cell data. *Nat. Biotechnol.* **34**, 637–645 (2016).

50. N. Stanley, T. Bonacci, R. Kwitt, M. Niethammer, P. J. Mucha, Stochastic block models with

multiple continuous attributes. *Appl. Netw. Sci.* **4**, 54 (2019).

51. G. Finak, A. McDavid, M. Yajima, J. Deng, V. Gersuk, A. K. Shalek, C. K. Slichter, H. W. Miller, M. J. McElrath, M. Prlic, P. S. Linsley, R. Gottardo, MAST: A flexible statistical framework for assessing transcriptional changes and characterizing heterogeneity in single-cell RNA sequencing data. *Genome Biol.* **16**, 1–13 (2015).

52. G. Korotkevich, V. Sukhov, A. Sergushichev, Fast gene set enrichment analysis, 1–29 (2016).

53. A. Subramanian, P. Tamayo, V. K. Mootha, S. Mukherjee, B. L. Ebert, M. A. Gillette, A. Paulovich, S. L. Pomeroy, T. R. Golub, E. S. Lander, J. P. Mesirov, *Proc. Natl. Acad. Sci.*, in press (available at http://www.pnas.org/content/102/43/15545.abstract).

54. A. R. Cillo, C. H. L. Kürten, T. Tabib, Z. Qi, S. Onkar, T. Wang, A. Liu, U. Duvvuri, S. Kim, R. J. Soose, S. Oesterreich, W. Chen, R. Lafyatis, T. C. Bruno, R. L. Ferris, D. A. A. Vignali, Immune Landscape of Viral- and Carcinogen-Driven Head and Neck Cancer. *Immunity*. **52**, 183-199.e9 (2020).

55. M. Efremova, M. Vento-Tormo, S. A. Teichmann, R. Vento-Tormo, CellPhoneDB: inferring cell–cell communication from combined expression of multi-subunit ligand–receptor complexes. *Nat. Protoc.* **15**, 1484–1506 (2020).

56. R. Browaeys, W. Saelens, Y. Saeys, NicheNet: modeling intercellular communication by linking ligands to target genes. *Nat. Methods*. **17**, 159–162 (2020).